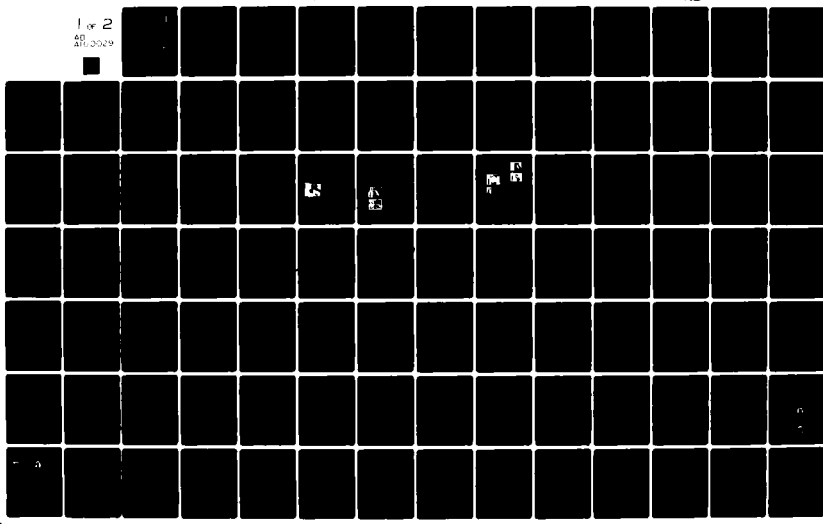


AD-A100 029 UTAH UNIV SALT LAKE CITY  
ELECTROMAGNETIC ENERGY ABSORPTION AND ITS DISTRIBUTION FOR MAN —ETC(U)  
NOV 78 O P GANDHI, J A D'ANDREA, M J HAGMANN DAMD17-47-C-4092  
UNCLASSIFIED NL  
UTEC-MD-78-189

F/6 6/18

1 of 2  
40 2029



PHOTOGRAPH THIS SHEET

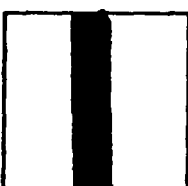
AD A100029

DTIC ACCESSION NUMBER



LEVEL

UTAH UNIV., SALT LAKE CITY



INVENTORY

ELECTROMAGNETIC ENERGY ABSORPTION AND ITS DISTRIBUTION FOR MAN  
AND ANIMALS AT DIFFERENT FREQUENCIES UNDER VARIOUS CONDITIONS.  
FINAL REPT. 1974 - 1978. NOV. 78. REPT. NO. UTEC-MD-78-189.

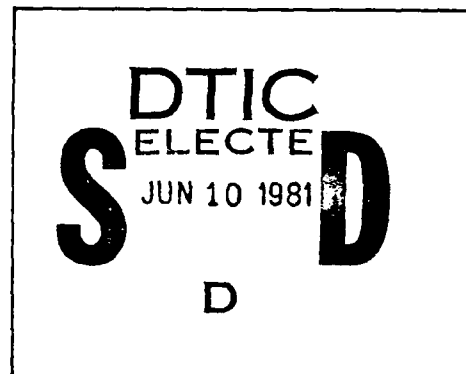
DOCUMENT IDENTIFICATION,  
CONTRACT DAMD17-74-C-4092

DISTRIBUTION STATEMENT A

Approved for public release;  
Distribution Unlimited

DISTRIBUTION STATEMENT

ACCESSION FOR	
NTIS	GRA&I
DTIC	TAB
UNANNOUNCED	
JUSTIFICATION	
BY	
DISTRIBUTION /	
AVAILABILITY CODES	
DIST	AVAIL AND/OR SPECIAL
A	
DISTRIBUTION STAMP	



DATE ACCESSIONED

DATE RECEIVED IN DTIC

PHOTOGRAPH THIS SHEET AND RETURN TO DTIC-DDA-2

AD

ELECTROMAGNETIC ENERGY ABSORPTION AND ITS DISTRIBUTION FOR MAN  
AND ANIMALS AT DIFFERENT FREQUENCIES UNDER VARIOUS CONDITIONS

FINAL REPORT

AD A1000029

Om P. Gandhi  
John A. D'Andrea  
Mark J. Hagmann

November 1978

Supported by  
U. S. Army Medical Research and Development Command  
Fort Detrick, Frederick, MD 21701

Contract No. DAMD 17-74-C-4092

University of Utah  
Salt Lake City, Utah 84112

DOD DISTRIBUTION STATEMENT

Approved for public release; distribution unlimited.

The findings in this report are not to be construed as  
an official Department of the Army position unless so  
designated by other authorized documents.

816 05018

## SECURITY CLASSIFICATION OF THIS PAGE (When Data Entered)

REPORT DOCUMENTATION PAGE		READ INSTRUCTIONS BEFORE COMPLETING FORM
1. REPORT NUMBER	2. GOVT ACCESSION NO.	3. RECIPIENT'S CATALOG NUMBER
4. TITLE (and Subtitle) Electromagnetic Energy Absorption and Its Distribution for Man and Animals at Different Frequencies under Various Conditions		5. TYPE OF REPORT & PERIOD COVERED Final Report, 1974-1978
7. AUTHOR(s) Om P. Gandhi, John A. D'Andrea, and Mark J. Hagmann		6. PERFORMING ORG. REPORT NUMBER UTEC MD 78-189
9. PERFORMING ORGANIZATION NAME AND ADDRESS University of Utah Salt Lake City, Utah 84112		10. PROGRAM ELEMENT, PROJECT, TASK AREA & WORK UNIT NUMBERS 62771A.3E162771A805.00.012
11. CONTROLLING OFFICE NAME AND ADDRESS U. S. Army Medical Research and Development Command Fort Detrick, Frederick, Maryland 21701		12. REPORT DATE November 1978
		13. NUMBER OF PAGES 107
14. MONITORING AGENCY NAME & ADDRESS (if different from Controlling Office)		15. SECURITY CLASS. (of this report) Unclassified
		15a. DECLASSIFICATION/DOWNGRADING SCHEDULE
16. DISTRIBUTION STATEMENT (of this Report)  Approved for public release; distribution unlimited.		
17. DISTRIBUTION STATEMENT (of the abstract entered in Block 20, if different from Report)		
18. SUPPLEMENTARY NOTES		
19. KEY WORDS (Continue on reverse side if necessary and identify by block number) Electromagnetic deposition and its distribution for man, numerical analysis and experimental simulation, free-space irradiation, ground and reflector effects, whole-body and head resonance frequencies, multianimal effects, simulation of man for 23-550 MHz, biological phantom materials to simulate tissue properties, multilayered model of man, design of a waveguide slot array for constant (over)		
20. ABSTRACT (Continue on reverse side if necessary and identify by block number) The whole-body absorption of electromagnetic waves by biological bodies is strongly dependent on the orientation of the electric field ( $\vec{E}$ ) relative to the longest dimension ( $L$ ) of the body. The highest rate of energy deposition occurs for $\vec{E} \parallel \hat{L}$ orientation for frequencies (65-70 MHz for an adult human being) such that the major length is approximately 0.36 to 0.4 times the free-space wavelength. Peaks of whole-body absorption for the other two configurations (major length oriented along the direction of propagation ( $k \parallel \hat{L}$ ) or along the (continued over)		

19. KEY WORDS (continued)

radiation intensity, behavioral experiments with laboratory rats, time to work stoppage at different frequencies.

20. ABSTRACT (continued)

vector of the magnetic field ( $\vec{H} \parallel \hat{L}$ ) occur for  $\lambda$  on the order of  $4\pi b$ , where  $2\pi b$  is the weighted average circumference of the animals.

Numerical calculations for a realistic block model of man have shown a fine structure to whole-body absorption at frequencies higher than the whole-body resonant frequency. Minor peaks in the supraresonance region are ascribed to maxima of energy deposition in the various body parts such as the arm and the head. For the  $E \parallel \hat{L}$ , supraresonant region, an average  $1/f$  dependence of the whole-body absorbed dose is obtained theoretically and experimentally to frequencies on the order of 4-8 times the resonance frequency.

The effect of highly conducting (metallic sheet) ground and reflecting surfaces on the electromagnetic absorption and its distribution has been studied. For a standing man model ( $\vec{E} \parallel \hat{L}$ ) with feet in conductive contact with a perfect ground, the new resonant frequency is roughly one-half that for free-space irradiation. At this lower resonance frequency, the mass normalized (specific) absorption rate (SAR) is about twice that at peak absorption frequency for free-space irradiation, and the ground effects are lost even for a 3-4" separation from the ground.

Maximum deposition of electromagnetic energy in the head region occurs for head-to-toe propagation at frequencies such that the head diameter is approximately 3.0 times the physical cross section. This value exceeds the ratio of nearly 1 reported previously for an isolated sphere model of the head.

A multilayered planar model is used to examine the dependence of whole-body power absorption on the configuration of surface layers, e.g., skin, fat, bone, muscle, which normally occur in biological bodies. It is found that the layering resonance for three-dimensional bodies (as opposed to geometrical resonance) can be predicted quite accurately by a planar model. Calculations for a multilayered prolate spheroidal model of man predict a whole-body layering resonance at 1.8 GHz with a power absorption 34 percent greater than that predicted by a homogeneous model.

Behavioral experiments with laboratory rats confirm the highlights of the above data.

### Summary

The whole-body absorption of electromagnetic waves by biological bodies is strongly dependent on the orientation of the electric field ( $\vec{E}$ ) relative to the longest dimension ( $L$ ) of the body. The highest rate of energy deposition occurs for  $\vec{E} \parallel \hat{L}$  orientation for frequencies (65-70 MHz for an adult human being) such that the major length is approximately 0.36 to 0.4 times the free-space wavelength. Peaks of whole-body absorption for the other two configurations (major length oriented along the direction of propagation ( $\vec{k} \parallel \hat{L}$ ) or along the vector of the magnetic field ( $\vec{H} \parallel \hat{L}$ )) occur for  $\lambda$  on the order of  $4\pi b$ , where  $2\pi b$  is the weighted average circumference of the animals.

Numerical calculations for a realistic block model of man have shown a fine structure to whole-body absorption at frequencies higher than the whole-body resonant frequency. Minor peaks in the supraresonance region are ascribed to maxima of energy deposition in the various body parts such as the arm and the head. For the  $\vec{E} \parallel \hat{L}$ , supraresonant region, an average  $1/f$  dependence of the whole-body absorbed dose is obtained theoretically and experimentally to frequencies on the order of 4-8 times the resonance frequency.

The effect of highly conducting (metallic sheet) ground and reflecting surfaces on the electromagnetic absorption and its distribution has been studied. For a standing man model ( $\vec{E} \parallel \hat{L}$ ) with feet in conductive contact with a perfect ground, the new resonant frequency is roughly one-half that for free-space irradiation. At this lower resonance frequency, the mass normalized (specific) absorption rate (SAR)

is about twice that at peak absorption frequency for free-space ir-radiation, and the ground effects are lost even for a 3-4" separation from the ground.

Maximum deposition of electromagnetic energy in the head region occurs for head-to-toe propagation at frequencies such that the head diameter is approximately 3.0 times the physical cross section. This value exceeds the ratio of nearly 1 reported previously for an isolated sphere model of the head.

A multilayered planar model is used to examine the dependence of whole-body power absorption on the configuration of surface layers, e.g., skin, fat, bone, muscle, which normally occur in biological bodies. It is found that the layering resonance for three-dimensional bodies (as opposed to geometrical resonance) can be predicted quite accurately by a planar model. Calculations for a multilayered prolate spheroidal model of man predict a whole-body layering resonance at 1.8 GHz with a power absorption 34 percent greater than that predicted by a homogeneous model.

Behavioral experiments with laboratory rats confirm the high-lights of the above data.

## FOREWORD

In conducting the research described in this report, the investigators adhered to the "Guide for Laboratory Animal Facilities and Care" as promulgated by the Committee on the Guide for Laboratory Animal Resources, National Academy of Sciences - National Research Council.

TABLE OF CONTENTS

	<u>Page</u>
Summary . . . . .	i
Foreword . . . . .	iii
Papers Published or Presented . . . . .	1
Invited Presentations and Seminars . . . . .	3
Professionals Partly Supported by the Contract . . . . .	4
Graduate Degrees Awarded . . . . .	5
Objectives. . . . .	6
Highlights of the Work Done on the Project . . . . .	6
A. Electromagnetic Energy Deposition in Man and Animals. .	6
Free-Space Irradiation Condition . . . . .	6
Electromagnetic Absorption in the Presence of Nearby Ground and Reflecting Surfaces . . . . .	8
Head Resonance. . . . .	11
Multianimal Effects . . . . .	11
B. Other Highlights of the Work Done on the Project . . .	12
Electromagnetic Absorption in a Multilayered Model of Man . . . . .	12
Behavioral and Thermal Effects of Microwave Irradiation at Resonant and Nonresonant Wavelengths . . . . .	13
Radiators for Microwave Biological Effects Research -- Waveguide Slot Array with Constant Radiation Intensity.	14
Biological Phantom Materials for Simulating Man at Different Frequencies . . . . .	15
Procedures for Improving Convergence of Moment-Method Solutions in Electromagnetics . . . . .	15
References . . . . .	17
Appendix A: Conditions of Strongest Electromagnetic Power Deposition in Man and Animals . . . . .	19

	<u>Page</u>
Appendix B: Numerical Calculation of Electromagnetic Energy Deposition for a Realistic Model of Man . . . . .	28
Appendix C: Part-Body and Multibody Effects on Absorption of Radio-Frequency Electromagnetic Energy by Animals and by Models of Man . . . . . . . . . . . . . . .	34
Appendix D: Numerical Calculation of Electromagnetic Energy Deposition in Models of Man with Grounding and Reflector Effects. . . . . . . . . . . . . . .	41
Appendix E: Some Recent Results on the Deposition of Electromagnetic Energy in Animals and Models of Man . . .	48
Appendix F: Head Resonance: Numerical Solutions and Experimental Results . . . . . . . . . . . . . . .	64
Appendix G: Electromagnetic Absorption in a Multilayered Model of Man . . . . . . . . . . . . . . .	69
Appendix H: Behavioral Effects of Resonant Electromagnetic Power Absorption in Rats . . . . . . . . .	75
Appendix I: Procedures for Improving Convergence of Moment-Method Solutions in Electromagnetics . . . . .	92
Appendix J: Improvement of Convergence in Moment-Method Solutions by the Use of Interpolants . . . . .	98

Papers Published or Presented

1. O. P. Gandhi, "Conditions of Strongest Electromagnetic Power Deposition in Man and Animals", *IEEE Transactions on Microwave Theory and Techniques*, Vol. MTT-23, December 1975, pp. 1021-1029.

Papers Presented at the 1975 USNC/URSI Meeting, Boulder, Colorado

2. O. P. Gandhi, K. Sedigh, G. S. Beck, and E. L. Hunt, "Distribution of Electromagnetic Energy Deposition in Models of Man with Frequencies Near Resonance", *Biological Effects of Electromagnetic Waves*, selected papers of the meeting, Vol. II, pp. 44-67 [HEW Publication (FDA) 77-8011].
3. J. A. D'Andrea, O. P. Gandhi, and R. P. Kesner, "Behavioral Effects of Resonant Electromagnetic Power Absorption in Rats", *Biological Effects of Electromagnetic Waves*, selected papers of the meeting, Vol. I, pp. 257-273 [HEW Publication (FDA) 77-8011].

Papers Presented at the 1976 USNC/URSI Meeting, Amherst, Massachusetts

4. O. P. Gandhi, E. L. Hunt, and J. A. D'Andrea, "Electromagnetic Power Deposition in Man and Animals with and without Ground and Reflector Effects", *Radio Science*, Vol. 12, No. 6(S), 1977, pp. 39-48.
5. M. J. Hagmann and O. P. Gandhi, "Radiators for Microwave Biological Effects Research -- Waveguide Slot Array with Constant Radiation Intensity", *Radio Science*, Vol. 12, No. 6(S), 1977, pp. 97-102.
6. J. A. D'Andrea, O. P. Gandhi, and J. L. Lords, "Behavioral and Thermal Effects of Microwave Radiation at Resonant and Nonresonant Wavelengths", *Radio Science*, Vol. 12, No. 6(S), 1977, pp. 251-256.
7. O. P. Gandhi and K. Sedigh, "Biological Phantom Materials for Simulating Man at Different Frequencies".

Papers Presented at the 1977 USNC/URSI Meeting, Airlie, Virginia

8. O. P. Gandhi and M. J. Hagmann, "Some Recent Results on Deposition of Electromagnetic Energy in Animals and Models of Man", published as "Part-Body and Multibody Effects on Absorption of Radio Frequency Electromagnetic Energy by Animals and by Models of Man", *Radio Science*, Vol. 14, No. 6(S), 1979, pp. 15-22.

9. M. J. Hagmann, O. P. Gandhi, and C. H. Durney, "Numerical Calculation of Electromagnetic Energy Deposition for a Realistic Model of Man", *IEEE Transactions on Microwave Theory and Techniques*, Vol. MTT-27, 1979, pp. 804-809.
10. M. J. Hagmann and O. P. Gandhi, "Numerical Calculation of Electromagnetic Energy Deposition in Man with Ground and Reflector Effects", *Radio Science*, Vol. 14, No. 6(S), 1979, pp. 23-29.

---

11. M. J. Hagmann, O. P. Gandhi, J. A. D'Andrea, and I. Chatterjee, "Head Resonance: Numerical Solutions and Experimental Results", paper presented at the 1978 MTT/IMPI/URSI meeting, Ottawa, Canada, *IEEE Transactions on Microwave Theory and Techniques*, Vol. MTT-27, 1979, pp. 809-813.
12. O. P. Gandhi and M. J. Hagmann, "Some Recent Results on Deposition of Electromagnetic Energy in Animals and Models of Man", *Proceedings of the Workshop on Physical Basis of Electromagnetic Interactions with Biological Systems*, University of Maryland, June 15-17, 1977, editors: L. S. Taylor and A. Y. Cheung, pp. 243-259.
13. M. J. Hagmann, O. P. Gandhi, and C. H. Durney, "Upper Bound on Cell Size for Moment-Method Solutions with Hard Scatterers", *IEEE Transactions on Microwave Theory and Techniques*, Vol. MTT-25, 1977, pp. 831-832.
14. M. J. Hagmann, O. P. Gandhi, and C. H. Durney, "Procedures for Improving Convergence of Moment-Method Solutions in Electromagnetics", *IEEE Transactions on Antennas and Propagation*, Vol. AP-26, 1978, pp. 743-748.
15. M. J. Hagmann, O. P. Gandhi, and C. H. Durney, "Improvements of Convergence in Moment-Method Solutions by the Use of Interpolants", *IEEE Transactions on Microwave Theory and Techniques*, Vol. MTT-26, 1978, pp. 904-908.
16. P. W. Barber, O. P. Gandhi, M. J. Hagmann, and I. Chatterjee, "Electromagnetic Absorption in a Multilayered Model of Man", *IEEE Transactions on Biomedical Engineering*, Vol. BME-26, 1979, pp. 400-405.
17. M. J. Hagmann, O. P. Gandhi, and C. H. Durney, "Improvement of Convergence in Moment-Method Solutions by the Use of Interpolants", paper presented at the 1978 IEEE/AP-S Symposium and USNC/URSI Meeting, Washington, D. C., May 15-19, 1978.

Invited Presentations and Seminars

1. December 1974, invited seminar at Bureau of Radiological Health, Rockville, Maryland, "Polarization and Frequency Effects on Whole Body Absorption of Electromagnetic Energy".
2. March 1977, invited seminar at a research meeting on Biological and Ecological Effects of Energy Transmission by Microwaves, NASA Ames Research Center, California; presentation: "Electromagnetic Power Deposition in Man and Animals".
3. April 1977, invited speaker to the Washington Regional Electromagnetic Bioeffects Seminar, "Electromagnetic Power Deposition in Man and Animals with and without Ground and Reflector Effects".
4. June 1977, invited participant in workshop on the Physical Basis of Electromagnetic Interactions with Biological Systems, University of Maryland, College Park, Maryland (supported by FDA and U. S. Navy); presentation: "Some Recent Results on Deposition of Electromagnetic Energy in Animals and Models of Man".
5. December 1977, invited seminar at DOE-NASA meeting on Biological and Ecological Effects of Microwave Beams from Satellite Power Stations, Reston, Virginia; presentation: "Microwave Absorption in Man and Animals".
6. May 1978, invited presentation at the Radiation Research Society Conference, Toronto, Canada; presentation: "Electromagnetic Energy Deposition in Man and Animals".
7. August 1978, invited seminars at Department of Occupational Health, Umeå, Sweden; Swiss Federal Institute of Technology, Zurich, Switzerland; and Royal Postgraduate Medical School, University of London, London, England; presentation: "Electromagnetic Energy Deposition in Man and Animals".
8. October 1978, invited seminar at the Department of Bioengineering, University of Pennsylvania; presentation: "Electromagnetic Energy Deposition in Man and Animals".
9. April 1979, invited presentation at New York Academy of Medicine meeting, New York, New York; presentation" "Electromagnetic Energy Deposition in Man and Animals".

Professionals Partly Supported by the Contract

Om P. Gandhi

John A. D'Andrea

Mark J. Hagmann

Peter W. Barber

Richard W. Grow

Graduate Degrees Awarded

John A. D'Andrea, Ph.D., 1976, dissertation: "Behavioral Effects  
of Resonant Electromagnetic Power Absorption in Rats".

Mark J. Hagmann, Ph.D., 1978, dissertation: "Numerical Studies  
of Absorption of Electromagnetic Energy by Man".

ELECTROMAGNETIC ENERGY ABSORPTION AND ITS DISTRIBUTION FOR MAN  
AND ANIMALS AT DIFFERENT FREQUENCIES UNDER VARIOUS CONDITIONS

Objectives

The objectives of the project were:

1. To quantify the electromagnetic power absorption and its distribution for man when subjected to radiation at different frequencies and under various exposure conditions.
2. To verify the important findings of part (1) by exposure of living organisms.

The experiments for man were performed with reduced proportionately-scaled models filled with 0.9 percent saline solutions and with biological-phantom materials developed to simulate electromagnetic properties of human tissue. The animal experiments consisted of microwave-induced convulsions and work stoppage in rats.

The purpose of the project was to develop an understanding that would lead to projections for humans.

Highlights of the Work Done on the Project

A. Electromagnetic Energy Deposition in Man and Animals\*

Free-Space Irradiation Condition

The condition that has been studied the most to date is that of

---

\* A paper based on these highlights will be submitted for publication in the *Proceedings of the IEEE* (January 1980) Special Issue on Biological and Ecological Effects and Medical Applications of Electromagnetic Energy.

free-space irradiation of single animals. The whole-body absorption of electromagnetic waves by biological bodies is strongly dependent on the orientation of the electric field ( $\vec{E}$ ) relative to the longest dimension ( $L$ ) of the body. The highest rate<sup>1</sup> of energy deposition occurs for  $\vec{E} \parallel \hat{L}$  orientation (see Appendix A), for frequencies such that the major length is approximately 0.36 to 0.4 times the free-space wavelength ( $\lambda$ ) of radiation. Peaks of whole-body absorption for the other two configurations (major length oriented along the direction of propagation ( $\vec{k} \parallel \hat{L}$ ) or along the vector of the magnetic field ( $\vec{H} \parallel \hat{L}$ ) have also been reported<sup>2</sup> for  $\lambda$  on the order of  $4\pi b$ , where  $2\pi b$  is the weighted average circumference of the animals.

Using prolate spheroidal and ellipsoidal equivalents of biological bodies, theoretical calculations have recently been given in a dosimetry handbook<sup>3</sup> for frequencies up to and slightly beyond the resonant region for the aforementioned polarizations  $\vec{E} \parallel \hat{L}$ ,  $\vec{k} \parallel \hat{L}$ , and  $\vec{H} \parallel \hat{L}$ . Numerical calculations for a realistic model<sup>4</sup> of man (see Appendix B) have shown a fine structure to whole-body absorption at frequencies higher than the whole-body resonant frequency. Minor peaks in the supraresonance region are ascribed to maxima of energy deposition in the various body parts such as the arm and the head<sup>5</sup> (see Appendix C for details).

For the supraresonant region, the  $\vec{E} \parallel \hat{L}$  orientation has been studied most extensively. An average  $1/f$  dependence of the whole-body absorbed dose is experimentally observed<sup>6</sup> to frequencies  $f$  on the order

of  $1.6 S_{res}$  times the resonant frequency  $f_r$ , where  $S_{res}$  is the relative absorption cross section at the resonant frequency.

Empirical equations for specific absorption rate (SAR) have been derived<sup>6</sup> for  $\vec{E} \parallel \hat{L}$  orientation and found to be fairly accurate for six animal species<sup>5</sup> from 25-g mice to 2250-g rabbits.

These equations are given in Table 1.

The coefficients in these empirical equations for man model are approximatley 63 percent of the live animal coefficients. Further research is needed to resolve this difference.

#### Electromagnetic Absorption in the Presence of Nearby Ground and Reflecting Surfaces

Only highly conducting (metallic sheet) ground and reflecting surfaces<sup>6,7</sup> of infinite extent have been studied to date (see Appendix D). For a standing man model with feet in conductive contact with a perfect ground, there is a drastic alteration in SAR as a function of frequency. For  $\vec{E} \parallel \hat{L}$  orientation the new resonant frequency is roughly one half that given by Eq. 1. At this lower resonance frequency, the SAR is about twice that at peak absorption frequency for free-space irradiation.

The nature of the ground effects on SAR (for  $\vec{E} \parallel \hat{L}$  orientation) is such that even a small separation<sup>7-9</sup> from ground (to break conductive contact) is sufficient to eliminate much of the ground effect (see Appendices D and E). For separations from ground more than 3-4", the total energy deposition and its distribution are identical to those for

Table 1. SAR for man models for conditions of free-space irradiation.

$\vec{E} \parallel \hat{L}$  Orientation

Peak absorption or resonant frequency:

$$f_r = 11.4 / L_{cm} \text{ GHz} \quad (1)$$

For subresonant region --  $0.5 f_r < f < f_r$ :

$$\text{SAR in mW/g for } 1 \text{ mW/cm}^2 \text{ incident plane waves} = 0.522 \frac{L_{cm}^2}{\text{weight in g}} \left( \frac{f}{f_r} \right)^{2.75} \quad (2)$$

For supraresonant frequency region --  $f_r < f < 1.6 S_{res} f_r$ :

$$\text{SAR in mW/g for } 1 \text{ mW/cm}^2 \text{ incident plane wave fields} = \frac{5.95}{f_{GHz}} \frac{L_{cm}}{\text{weight in g}} \quad (3)$$

where  $L_{cm}$  is the long dimension of the body in centimeters and

$$S_{res} = 0.481 \sqrt{\frac{L_{cm}^3}{\text{weight in g}}} \quad (4)$$

free-space irradiation conditions. Even for a man model in conductive contact with a perfect ground, the energy deposition in the supraresonance region ( $f > 2-3 f_r$ ) is comparable<sup>7</sup> to that for conditions of free-space irradiation.

Other orientations and/or finite conductivity ground effects on SAR have not been studied to date.

For highly conducting (metallic sheet) reflecting surfaces of flat and 90°-corner types, enhancements<sup>6</sup> in SAR by factors as large as 27 have been observed for  $\vec{E} \parallel \hat{L}$  orientation. Most of the work to date has concentrated on frequencies close to the resonance region. The observed enhancement factors are explained<sup>6</sup> on the basis of antenna theory.<sup>10</sup> Indeed, for incident plane waves for  $\vec{E} \parallel \hat{L}$  orientation, most of the observed results are as though the target acted like a pick-up half-wave dipole with reflecting surfaces in close vicinity.

Finite conductivity, finite size reflecting surfaces and other orientations have not been considered to date. Also the results for frequencies higher than about 8.5 times the resonant frequency (550 MHz for man) have not been obtained even for highly conducting reflectors.

Enclosed structures such as rooms, etc., may act as lossy resonators with electromagnetic fields coupling in from windows. If such structures were to have highly reflecting walls, field enhancements by two to three orders of magnitude may indeed be possible. However, since typically encountered walls are not very reflecting, it is expected that field enhancements by more than a factor of 5-10 may not occur realistically. Research into these structures is needed in order

to describe the nature of field enhancements.

#### Head Resonance

We have recently identified a frequency region for the highest rate of energy deposition in the head. The head resonance<sup>5,8,11</sup> (see Appendices C, E, and F) occurs at frequencies such that the head diameter is approximately one quarter of the free-space wavelength. For the intact (adult) human head, the resonance frequency is estimated to be on the order of 350-400 MHz. At head resonance, the absorption cross section for the head region is approximately 3.0 times the physical cross section with a volume averaged SAR that is about 3.3 times the whole-body averaged SAR. Both values greatly exceed numbers reported earlier<sup>12,13</sup> for spherical models of the *isolated* human head. Also numerical calculations<sup>11</sup> (Appendix F) using 144 cubical cells of various sizes to fit the shape of the human head (340 cells for the total body) give local SARs at hot spots that are about 5 times the head-average values.

We feel that the phenomenon of head resonance may be important in the study of behavioral effects, blood-brain barrier permeability, cataractogenesis, and microwave bioeffects.

#### Multianimal Effects<sup>5</sup>

It has been shown (see Appendix C for details) that for resonant biological bodies close to one another, the antenna theory may be used to predict the modification in SAR relative to free-space values. For

two resonant targets separated by  $0.65$  to  $0.7 \lambda$ , the highest SAR, 150 percent of the free-space value has been experimentally observed for anesthetized rats and models of man for  $\vec{E} \parallel \hat{L}$  orientation for frontally (broadside) incident plane waves. For three animals in a row with an interanimal spacing of  $0.65 \lambda$ , the central animal SAR is observed to be roughly two times, while the two end animals receive an SAR that is approximately 1.5 times that for an isolated animal.

Full implications of the multibody effects on SAR are not completely understood, even though preliminary experimental data<sup>5</sup> show that similar enhancements may also occur for subresonance and supreresonance regions. Furthermore, other orientations, irregular spacings, and nonfree-space exposure conditions have not been considered to date.

#### B. Other Highlights of the Work Done on the Project

##### Electromagnetic Absorption in a Multilayered Model of Man

A multilayered planar model is used (see Appendix G) to examine the dependence of whole-body power absorption on the configuration of surface layers, e.g., skin, fat, muscle, which normally occur in biological bodies. It is found that the layering resonance for three-dimensional bodies (as opposed to the geometrical resonance) can be predicted quite accurately by a planar model. Calculations for a multilayered prolate spheroidal model of man predict a whole-body layering resonance at 1.8 GHz with a power absorption 34 percent greater than that predicted by a homogeneous model.

Behavioral and Thermal Effects of Microwave Irradiation at Resonant and Nonresonant Wavelengths

The details of these studies are given in Appendix H.

Behavioral and thermal effects of radiating an animal with differing wavelengths of microwave energy at the same power density were investigated in the first of two studies. Five Long-Evans rats were trained to perform a lever-pressing task and were rewarded with food on a variable interval schedule of reinforcement. Rats were individually exposed in random order to 400-, 500-, 600-, and 700-MHz CW radiation at a power density of  $20 \text{ mW/cm}^2$  with the long axis of the rat's body parallel to the vector of the electric field. Radiation at all wavelengths produced rises of body temperature and stoppage of lever pressing. The averaged rise in body temperature was greatest and work stoppage was most rapid during exposures at 600 MHz. In the second study, six rats were exposed in random order to 600-MHz CW radiation at power densities of 5, 7.5, 10, and  $20 \text{ mW/cm}^2$  while performing the same behavioral task. Exposures at 10 and  $20 \text{ mW/cm}^2$  resulted in work stoppage, while exposures at 5 and  $7.5 \text{ mW/cm}^2$  did not. In addition, three of the rats were subsequently exposed while responding to 600-MHz pulsed radiation (1000 pps, 3- or 30- $\mu\text{s}$  pulse durations at a peak power density of  $170 \text{ mW/cm}^2$  (averaged 0.51 and  $5.1 \text{ mW/cm}^2$ ). No work stoppage occurred to pulsed radiation. Taken in sum, the data show that the mature Long-Evans rat is resonant at a frequency near 600 MHz while work stoppage during short-term exposures to 600-MHz radiation occurs at a power density between 7.5 and  $10 \text{ mW/cm}^2$ .

Radiators for Microwave Biological Effects Research --  
Waveguide Slot Array with Constant Radiation Intensity

Microwave biological studies with large targets or multiple targets require a large working area that provides near-uniform exposures to energy. At high microwave frequencies where high power sources are not readily available, it is desirable to use a radiator that provides a constant intensity beam so that the working area may receive almost all of the radiated energy.

Several synthesis procedures have been used for design of a longitudinal shunt slot array having a pattern with nearly constant radiation intensity over the beam width and zero intensity outside. A beam width of 15.5° was chosen as being small enough for a radiated beam to approximate a plane wave yet give enough divergence for convenient chamber divisions. Discontinuities in the desired pattern force the Fourier-synthesized pattern to have significant errors due to overshoot and ripple. Solutions developed on the basis of Fejér sums and Lanczos weighted least squares gave patterns with objectionable rounding. A new procedure based on weighted least squares was developed for optimum characteristics and both the new procedure and its application to a practical design are described in reference 14.

A longitudinal-shunt slot array with reflectors has been designed, built, and tested. The antenna is easily matched near the design frequencies of 10.0-10.4 GHz. The radiation pattern has an intensity within ±0.5 dB over a total angle of 15.6° in the H plane and 15.5° in the E plane. Gain is 19.7 dB which is 3.9 dB above that of a horn with a

similar aperture area. By using energy-absorbing material, it is possible to produce a pattern in which the fields drop suddenly from the nearly constant values to nearly zero.

Biological Phantom Materials for Simulating Man at Different Frequencies

Biological phantom materials were developed for simulating man over the frequency range 13-230 MHz (including the important resonance regions of 33 and 65 MHz). These materials have been used to fill the eight proportionately-scaled figurines for dosimetric measurements at 300, 400, 600, 915, and 985 MHz. The compositions and their measured properties are given in Appendix A of Annual Report No. 2.

Procedures for Improving Convergence of Moment-Method Solutions in Electromagnetics

The value of numerical solutions in dosimetry may be limited by both the accuracy of the model as a representation of the target animal and the accuracy of the computations for the model. Accurate numerical procedures have been developed for use with crude models such as the sphere, infinite cylinder, ellipsoid, and spheroid. We have used moment-method solution of the electric field volume integral equation so that an array of cubes of different sizes and compositions may be used to better represent the shape of the target animal. In order to allow a maximum number of cubes for increased detail in the representation of arms, legs, etc., we have used a pulse function basis in the moment-method solution. Others have also used pulse function solutions

for block models in geophysics and in dosimetry, but we have addressed the issues of both estimating and reducing the errors caused by the use of pulse functions.

A pulse function basis requires the assumption that the cells are small enough that the electric field may be represented by a constant complex vector within each cell. Solutions previously reported by others for a block model of man have a ratio of 239:1 for energy deposition in one pair of adjacent cells at 10 MHz. We expect that large errors are present in solutions exhibiting large cell-to-cell variations. Our first publication regarding the use of pulse functions is Appendix M which establishes an upper bound on cell size. Such a criterion was not previously available for use with moment-method solutions. After defining the source of error, our next task was to reduce the error. Appendix I describes several novel procedures which we discovered for reducing the error in solutions of 2-D electromagnetics problems. We were not able to extend the new procedures to 3-D solutions, but we found a different method which is useful for improving convergence in 3-D problems which is described in Appendix J. Armed with both our convergence criterion (Reference 15) and a novel method of improving convergence (Appendix J), we have proceeded to obtain numerical solutions for a realistic model of man both in free-space and under other conditions such as in the presence of a ground plane or flat or 90° corner reflectors. Such applications are described in other publications referenced earlier in this report.

### References

1. O. P. Gandhi, "Conditions of Strongest Electromagnetic Power Deposition in Man and Animals", *IEEE Transactions on Microwave Theory and Techniques*, Vol. MTT-23, 1975, pp. 1021-1029 (Appendix A).
2. O. P. Gandhi, "Polarization and Frequency Effects on Whole Animal Absorption of RF Energy", *Proceedings of the IEEE*, Vol. 62, 1974, pp. 1166-1168.
3. C. C. Johnson, C. H. Durney, P. W. Barber, H. Massoudi, S. J. Allen, and J. C. Mitchell, "Radiofrequency Radiation Dosimetry Handbook", Report SAM-TR-76-35, USAF School of Aerospace Medicine, Brooks Air Force Base, Texas 78235, September 1976.
4. M. J. Hagmann, O. P. Gandhi, and C. H. Durney, "Numerical Calculation of Electromagnetic Energy Deposition for a Realistic Model of Man", paper presented at the 1977 International Symposium on the Biological Effects of Electromagnetic Waves, Airlie, Virginia, October 30-November 4; to be published in *IEEE Transactions on Microwave Theory and Techniques* (Appendix B).
5. O. P. Gandhi, M. J. Hagmann, and J. A. D'Andrea, "Some Recent Results on Deposition of Electromagnetic Energy in Animals and Models of Man", paper presented at the 1977 International Symposium on the Biological Effects of Electromagnetic Waves, Airlie, Virginia, October 30-November 4; *Radio Science*, Vol. 14, No. 6(S), 1979, pp. 15-21 (Appendix C).
6. O. P. Gandhi, E. L. Hunt, and J. A. D'Andrea, "Deposition of Electromagnetic Energy in Animals and in Models of Man with and without Grounding and Reflector Effects", *Radio Science*, Vol. 12, November/December 1977, pp. 39-47; *Biological Effects of Electromagnetic Waves, Selected Papers of the USNC/URSI Annual Meeting*, Amherst, Massachusetts.
7. M. J. Hagmann and O. P. Gandhi, "Numerical Calculation of Electromagnetic Energy Deposition in Man with Ground and Reflector Effects", paper presented at the 1977 International Symposium on the Biological Effects of Electromagnetic Waves, Airlie, Virginia, October 30-November 4; *Radio Science*, Vol. 14, No. 6(S), 1979, pp. 23-29 (Appendix D).
8. O. P. Gandhi and M. J. Hagmann, "Some Recent Results on Deposition of Electromagnetic Energy in Animals and Models of Man", invited paper presented at the Workshop on Physical Basis of Electromagnetic Interactions with Biological Systems, University of Maryland, June 15-17, 1977; published in the proceedings of the workshop, editors L. S. Taylor and A. Y. Cheung, pp. 243-259 (Appendix E).

9. O. P. Gandhi, J. A. D'Andrea, B. K. Jenkins, J. L. Lords, J. R. Mijanovich, and K. Sedigh, "Behavioral and Biological Effects of Resonant Electromagnetic Absorption in Rats", Technical Report UTEC MD-75-174 under contract No. DAMD 17-74-C-4092, Microwave Device and Physical Electronics Laboratory, University of Utah, Salt Lake City, Utah 84112, June 30, 1975.
10. H. Jasik (Ed.), *Antenna Engineering Handbook*, McGraw-Hill, New York, 1961, Chapter 11.
11. M. J. Hagmann, O. P. Gandhi, J. A. D'Andrea, and I. Chatterjee, "Head Resonance: Numerical Solutions and Experimental Results", paper presented at the 1978 MTT/IMPI/URSI meeting, Ottawa, Canada, June 1978; published in *IEEE Transactions on Microwave Theory and Techniques*, Vol. MTT-27, 1979, pp. 809-813 (Appendix F).
12. W. T. Joines and R. J. Spiegel, "Resonance Absorption of Microwaves by the Human Skull", *IEEE Transactions on Biomedical Engineering*, Vol. BME-21, 1974, pp. 46-48.
13. C. M. Weil, "Absorption Characteristics of Multilayered Sphere Models Exposed to UHF/Microwave Radiation", *IEEE Transactions on Biomedical Engineering*, Vol. BME-22, 1975, pp. 468-476.
14. M. J. Hagmann and O. P. Gandhi, "Radiators for Microwave Biological Effects Research -- Waveguide Slot Array with Constant Radiation Intensity", *Radio Science*, Vol. 12, No. 6(S), 1979, pp. 97-102.
15. M. J. Hagmann, O. P. Gandhi, and C. H. Durney, "Upper Bound on Cell Size for Moment-Method Solutions", *IEEE Transactions on Microwave Theory and Techniques*, Vol. MTT-25, 1977, pp. 831-832.

## APPENDIX A

IEEE TRANSACTIONS ON MICROWAVE THEORY AND TECHNIQUES, VOL. MTT-23, NO. 12, DECEMBER 1975

1021

# Conditions of Strongest Electromagnetic Power Deposition in Man and Animals

O. P. GANDHI, SENIOR MEMBER, IEEE

**Abstract**—Strongest power deposition for biological bodies is found for fields polarized along the longest dimension for frequencies such that the major length is about 0.4 times the free-space wavelength of radiation. Peak absorption in the presence of ground effects is observed at frequencies about one-half as much as for bodies isolated in free space. At resonance, an effective absorption area 3–4 times the shadow cross section is measured. Using biological-phantom figurines of the human body, distribution of power absorption is determined. Maximum power deposition is observed for the neck region. Initial experiments with anesthetized and dead rats have confirmed this observation.

## INTRODUCTION

**B**ECAUSE of the expanding uses of electromagnetic (EM) radiation, it has become necessary to establish the most hazardous conditions of exposure to such radiation for humans. In particular, it is important to know the frequency regions of most absorption for various orientations of the body relative to the polarization of incident waves and how the absorption cross section varies with frequency of EM radiation. It is also important to determine the distribution of power absorption in the body to ascertain locations of maximum deposition particularly close to resonant frequencies. This knowledge is vital in evaluating and establishing radiation safety standards.

Based on our previous experiments [1] with rats and biological-phantom and saline-filled prolate spheroidal bodies, strongest whole-body absorption was found for EM fields polarized with electric field along the long dimensions of the bodies. EM power absorption was measured for bodies of fixed size at various frequencies using a parallel-plate waveguide as a transmission medium of plane waves and compared [2] with data obtained from fixed-frequency free-space irradiation exposures of bodies of varying sizes. The salient features of the experimentally observed results (qualitatively sketched in Fig. 1) are as follows.

- 1) The  $\mathbf{E} \parallel \hat{\mathbf{L}}$  orientation is found to be the most absorbing, and  $\mathbf{H} \parallel \hat{\mathbf{L}}$  the least absorbing, with the configuration  $\mathbf{k} \parallel \hat{\mathbf{L}}$  only slightly more absorbing than the  $\mathbf{H} \parallel \hat{\mathbf{L}}$  orientation. The vectors  $\mathbf{E}$ ,  $\mathbf{H}$ , and  $\mathbf{k}$  are along the

Manuscript received April 15, 1975; revised August 26, 1975. This work was supported by the U. S. Army Medical Research and Development Command under Contract DAMD 17-74-C-4092.

The author is with the Department of Electrical Engineering, University of Utah, Salt Lake City, Utah 84112. He is also a consultant to the Division of Neuropsychiatry, Walter Reed Army Institute of Research, Washington, D. C. 20012.

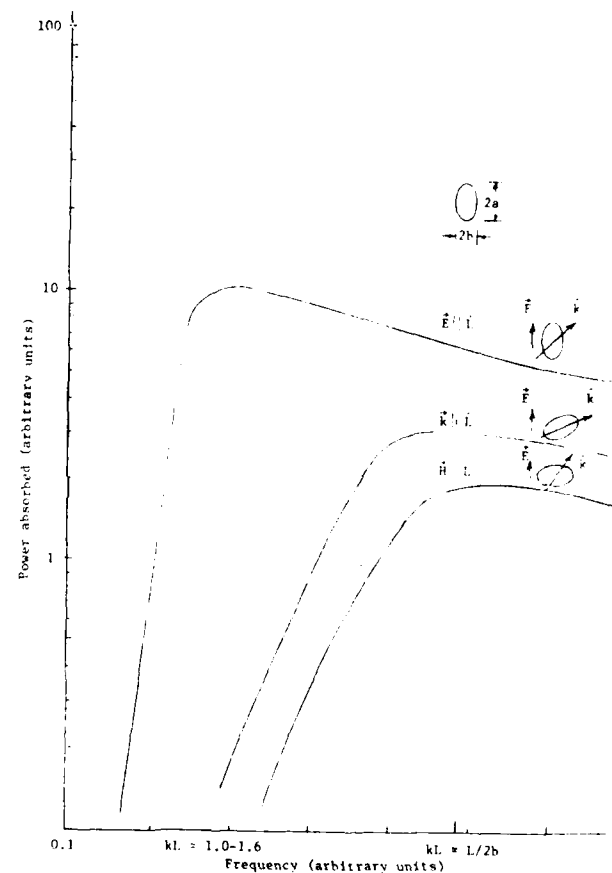


Fig. 1. Typical RF absorption curves for animals and bodies of prolate-spheroidal shape obtained with a parallel-plate waveguide. Symbols with arrows above are represented by boldface italic in text.

electric and magnetic fields, and along the direction of propagation, respectively, and  $\hat{\mathbf{L}}$  is along the major length  $L$  of the body. These experimental results are in qualitative agreement with recent theoretical results [3] on power absorption in homogeneous lossy prolate spheroids. Quantitative comparison has not been possible because of the long-wavelength ( $kL \gtrsim 0.6$ ) approximation of the theory. By contrast, the experimental results pertain mostly to frequencies on the order of resonant and higher frequencies ( $kL \gtrsim 1.0$ ).

- 2) The frequencies of peak absorption occur in the reverse order. Maximum absorption for  $\mathbf{E} \parallel \hat{\mathbf{L}}$  occurs at the lowest frequency with  $kL = 2\pi L/\lambda$  on the order of

**TABLE I**  
**ACTUAL AND EQUIVALENT PROLATE SPHEROIDAL DIMENSIONS FOR ANESTHETIZED RATS OF DIFFERENT WEIGHTS**

Weight of the Rat in Grams	Rat Length L from Nose to Base of Tail cm	Measured Circumference of the Animal cm	Nominal Circumference* 2b in cm	Aspect Ratio L/2b of Equivalent Prolate Spheroid
96	15.5	11.5 (body) max. 9.0 (head)	10.60	4.50
158	18.0	13.5 (body) max. 9.0 (head)	12.62	4.30
261	21.0	15.0 (body) max. 10.0 (head)	15.32	4.30
390	23.5	18.0 (body) max. 11.0 (head)	17.70	4.35

\* This is calculated from the relationship  $2/3 \pi b^2 \rho = W$ .

1.0 to 1.6 ( $L/\lambda \approx 0.16$  to 0.25). Peak absorption for  $\mathbf{k} \parallel \hat{\mathbf{L}}$  and  $\mathbf{H} \parallel \hat{\mathbf{L}}$  orientations occurs at successively higher frequencies, with  $kL$  for these configurations on the order of  $L/2b$  where  $2b$  is the length of the equivalent prolate spheroidal body<sup>1</sup> along the minor axes (see Table I for numbers illustrative of 90–400-g rats). These values of  $kL$  for resonance in the different orientations are obtained approximately by requiring that for a sphere [4], [5] the shortest circumference for the lossy creeping waves launched at the center of the shadow plane be  $0.5 \lambda$ .

3) In the frequency region immediately below resonance, absorption diminishes rapidly with frequency. An  $f^{-0.75}$  dependence similar to that for spheres is observed.

4) There is an excellent correlation of the results obtained from the parallel-plate waveguide with the free-space irradiation results [1], [2]. The only exception is that maximum absorption in the free-space case occurs for body size of about  $0.4 \lambda$ , i.e., at approximately twice the frequency observed in the parallel-plate waveguide situation. The reason for this may be that while a body isolated in free space is required to be approximately  $0.4 \lambda$  for resonance, the same condition is met in the presence of a ground plane (such as in the parallel-plate waveguide) with only a  $0.2\lambda$  body and its image in the ground plane acting together.

#### CORRELATION WITH LETHALITY RESULTS

A study [6] has just been completed at Walter Reed Army Institute of Research, Washington, D. C., on the lethality of 100–125- and 380–420-g rats and 25–35-g mice when exposed to microwave radiation at 710, 985, 1700, 2450, and 3000 MHz. The choice of frequencies was dictated by the anechoic chamber facilities available at Walter Reed Laboratories. The time to convulsion was

measured for  $\mathbf{E} \parallel \hat{\mathbf{L}}$  and  $\mathbf{H} \parallel \hat{\mathbf{L}}$  configurations. At each frequency, eleven animals were studied for each of the two orientations picked to correspond to the maximum and minimum absorbing configurations of Fig. 1. The lethality data correlate well with our results [1], [2] obtained from the modeling experiments. In particular, the following points of agreement are noteworthy.

- 1) The time to convulsion in the  $\mathbf{E} \parallel \hat{\mathbf{L}}$  orientation is always shorter than that for the  $\mathbf{H} \parallel \hat{\mathbf{L}}$  orientation.<sup>2</sup>
- 2) On the low-frequency side of resonance, the time to convulsion rises very rapidly, corresponding to a fast diminishing absorption in this region (see Fig. 1).
- 3) The minimum time to convulsion for  $\mathbf{H} \parallel \hat{\mathbf{L}}$  orientation occurs for  $kL \approx 4.4$ . From Table I, the nominal  $L/2b$  for rats of different weights is on the order of 4.4. The lethality results are consequently in agreement with the parallel-plate waveguide results for resonant absorption at  $kL \approx L/2b$ .
- 4) For the  $\mathbf{E} \parallel \hat{\mathbf{L}}$  configuration, minimum time to convulsion is obtained at frequencies such that the length from the animal's eyes to the base of the tail is approximately  $0.4 \lambda$ . This is in agreement with the free-space experiments described in the following (see Fig. 2) and also in [1].

#### SCALING

To evaluate the validity of scaling, free-space heating experiments were repeated<sup>3</sup> at 710 MHz for saline-filled prolate spheroidal bodies ( $L/2b = 6$  corresponding to humans) of major length varying from 7.6 to 25.4 cm. The temperature increase for a 5-min exposure to 100-mW/cm<sup>2</sup> radiation is plotted in Fig. 2. From the amount of energy absorbed, the relative absorption coefficient [7]  $S$

<sup>1</sup> The dimension  $2b$  for an equivalent prolate spheroid is calculated from the expression  $2/3 \pi b^2 L \rho = W$ , where  $W$  is the weight of the body and  $\rho$  is the average mass density of nearly 1 g/cm<sup>3</sup>. The nominal circumference  $2b$  so calculated has been found to correspond well to the average circumference actually measured for rats of weights varying from 90 to 400 g (see Table I).

<sup>2</sup> The only exception to this observation is 400-g rats at 2450 and 3000 MHz. For these animals, such frequencies are 4–5 times higher than the resonant frequency of the  $\mathbf{E} \parallel \hat{\mathbf{L}}$  orientation. A considerably reduced total power deposition under these circumstances may well be the reason for this anomaly.

<sup>3</sup> Experiments were previously done at 1700 MHz with smaller size prolate spheroidal bodies with  $L$  of 4.8, 6, 7.2, 9.6, and 14.4 cm (see [1]).

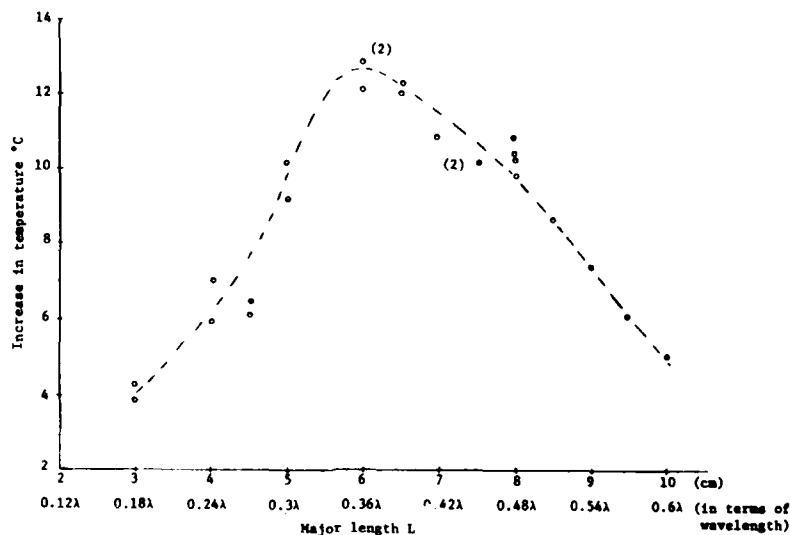


Fig. 2. Temperature rise in saline-filled prolate spheroids with an aspect ratio  $L/2b$  of 6. Frequency, 710 MHz; ir-radiation time, 5 min; incident power density, 100 mW/cm<sup>2</sup>; polarization,  $E \parallel L$ .

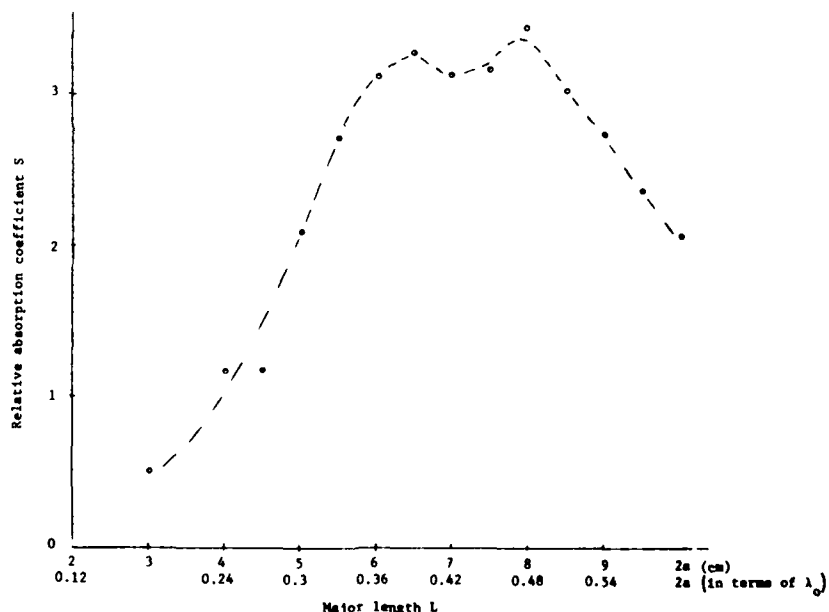


Fig. 3. Relative absorption coefficient  $S$  for different size prolate spheroids ( $L/2b = 6$  in each case). Polarisation:  $E \parallel L$ .

is calculated<sup>4</sup> and is plotted in Fig. 3. Maximum absorption is observed, as before [1], [2], for bodies of major length on the order of  $0.38\text{--}0.48\lambda$ , and whole-body deposition of about 3.5 times as much as that called for by the shadow area is measured. This verifies experimentally the concept of scaling. Bodies scaled down in all dimensions

result in peak absorption frequencies scaled up by the same factor and vice versa.

#### CORE TEMPERATURE OF RATS EXPOSED IN DIFFERENT ORIENTATIONS

In order to dramatize the polarization-dependent variability of the EM hazard, 250-g<sup>4</sup> Wistar rats were exposed to 100-mW/cm<sup>2</sup> fields. The rectal temperature of the animal was measured under irradiation, using the

<sup>4</sup> The relative absorption coefficient  $S$  is defined as the absorption cross section divided by the physical-shadow cross section. Power absorbed in milliwatts =  $(4180 \times \text{temperature increase of the body} \times \text{weight in grams})/\text{irradiation time in seconds}$ . This divided by the incident field intensity in milliwatts/square centimeter gives the absorption cross section.

<sup>5</sup> This particular weight was selected to observe the  $L \approx 0.4\lambda$  condition for maximum absorption in the free space.

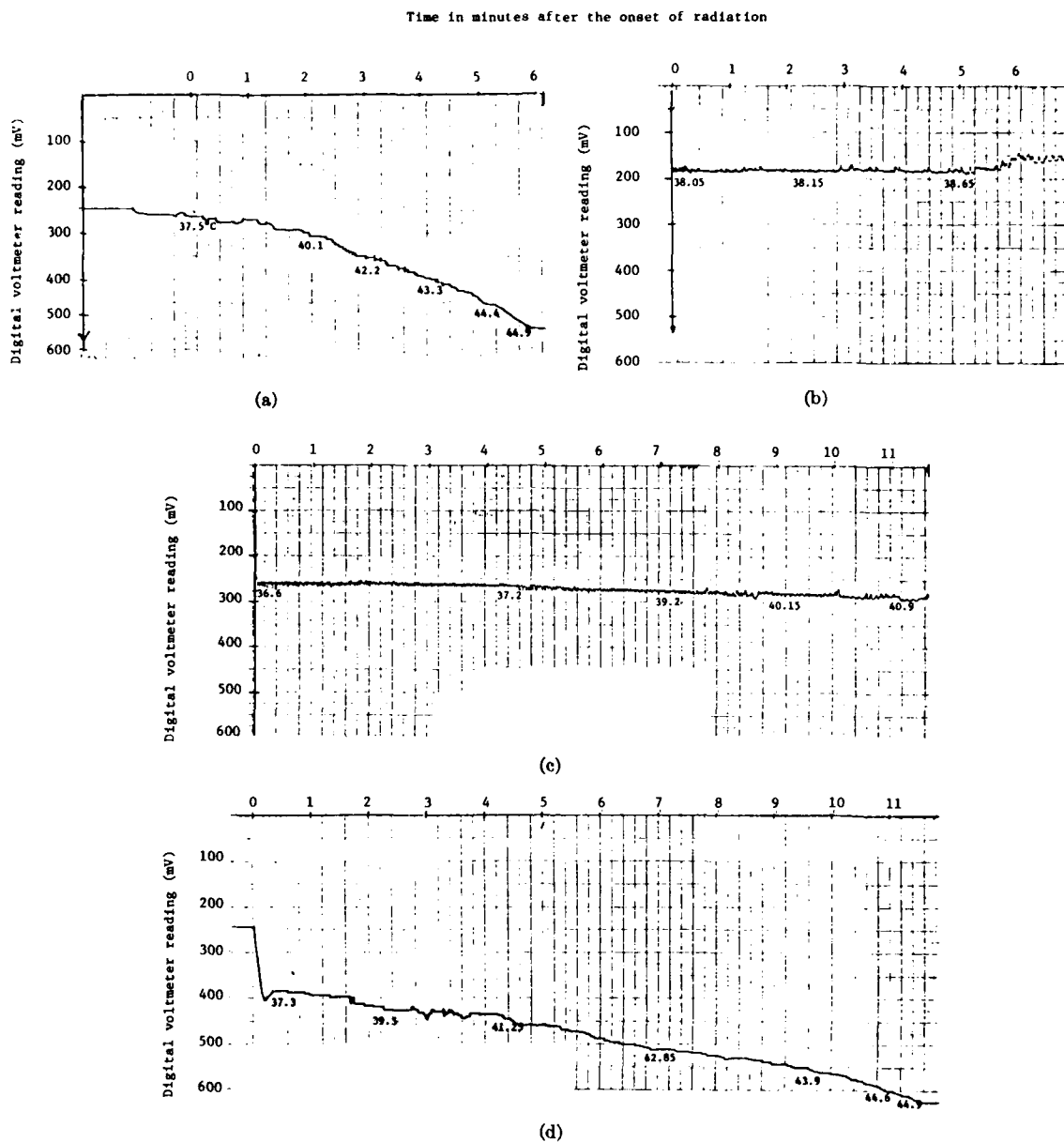


Fig. 4. Core temperature of 250-g rats exposed to 710-MHz radiation. (a) Orientation  $E \parallel \hat{L}$ ; incident power density,  $100 \text{ mW/cm}^2$ . (b) Orientation  $K \parallel \hat{L}$ ; incident power density,  $100 \text{ mW/cm}^2$ . (c) Orientation  $H \parallel \hat{L}$ ; incident power density,  $100 \text{ mW/cm}^2$ . (d) Orientation  $E \parallel \hat{L}$ ; incident power density,  $50 \text{ mW/cm}^2$ .

relatively nonperturbing liquid-crystal fiberoptic temperature probe [8]. The digital voltmeter reading as a function of time was recorded and is given in Fig. 4(a), (b), and (c) for the three orientations. The core temperature read off the calibration chart of the probe is marked alongside the curves in Fig. 4. For an incident power density of  $50 \text{ mW/cm}^2$  [Fig. 4(d)], the power deposition in the  $E \parallel \hat{L}$  orientation was still much higher than that for the other two configurations at  $100 \text{ mW/cm}^2$ . The increase in animal temperature as a function of time for the two power densities in the  $E \parallel \hat{L}$  orientation is plotted in Fig. 5. For this configuration, the relative absorption

coefficients  $S$  of 3.8 and 4.26 are calculated from the initial slopes of the temperature-rise curves for  $100$ - and  $50\text{-mW/cm}^2$  incident field intensities, respectively. This may be compared to  $S$  on the order of 3.5 for resonant-size saline-filled prolate spheroids (Fig. 3).

#### DISTRIBUTION OF POWER DEPOSITION— “HOT SPOTS”

To determine the distribution of power deposition, an 18.4-cm-tall figurine of the female body has been used as a mold to form a cavity in styrofoam. The size of the figurine has been selected such as to allow resonance (Fig. 3) at

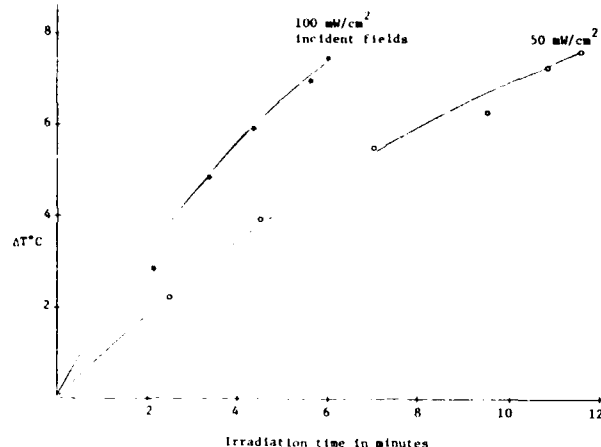


Fig. 5. Core temperature increase of 250-g Wistar rats exposed to 710-MHz free-space radiation ( $E \parallel \hat{L}$  orientation).



Fig. 6. Photograph of the parallel-plate radiation chamber.

710 MHz for free-space radiation ( $L/\lambda \approx 0.44$ ) and at a frequency about half as much in the parallel-plate radiation chamber. In order to simulate ground effects on EM power absorption, a larger parallel-plate radiation chamber (Fig. 6) has been designed and fabricated. For the chamber, the central working area<sup>6</sup> consists of a copper plate of 63.5-cm width separated by a 25.4-cm clearance from the ground plate of 117-cm width. The overall transmission length of 198 cm is occupied by two symmetrical tapered sections of 61-cm axial length, the central working area of 61-cm length, and the 7.5-cm end sections connected to UG58/U input and output coaxial connectors.

From EM field theory, a body reduced by a factor of  $\beta$  in all dimensions may be used to obtain RF absorption

<sup>6</sup> The uniformity of fields in the central working area was established by heating a 19-cm-long saline-filled prolate spheroid in the  $E \parallel \hat{L}$  orientation. For the spheroid placed at the center of the plates, a temperature increase of 1.23°C was measured for an incident field intensity of 49.10 mW/cm<sup>2</sup> at 360 MHz. By comparison, a temperature increase of 1.15°C at 48.88 mW/cm<sup>2</sup> was observed for the same spheroid placed 10.2 cm off the center line.

characteristics of the full-scale body, provided an irradiation frequency scaled up by a factor of  $\beta$  is used. However, it is necessary that the complex permittivity ( $\epsilon_1 - j\sigma/\omega_0$ ) represented by the scaled-down model correspond to the value at the lower frequency characteristic of the whole body. With these scaling precautions, the distribution of power deposition in the reduced scale model is identical (though the magnitudes are higher by a factor of  $\beta$ ) to that of the full-scale body. Since the projected frequency of maximum absorption for adult humans is on the order of 65–75 MHz in free space and about half as much in the presence of ground effects, the biological-phantom material that is used should have the dielectric properties of humans in that frequency range. A composition [9] of the material with 3.26 percent NaCl, 8.74 percent Superstuff (obtained from Wiamo Manufacturing Company, San Gabriel, California), and 87.0 percent water has a measured dielectric constant of 66 and a conductivity of 4.39 mho/m. For use at a frequency of 350 MHz, this corresponds to  $\epsilon_r = 66 - j225.6$ . By comparison, for muscle, skin, and tissues with high water content,  $\epsilon_r = 88 - j250$  at 50 MHz [4]. Because of the relative closeness of the two dielectric constants, the mixture of this composition was used to fill the figurine-shaped cavity for experiments in the parallel-plate radiation chamber.<sup>7</sup> Temperature under irradiation was recorded using the liquid-crystal temperature probe [8]. From the increase in temperature, the absorbed power density in milliwatts/gram was calculated from the relationship [7]  $(4180 \times \text{temperature increase})/\text{irradiation time in seconds}$ . The absorption coefficient  $\alpha$ ,<sup>8</sup> defined as milliwatts/gram of absorbed power/milliwatts/square centimeter of incident field intensity for various parts of the body, has been calculated and is given in Table II. For  $E \parallel \hat{L}$  orientation, the strongest intensity of power deposition is observed in the neck area of the body. For the density of power absorption this is followed by the shins, the thighs, the chest, the eyes, and the pudendal region, in that order. In Fig. 7 the thermographic record of the temperature before and after 1 min of free-space irradiation with a field intensity of 100 mW/cm<sup>2</sup> at 710 MHz is shown. The pattern of power deposition bears a remarkable resemblance to the distribution obtained in the parallel-plate radiation chamber.

In order to obtain a quantitative information on the power deposition under free-space irradiation conditions, a 12.1-cm resonant-size ( $L/\lambda \approx 0.4$ ) figurine was used at 985 MHz.<sup>9</sup> A field intensity of 100 mW/cm<sup>2</sup> was used to

<sup>7</sup> For free-space irradiation experiments, the composition of the material used is 9.25 percent NaCl, 8.25 percent Superstuff, and 82.5 percent water. This mixture, having a measured dielectric constant of 66 and a conductivity of 10.09 mho/m, corresponds to a complex relative permittivity  $\epsilon_r$  of 66 - j255 when used at 710 MHz.

<sup>8</sup> The parameters  $S$  and  $\alpha$  are related in that  $S = (\alpha \times \text{weight of the body})/(\text{shadow area of the body})$ . For animals and other bodies of irregular shape,  $S$  is a more difficult parameter to calculate because of the difficulty in evaluating the shadow area of these bodies.

<sup>9</sup> E. L. Hunt of the Department of Microwave Research, Walter Reed Army Institute of Research, Washington, D. C., participated in these experiments.

TABLE II  
MEASURED DISTRIBUTION OF POWER DEPOSITION IN AN 18.4-CM-TALL  
BIOLOGICAL-PHANTOM HUMAN FIGURINE (PARALLEL-PLATE  
WAVEGUIDE RADIATION CHAMBER)

Frequency MHz	$\alpha/L$	$\alpha_{\text{Neck}}$	$\alpha_{\text{Shin}}$	$\alpha_{\text{Eyes}}$	$\alpha_{\text{Pudendal}}^*$ Region
$\hat{E} \parallel \hat{L}$ orientation					
230	0.141	2.895			
240	0.147	3.381	0.788		0.155
270	0.166		1.927		
300	0.184	5.097	2.256	0.840	0.442
320	0.196	5.367			
350	0.215	6.761	1.863		
380	0.233		4.368	1.148	
395	0.242	6.153			
$\hat{E} \parallel \hat{k}$ orientation					
395	0.242	0.094			
$\hat{H} \parallel \hat{L}$ orientation					
100	0.184	0.130			

Note: Symbols with arrows above are represented by boldface italic in text.

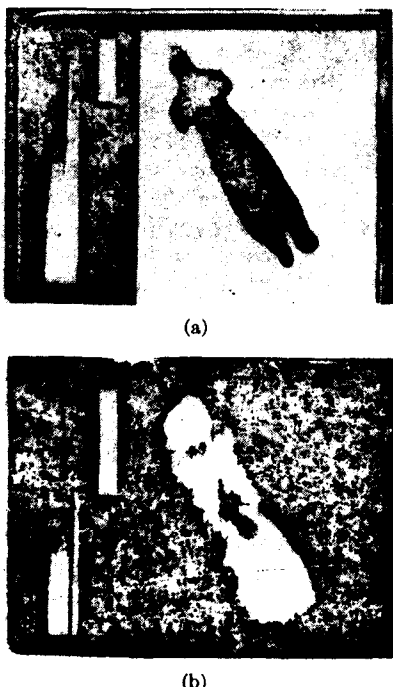


Fig. 7. The thermographic recording of the central section of an 18.4-cm biological-phantom figurine before and after free-space plane-wave irradiation for 1 min at 100 mW/cm<sup>2</sup> at 710 MHz ( $L/\lambda \sim 0.44$ ). (a) Before exposure to radiation, 8.5°C baseline; 3°C full scale. (b) After irradiation in the  $E \parallel L$  configuration; waves incident on the front side of the body, 6°C baseline; 10°C full scale.

speed up the heating process and thus reduce the heat diffusion to cooler areas of the body. Temperature under irradiation was recorded using the liquid-crystal temperature probe. Due to the extremely large energy deposition

rate for the neck region, exposure times on the order of 5 s were used when measuring temperature increases for this part of the body. Irradiation times of 10–20 s were used for measurements in other parts of the body. The measured rates of temperature rise are used to calculate the  $\alpha$ 's for various parts of the body in a 1.75-m man and these are given in Table III. The patterns of power deposition obtained from both the parallel-plate waveguide radiation chamber and free-space irradiation are very similar. For the  $E \parallel \hat{L}$  resonance condition, the very maximum power deposition is observed for the neck region of the body. Under both free-space and parallel-plate waveguide irradiation conditions, an  $\alpha$  parameter of approximately 20 times the whole-body average is observed for the neck region of the body.

A point of concern is the much lower values observed in the parallel-plate radiation chamber as compared to the values measured under free-space irradiation. This may be seen by comparing the values in Table II to those of column 3 of Table III. The fact that a larger scaling factor  $\beta$  is used for the 12.1-cm figurine than for the 18.4-cm figurine should account only for a factor of 1.52 in going from Table II to Table III. Somewhat reduced values in Table II will also be expected because of lower field intensities and the resultant heat diffusion, particularly from hot spots. In order to create a more satisfactory representation of the real-life ground effects, a monopole-above-ground radiation has been designed and is currently under construction at our laboratory. The new radiation chamber is sketched in Fig. 8. The radiator consists of a 45° corner reflector in conjunction with a quarter-wave monopole above ground. The gain of such an antenna has been calculated [10] and is tabulated in Table IV. For the antenna-to-corner spacing of 0.65  $\lambda$ , the calculated radiation pattern of the antenna system is plotted in Fig. 9. The field intensity at a far-field distance of 6 ft for 350 W of radiated power may be as high as 60 mW/cm<sup>2</sup>. Such field intensities are adequate for the planned experiments. The radiation chamber is being constructed with the provision for alterations for use at different frequencies in the 300–1000-MHz band. Such a radiation chamber is not easily amenable to wide-band whole-body absorption measurements such as have been possible in the parallel-plate transmission line using a network analyzer. The monopole-above-ground radiation chamber will, however, offer a real-life simulation of ground effects on EM power absorption in man and animals.

A significant result of the experiments with biological-phantom figurines is that a high power deposition in the neck region is observed. Power absorption coefficient  $\alpha = 6.76$  for the neck region for  $E \parallel \hat{L}$  orientation is over 17 times larger than the average value for saline-filled prolate spheroids of the same overall dimension (see Table V for whole body or average  $\alpha$  for a 19-cm saline-filled prolate spheroid at different frequencies). For  $k \parallel \hat{L}$  and  $H \parallel \hat{L}$  orientations, the rate of heating is minimal (Table II) and this, for the neck region, is a factor of 40 to 50 times smaller than the rate for the  $E \parallel L$  configuration. For these orientations the results once again are in agree-

**TABLE III**  
**RATES OF ENERGY DEPOSITION IN VARIOUS PARTS OF THE BODY**  
**MEASURED DATA AND PROJECTED RATES OF ENERGY DEPOSITION IN A 1.75-M MAN**

Region of the Body	985 MHz Resonant Size (12.1 cm; $L = 0.4 \lambda$ ) Biological-Phantom Figurine		1.75 m Man, 67.9 MHz		
	Rate of Temperature Increase at 100 mW/cm <sup>2</sup> °C/Min.	$\alpha$ (W/kg)/(mW/cm <sup>2</sup> )	$\alpha$ (W/kg)/(mW/cm <sup>2</sup> )	Rate of Energy Deposition	
				For Incident Fields of 10 mW/cm <sup>2</sup> W/kg	For Incident Fields of 50 mW/cm <sup>2</sup> W/kg
<b>Neck:</b>					
Upper part	128.3	89.38	6.16	61.67	308.10
Lower part*	65.2	45.42	3.13	31.31	156.57
Shins	9.5	6.62	0.46	4.56	22.80
Thighs	10.8	7.52	0.52	5.19	25.95
Chest	6.64	6.02	0.41	4.15	20.75
Pudendal Region	3.2	2.23	0.15	1.54	7.7
Eyes	0.9	0.63	0.043	0.43	2.15
Arms	?	?	?	?	?

Note:  $E \parallel \hat{L}$  resonance condition ( $L/\lambda = 0.4$ ).

\* The rate of temperature rise for the lower part of the neck is considerably lower because of its vicinity close to the torso which provides a large heat drain.

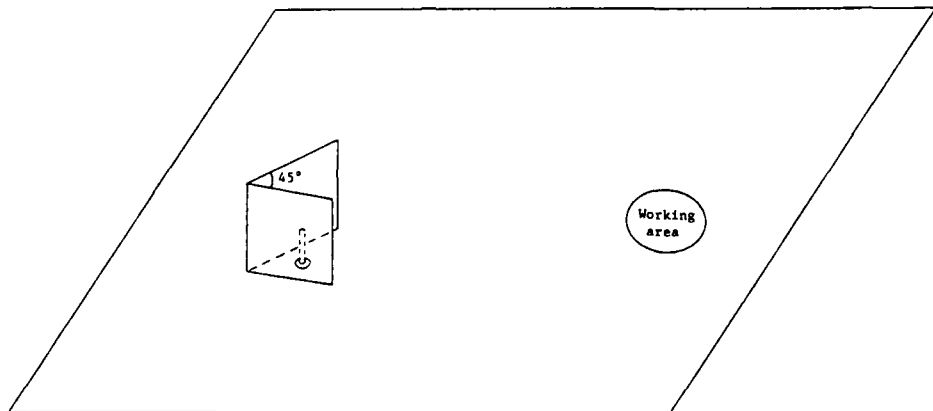


Fig. 8. A monopole antenna in a 45° corner reflector.

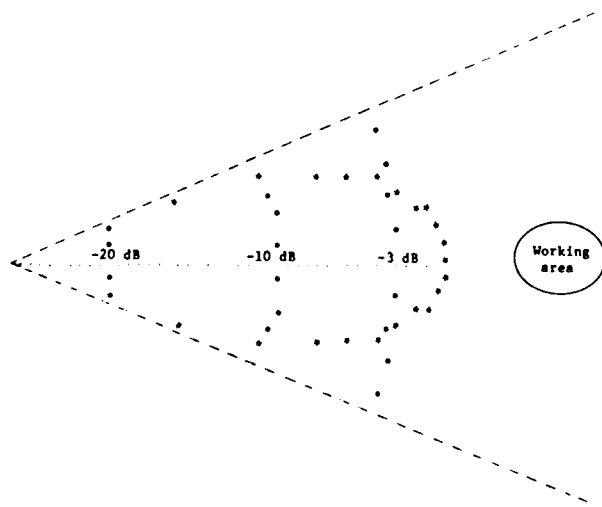


Fig. 9. Calculated radiation pattern at the ground plane of a monopole in a 45° corner reflector.

**TABLE IV**  
**CALCULATED FIELD INTENSITIES DUE TO A QUARTER-WAVE MONPOLE IN A 45° CORNER REFLECTOR**

$\frac{R}{\lambda}$	Driving Power Impedance Ohms	Calculated Gain of the Antenna	Field Intensity at R = 6 feet mW/cm <sup>2</sup>
0.55	$16 + j56.5$	75	62.4
0.6	$23.5 + j64.6$	79.3	66.0
0.65	$32 + j65.0$	82.7	68.9
0.7	$47.5 + j61.4$	73.1	60.9
0.75	$59.5 + j59.7$	70.87	59.0

Note: Transmitter Power = 350 W.

TABLE V  
ABSORPTION PARAMETER  $\alpha$  OF A 19-CM SALINE-FILLED PROLATE SPHEROID AS A FUNCTION OF FREQUENCY

Frequency MHz	Number of Measurements	$L/\lambda$	$\alpha$ (average)
240	1	0.152	.2945
260	3	0.165	.3097
300	3	0.190	.3989
320	2	0.203	.3214
360	3	0.229	.4089
380	4	0.241	.4908
395	6	0.251	.3786

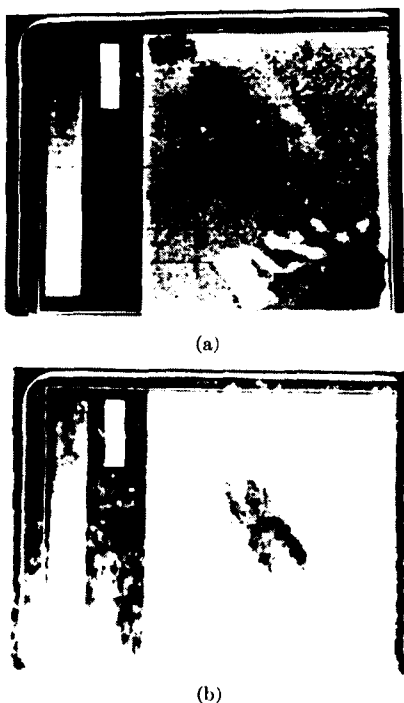
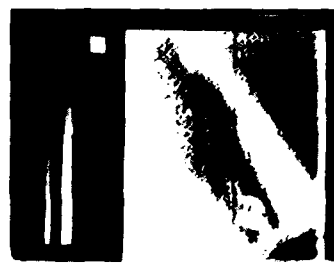


Fig. 10. Thermographic recording of the central section of an 18.4-cm biological-phantom figurine; free-space irradiation of 710 MHz (temperature of the body before irradiation  $\sim 7$  °C). (a) After irradiation in the  $E \parallel L$  configuration for 10 min at 100 mW/cm<sup>2</sup>; baseline 8°C; 3°C full scale. (b) After irradiation in the  $H \parallel L$  configuration for 10 min at 100 mW/cm<sup>2</sup>; baseline 8°C; 3°C full scale.

ment with those obtained from free-space irradiation. For up to 10 min of exposure to 710-MHz free-space fields of intensity 100 mW/cm<sup>2</sup>, negligible modifications of the temperature pattern were observed, and this is illustrated in Fig. 10.

The thermographic record of the temperature before and after 1 min of free-space irradiation ( $E \parallel L$  orientation) at 2450 MHz is shown in Fig. 11. Maximum heating at 2450 MHz ( $L/\lambda = 1.5$ ), approximately 3.75 times the resonant frequency, is still observed in the neck, the arms, and the legs. As expected, the temperature rise is considerably lower than that for 710-MHz radiation. Also, the torso is heated hardly at all, which is a feature distinct from the power distribution at the resonant frequency of 710 MHz (Fig. 7). The quantitative values of  $\alpha$  measured with



(a)



(b)

Fig. 11. The thermographic recordings of the central section of an 18.4-cm biological-phantom figurine before and after free-space plane-wave irradiation for 1 min at 100 mW/cm<sup>2</sup> at 2450 MHz ( $L/\lambda = 1.50$ ). (a) Before exposure to radiation, 8.6°C baseline, 1°C full scale. (b) After irradiation in the  $E \parallel L$  configuration; waves incident on the front side of the body; 10°C black level; 1°C full scale.

the liquid-crystal temperature probe for a somewhat smaller size figurine are given in Table VI. The hottest parts of the body are the neck, the legs, and the arms.

The large power deposition observed in the neck region of the figurines has prompted us to look for similar effects in animals. Initial measurements<sup>10</sup> conducted with the liquid-crystal probe implanted subcutaneously in the neck region of anesthetized 388-g long Evans rats have shown  $\alpha = 0.479$  at 360 MHz as against  $\alpha = 0.38$  for the deep rectal region. For dead animals, on the other hand, the corresponding numbers are  $\alpha = 0.855$  for the neck region and  $\alpha = 0.231$  for the core of the animal. Further experiments are currently in progress to ascertain the nature of neck heating and its biological implications. Since reports in the literature suggest that continued low-level exposure to microwave irradiation in both humans [11] and animals [12] produces fatigue and hypoactivity, the possibility exists that this may be linked to the heating in the neck region. The heating in the neck area may produce changes in circulating blood hormones such as thyroxine. In future experiments, blood thyroxine levels will be examined by serum thyroxine and protein-bound iodine-level assay techniques.

## SUMMARY

The RF power deposition is found to vary significantly with orientation and with frequency. The strongest absorption is found for waves polarized along the long di-

<sup>10</sup> These experiments are being performed by J. D'Andrea of our laboratory.

TABLE VI  
 $E \parallel \hat{L}$ , OFF-RESONANCE CONDITION ( $L/\lambda = 0.985$ )  
 MEASURED DATA AND PROJECTED RATES OF ENERGY DEPOSITION IN A 1.75-M MAN

Region of the Body	2450 MHz 12.1 cm Biological-Phantom Figurine $L/\lambda = 0.985$			1.75 m Man, 169 MHz		
	Rate of Temperature Increase at 100 mW/cm <sup>2</sup>		(W/kg)/(mW/cm <sup>2</sup> )	Rate of Energy Deposition		Fields of 10 mW/cm <sup>2</sup> W/km
	*°C/Min	(W/kg)/(mW/cm <sup>2</sup> )		For Incident	For Incident	
Neck	5.6	3.90	0.17	2.69	13.45	
Shins	4.6	3.20	0.22	2.21	11.05	
Arms	3.05	2.12	0.15	1.46	7.30	
Thighs	2.05	1.43	0.1	0.99	4.95	
Chest	1.2	0.84	0.06	0.58	2.9	
Elves	0.425	0.3	0.02	0.21	1.05	
Groin	0.2	0.14	0.01	0.1	0.5	

mension of bodies at frequencies such that the major length is approximately 0.4 times the wavelength of radiation for bodies in free space. Peak absorption, in the presence of ground effects, is observed at frequencies about one-half as much as bodies isolated in free space. A significant result of the experiments with biological-phantom figurines is that a high rate of energy deposition is observed for the neck region. Power absorption coefficient  $\alpha$  for the neck region for  $E \parallel \hat{L}$  orientation is about 20 times larger than the whole-body average. This may be biologically significant and is being investigated further. Initial experiments with anesthetized and dead rats have indeed demonstrated a higher power deposition in the neck region than in the core of the animals. For figurines for  $k \parallel \hat{L}$  and  $H \parallel \hat{L}$  orientations, the rate of heating is minimal, and for the neck region is a factor of 40 to 50 times smaller than the rate for the  $E \parallel \hat{L}$  resonance condition. The frequencies of maximum absorption for adult humans is projected to be on the order of 65–75 MHz for free-space conditions and about half as much in the presence of ground effects.

#### ACKNOWLEDGMENT

The author wishes to thank E. L. Hunt who participated in parts of this work. The assistance of P. Brown and D. Hawkins of the Walter Reed Army Institute of Research is gratefully acknowledged. The author has also enjoyed the support of his students, in particular, J. D'Andrea, G. Beck, and T. Gustafson, in several facets of this work. The experiments with free-space irradiation were performed in the anechoic chambers at the Department of

Microwave Research, Walter Reed Army Institute of Research, Washington, D. C.

#### REFERENCES

- [1] O. P. Gandhi, "Polarization and frequency effects on whole animal absorption of RF energy," *Proc. IEEE (Lett.)*, vol. 62, pp. 1171–1175, Aug. 1974.
- [2] —, "Strongest dependence of whole animal absorption on polarization and frequency of radio-frequency energy," *Ann. N. Y. Acad. Sci.*, vol. 247, pp. 532–538, Feb. 1975.
- [3] C. H. Durney, C. C. Johnson, and H. Massoudi, "Long-wavelength analysis of plane wave irradiation of a prolate spheroid model of man," *IEEE Trans. Microwave Theory Tech.*, vol. MTT-23, pp. 246–253, Feb. 1975.
- [4] C. C. Johnson and A. W. Guy, "Nonionizing electromagnetic wave effects in biological materials and systems," *Proc. IEEE*, vol. 60, pp. 692–718, June 1972.
- [5] T. B. A. Senior and R. F. Goodrich, "Scattering by a sphere," *Proc. Inst. Elec. Enq.*, vol. 111, pp. 907–916, 1964.
- [6] J. Schrot, T. D. Hawkins, and S. H. Githens, "Microwave frequency and E-field orientation interact with animal size," presented at the 1975 USNC/URSI-IEEE Conf., Boulder, Colo., Oct. 20–23, 1975.
- [7] A. Anne, M. Saito, O. M. Salati, and H. P. Schwart, "Relative microwave absorption cross sections of biological significance," in *Biological Effects of Microwave Radiation*, vol. 1. New York: Plenum, 1960, pp. 153–177.
- [8] T. C. Rozzell, C. C. Johnson, C. H. Durney, J. L. Lords, and R. G. Olsen, "A nonperturbing temperature sensor for measurements in electromagnetic fields," *J. Microwave Power*, vol. 9, pp. 241–249, Sept. 1974.
- [9] A. W. Guy, C. C. Johnson, J. C. Lin, A. F. Emery, and K. K. Kranning, "Electromagnetic power deposition in man exposed to HF fields and the associated thermal and physiologic consequences," USAF School of Aerospace Medicine, Brooks Air Force Base, Tex. Rep. SAM-TR-73-13, Dec. 1973.
- [10] O. P. Gandhi, "A computer program for calculating the radiation pattern of a general antenna array," *IEEE Trans. Educ. (Corresp.)*, vol. E-17, pp. 124–126, May 1974.
- [11] C. Silverman, "Nervous and behavioral effects of microwave radiation in humans," *J. Epidemiology*, vol. 97, pp. 21–224, Apr. 1973.
- [12] S. F. Korbel, "Behavioral effects of low intensity UHF radiation," in *Proc. 1969 Symp. Biological Effects and Health Implications of Microwave Radiation*, Sept. 17–19, 1969.

## APPENDIX B

804

IEEE TRANSACTIONS ON MICROWAVE THEORY AND TECHNIQUES, VOL. MTT-27, NO. 9, SEPTEMBER 1979

# Numerical Calculation of Electromagnetic Energy Deposition for a Realistic Model of Man

MARK J. HAGMANN, MEMBER, IEEE, OM P. GANDHI, FELLOW, IEEE, AND CARL H. DURNEY,  
MEMBER, IEEE

**Abstract**—Numerical calculations of absorbed energy deposition have been made for a block model of man that is defined with careful attention given to the biometric and anatomical features of a human being. Calculated post-resonant absorption and distribution of energy deposition through the body have better agreement with experimental results than previous calculations made using less realistic models.

Manuscript received September 18, 1978, revised April 9, 1979.  
The authors are with the Departments of Electrical Engineering and Bioengineering, University of Utah, Salt Lake City, UT 84112.

### I. INTRODUCTION

WE HAVE used numerical methods with a realistic model to calculate the deposition of electromagnetic energy in man. A block model of man was chosen to allow maximum freedom in defining both the shape and content of the model. We have used the moment-method solution of the electric-field integral equation with a pulse function basis and delta functions for testing [1], [2]. The

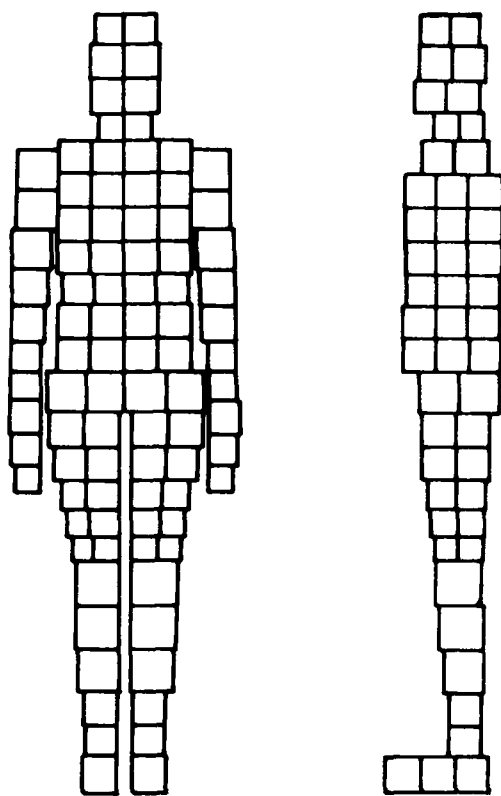


Fig. 1. Improved model of man.

following sections of this paper contain brief descriptions of the improved model and numerical methods, as well as a comparison of the calculations with other numerical and experimental results.

## II. DESCRIPTION OF THE MODEL

We have given careful attention to biometric and anatomical diagrams in defining the shape and content of a model having improved realism. A total of 180 cubical cells of various sizes was used to obtain a best fit of the contour on diagrams of the 50th percentile standard man [3]. Sizes and placement of the cells are shown in Fig. 1. Height of the model is 1.75 m.

Partitioning of bone, fat, skin, muscle, lung tissue, air, heart, brain, kidney, liver, and spleen through the cells was done with the aid of anatomical cross sections [4], [5]. Whole-body volume fractions of each tissue type are in agreement with published values. The volume-weighted complex permittivity of each cell was found using properties reported in the literature [6]–[8].

We have forced a plane of symmetry between the left and right body halves in selecting the size, placement, and volume-weighted complex permittivities of the cells. The symmetry has been utilized so that the size of the matrix used in the numerical solutions is determined by 90 cells rather than the total of 180 cells. The symmetry may only

be utilized for incident fields in which both  $E$  and  $k$  are contained in the plane of symmetry.

## III. SOLUTION OF THE MATRIX EQUATION

Since one plane of symmetry is used and there are three unknown field components in each cell, the matrix is 270 by 270 complex, which corresponds to a system of 540 simultaneous equations in 540 real unknowns. Solution of the matrix equation is complicated by the matrix being both full and asymmetric. Utilizing symmetry, or cells having different sizes or permittivities, would each be sufficient to destroy symmetry of the matrix.

We have used the successive overrelaxation (SOR) method [9] for iterative solution of the matrix equation. It is known that a matrix having at least one complex eigenvalue, as in the present case, will not allow convergence with SOR unless all eigenvalues have real parts with magnitudes less than unity. Convergence of SOR has the further restriction that the relaxation parameter must be less than a critical value that depends upon the matrix [9]. We have found that convergence with SOR requires a relaxation factor less than unity at 10 MHz, and the critical value decreases with increasing frequency until it reaches zero near 90 MHz. Convergence with SOR is not possible at frequencies exceeding 90 MHz with the present model of man, so we have been forced to use Gauss-Jordan and other noniterative methods [10]. In the present problem when SOR may be used in place of noniterative methods, the computer time is typically reduced by about a factor of four.

We have ordered numbering of cells in the model in such a way that the difference between the numbers for two cells is an increasing function of the distance between the cells. We have formed the matrix using an array of  $3 \times 3$  blocks for each cell pair which is inside-out from the structure used previously [11]. The two changes just described have caused the matrix to have a rapid decrease in magnitude of the elements with increasing distance from the diagonal. For all frequencies used so far with the realistic model of man (10–600 MHz), the only matrix elements having appreciable magnitude are contained in a band about the diagonal, which amounts to approximately 10 percent of the entire matrix. The approximation of forced banding may be applied to such a matrix to allow either a large reduction in cost of computations or a significant increase in number of cells [12]. We have not yet implemented forced banding, but we estimate that the method will allow enough cells so that reliable calculations may be made for a realistic model of man to frequencies as high as 2450 MHz.

## IV. CONVERGENCE CONSIDERATIONS

Numerical solutions using a pulse function basis can only be exact if there is no variation of  $E$  within each cell of the model. Solutions having large differences in calculated energy deposition for adjacent cells must have signi-

fificant variation of  $\vec{E}$  within the cells, which suggests lack of convergence. Previously reported solutions for block models of man have a ratio of 239:1 for energy deposition in one pair of adjacent cells at 10 MHz [1]. The arrangement and different sizes of cells in the present model cause the maximal ratio of energy deposition for a pair of adjacent cells to be 8:1 at the same frequency.

If  $\Delta$  is the side of a cubical cell and  $k$  represents the magnitude of the complex propagation vector within the cell, then substantial variation of the electric field must occur within the cell if  $k\Delta \approx \lambda/6$  [13]. Thus the pulse function approximation may not be justified at frequencies above 200 MHz with the new model, suggesting an increasing error at higher frequencies. Volume-weighting of the complex permittivity within each cell may also be unjustified at frequencies above 200 MHz though the results appear reasonable to at least 500 MHz.

A numerical solution using a pulse function basis results in a single value representing  $\vec{E}$  within each cell. It is possible to use the  $E$  values to calculate  $1/2\sigma\vec{E}\cdot\vec{E}^*$  for each cell, and to use a volume average to estimate the specific absorption rate (SAR). Large numbers of cells must be used in order to find accurate values of SAR by such a procedure. For example, our calculations of the SAR of a 12-cm muscle cube at 1 MHz show an error of 37 percent with 8 cells, 26 percent with 27 cells, and 20 percent with 64 cells. The delta functions used for testing enforce the integral equation at the center of each cell so that the calculated  $\vec{E}$  values are most representative of the cell centers. Inspection of the solutions suggests that the local values of  $\vec{E}$  have appreciably less error than occurs in the SAR.

If there is much variation of  $\vec{E}$  within a scattering body, then even if we had exact values of  $\vec{E}$  at the cell centers, appreciable error would be expected in the calculated SAR. The  $N$ , supposedly exact, local values of energy deposition constitute samples of an otherwise unknown population so that if large cell-to-cell variation is present, statistical procedures may be used to calculate confidence limits for values of whole-body or part-body SAR [14]. For man at 80 MHz with  $E \parallel \vec{I}$  and  $k$  front-to-back, the 80-percent confidence limits for whole-body SAR are  $\pm 12.2$  percent of the mean for the realistic model of man, and  $\pm 14.9$  percent of the mean for calculations reported earlier having somewhat greater cell-to-cell variation [1].

We have found that accuracy is improved by using a three-dimensional interpolant with the  $E$  values initially calculated for each cell to account for some of the variation of  $\vec{E}$  within each cell [15]. Triangular and triquadratic interpolants have both been used to estimate the variation of  $\vec{E}$  between the cell centers. The interpolant is integrated in calculating the SAR. For the 12-cm muscle cube at 1 MHz, the SAR found with 27 cells and the triquadratic interpolant have error comparable with the calculation based on 64 cells without the interpolant. The increase in cost due to use of the interpolant is about 1 percent. All

values of energy absorption in this paper have been calculated using interpolants.

## V. COMPARISON OF CALCULATIONS WITH OTHER RESULTS

Fig. 2 shows the values of whole-body SAR calculated for man in free space with  $E \parallel \vec{I}$  and an incident intensity of 1 mW/cm<sup>2</sup>. Points on Fig. 2 represent the results of numerical solutions for the realistic model of man, both with and without the use of an interpolant. The homogeneous approximation of two-thirds the complex permittivity of muscle was used in all calculations for the figure. It is seen in Fig. 2 that the fractional correction which is made by the interpolant increases at high frequencies where increasing error is expected.

Values of whole-body SAR below resonance in Fig. 2 are typically within 10 percent of values calculated for prolate-spheroidal and ellipsoidal models using the same homogeneous approximation of complex permittivity [16]. Experimental results have shown that the SAR for  $E$  polarization is inversely proportional to frequency for frequencies from about 1 to 6 times that of resonance [17], [18]. For small animals, such as the rat, the high value of the resonant frequency allows a reduced magnitude for the relative permittivity of tissue so that post-resonant calculations for prolate-spheroidal models may be made using the extended boundary condition method [16]. Such results show the experimentally observed  $1/f$  behavior, but the calculations there cannot be directly applied to man. A  $1/f$  dependence of the post-resonant SAR is also expected from antenna theory. The anticipated  $1/f$  post-resonant behavior is evident in Fig. 2. Further numerical solutions suggested a significantly faster roll off between  $f^{-1/3}$  and  $f^{-1/4}$  [1].

Fig. 3 also shows the whole-body SAR of man in free space with  $E \parallel \vec{I}$  and an incident intensity of 1 mW/cm<sup>2</sup>. The solid curve in Fig. 3 was obtained by splining the 20 values obtained in numerical solutions for the homogeneous realistic model of man. Points on Fig. 3 represent experimental values obtained for human-shaped figurines filled with saline or biological phantom mixtures [17], [18]. The numerical solutions suggest that the resonant frequency is 77 MHz which is somewhat higher than the value of 68–71 MHz determined experimentally.

An important contribution that can be expected from numerical solutions for a realistic model of man is the distribution of energy deposition through the model. Prolate-spheroidal and ellipsoidal models cannot be expected to provide an accurate description of the distribution of energy deposition since the distribution is strongly dependent upon detailed geometry. When the homogeneous approximation of complex permittivity is used, the distribution of energy deposition in the realistic model of man is in good agreement with that found experimentally for homogeneous models [17], [18]. Table I contains numerical and experimental values for the distribution of energy

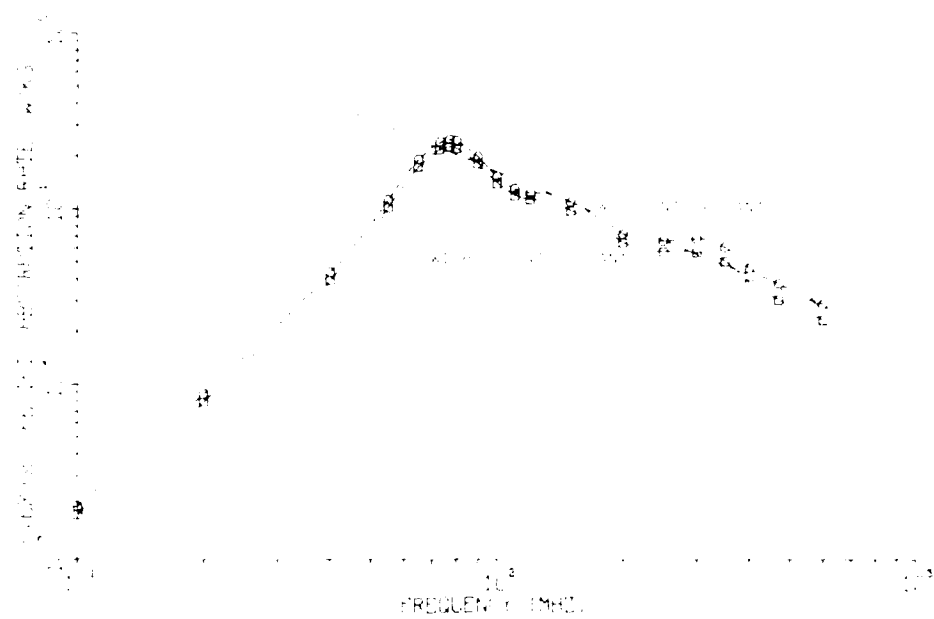


Fig. 2. Whole-body SAR for homogeneous model of man in free space.  $E/E_0 k$  front-to-back  
incident intensity = 1 mW/cm<sup>2</sup>.

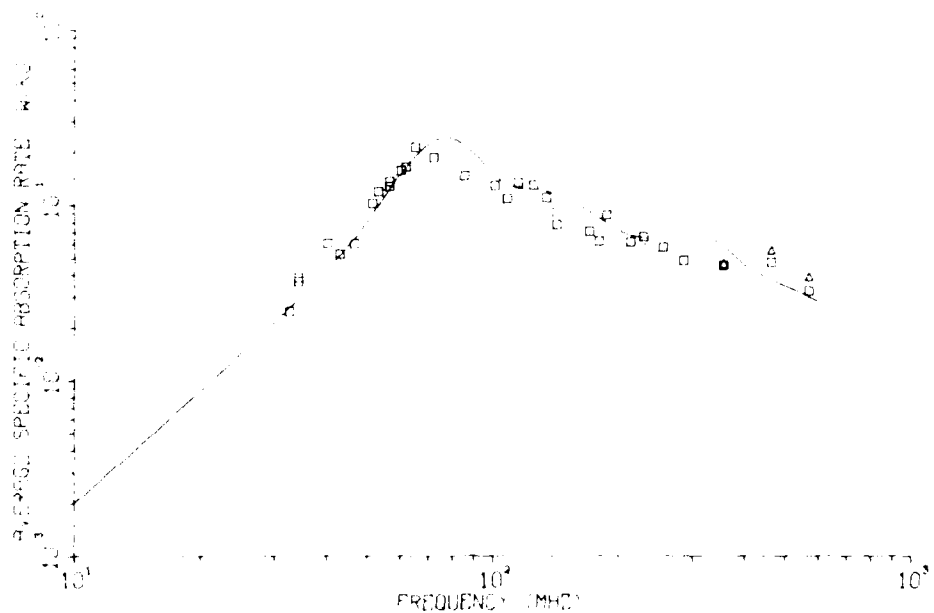


Fig. 3. Whole-body SAR for homogeneous model of man in free space.  $E/E_0 k$  front-to-back,  
incident intensity = 1 mW/cm<sup>2</sup>. Squares represent experimental points for saline-filled figurines.  
Triangles represent experimental values for figurines containing biological phantom mixtures.

TABLE I  
DISTRIBUTION OF ENERGY DEPOSITION FOR MAN NEAR RESONANCE IN FREE SPACE<sup>1</sup>

Region	Front Layer	Middle Layer	Back Layer
Head	1.0	1.0	1.0
Neck	1.0	1.0	1.0
Trunk	1.0	1.0	1.0
Arms	1.0	1.0	1.0
Legs	1.0	1.0	1.0
Total	1.0	1.0	1.0

<sup>1</sup>All values are in units watts per kilogram ( $\text{W}/\text{kg}$ ) for incident intensity of  $1 \text{ mW/cm}^2$ ;  $F = 1$ , front-to-back.

<sup>2</sup>Phantom models of man [Gandhi *et al.*, 1975].

<sup>3</sup>[Chen *et al.*, 1977].

<sup>4</sup>Calculations for a realistic model of man by the authors.

<sup>5</sup>Commercial dolls used as forms for the phantoms are thought to have exaggerated neck constriction. Neck heating for the dolls is about ten times that of the expected for man.

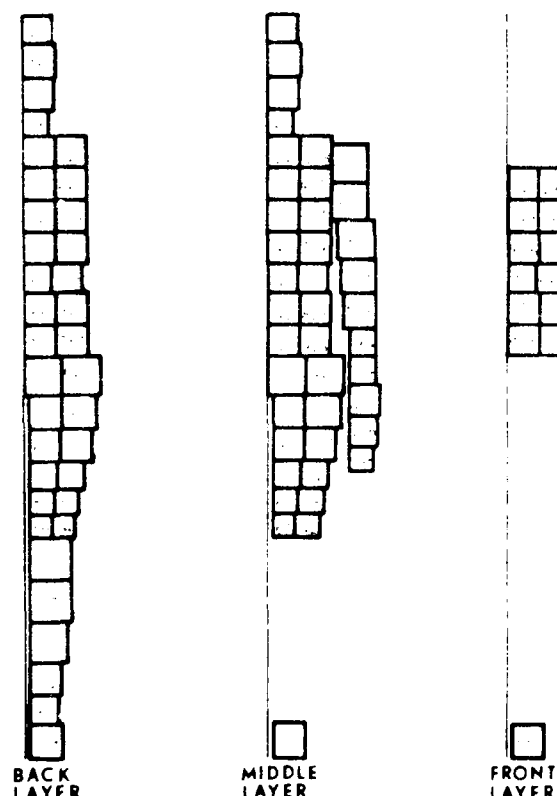


Fig. 4. Local SAR values ( $\text{watts}/\text{kg}$  per  $\text{mW}/(\text{cm}^2)$ )  $\times 100$  for homogeneous model of man with vertical polarization at 80 MHz.

deposition for man near resonance in free space. The deposition of energy in the regions of the eye, heart, thigh, and calf has been severely underestimated in previous calculations made with less realistic models [1], [11].

When the inhomogeneous complex permittivities are used with the model, a change of less than 2 percent typically occurs in the whole-body average SAR, but the distribution of energy deposition is changed. Figs. 4 and

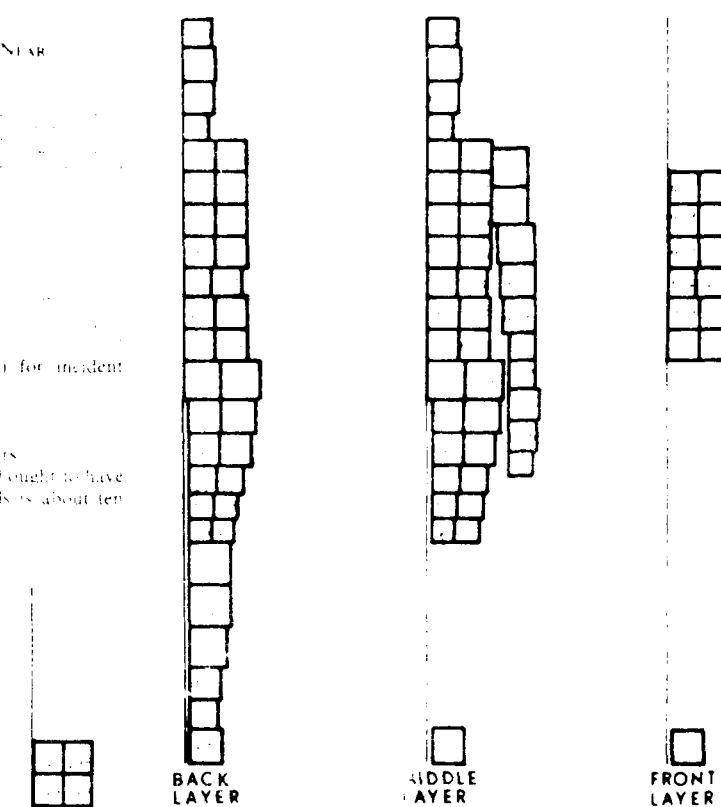


Fig. 5. Local SAR values ( $\text{watts}/\text{kg}$  per  $\text{mW}/(\text{cm}^2)$ )  $\times 100$  for inhomogeneous model of man with vertical polarization at 80 MHz.

5 illustrate the distribution of absorbed energy in man at 80 MHz in free space for the homogeneous and inhomogeneous models, respectively. One difference is that the inhomogeneous model has reduced absorption in regions with high bone content. Earlier workers have not reported results for inhomogeneous models having a cell-by-cell representation of the dielectric properties.

## VI. CONCLUSIONS

Numerical calculations of absorbed energy deposition have been made for a model of man that has been made with careful attention to both biometric and anatomical diagrams. A total of 180 cells was used in the model, which is a relatively large number for numerical solutions but facilitates accurate modeling.

Calculated post-resonant absorption and distribution of energy deposition through the body have been found to have better agreement with experimental results than previous calculations made using less realistic models.

## ACKNOWLEDGMENT

The authors wish to thank Dr. G. W. Hohmann of the Department of Geology and Geophysics at the University of Utah, Salt Lake City, for use of his computer program which was the starting point for the numerical methods used in the current work.

## REFERENCES

- [1] K. M. Chen and B. S. Guru, "Induced EM field and absorbed power density inside human torsos by 1 to 500 MHz EM waves," Tech. Rep. no. 1, under NSF Grant ENG 74-12603, 1976.
- [2] G. W. Hohmann, "Three-dimensional polarization and electromagnetic modeling," *Geophys.*, vol. 40, pp. 309-324, 1975.
- [3] N. Diffring, A. R. Iliev, and J. C. Bardagy, *Humaniele I, 2, 3*, Cambridge, MA: MIT Press, 1974.
- [4] D. J. Morton, *Manual of Human Cross Section Anatomy* (2nd edition), Baltimore, MD: Williams and Wilkins, 1944.
- [5] A. C. Eyclesheimer and D. M. Schoenmaker, *Cross-Section Anatomy*, New York: D. Appleton, 1911.
- [6] C. C. Johnson and A. W. Guy, "Nonionizing electromagnetic wave effects in biological materials and systems," *Proc. IEEE*, vol. 60, pp. 692-718, 1972.
- [7] C. C. Johnson, C. H. Durney, and H. Massoudi, "Long wavelength electromagnetic power absorption in prolate spheroidal models of man and animals," *IEEE Trans. Microwave Theory Tech.*, vol. MTT-23, pp. 739-747, 1975.
- [8] H. P. Schwan, "Electrical properties of tissue and cell suspensions," in *Advances in Biological and Medical Physics*, vol. V, J. H. Lawrence and C. A. Tobias, Eds., New York: Academic Press, 1957, pp. 147-209.
- [9] D. M. Young, *Iterative Solution of Large Linear Systems*, New York: Academic, 1971.
- [10] B. Carnahan, H. A. Luther, and J. O. Wilkes, *Applied Numerical Methods*, New York: Wiley, 1969.
- [11] K. M. Chen and B. S. Guru, "Internal EM field and absorbed power density in human torsos induced by 1-500 MHz EM waves," *IEEE Trans. Microwave Theory Tech.*, vol. MTT-25, pp. 746-756, 1977.
- [12] A. J. Poggio and F. K. Miller, "Integral equation solutions of three-dimensional scattering problems," in *Computer Technique for Electromagnetics*, R. Mittra, Ed., New York: Pergamon, 1973, pp. 159-264.
- [13] M. J. Hagmann, O. P. Gandhi, and C. H. Durney, "Upper bound on cell size for moment-method solutions," *IEEE Trans. Microwave Theory Tech.*, vol. MTT-25, pp. 831-832, 1977.
- [14] W. Mendenhall and R. L. Scheaffer, *Mathematical Statistics with Applications*, North Scituate, MA: Duxbury, 1973.
- [15] M. J. Hagmann, O. P. Gandhi, and C. H. Durney, "Improvement of convergence in moment-method solutions by the use of interpolants," *IEEE Trans. Microwave Theory Tech.*, vol. MTT-26, pp. 904-908, 1978.
- [16] C. C. Johnson, C. H. Durney, P. W. Barber, H. Massoudi, S. J. Allen, and J. C. Mitchell, "Radiofrequency radiation dosimetry Handbook," USAF Rep. SAM-TR-76-35, 1976.
- [17] O. P. Gandhi, K. Sedigh, G. S. Beck, and E. L. Hunt, "Distribution of electromagnetic energy deposition in models of man with frequencies near resonance," in *Biological Effects of Electromagnetic Waves, selected papers of the USNC-URSI annual meeting*, Boulder, CO, Oct. 20-23, 1975, vol. II, C. C. Johnson and M. J. Shore, eds.: HEW Publication (FDA) 77-801E, U.S. Government Printing Office, Washington, DC 20402.
- [18] O. P. Gandhi, E. L. Hunt, and J. A. D'Andrea, "Electromagnetic power deposition in man and animals with and without ground and reflector effects," *Radio Sci.*, vol. 12, no. 6(S), pp. 39-47, 1977.

## APPENDIX C

*Radio Science Volume 14, Number 6S, pages 15-21, November-December 1979*

### Part-body and multibody effects on absorption of radio-frequency electromagnetic energy by animals and by models of man

*O. P. Gandhi; M. J. Hagmann, and J. A. D'Andrea*

*Departments of Electrical Engineering and Bioengineering, University of Utah, Salt Lake City, Utah 84112*

(Received November 4, 1977.)

Fine structure in the whole-body resonant curve for radio-frequency energy deposition in man can be attributed to part-body resonances. As for head resonance, which occurs near 350 MHz in man, the absorptive cross section is nearly three times the physical cross section of the head. The arm has a prominent resonance at 150 MHz. Numerical solutions, antenna theory, and experimental results on animals have shown that whole-body energy deposition may be increased by 50 percent or more because of multiple bodies that are strategically located in the field. Empirical equations for SARs are also presented along with test data for several species of laboratory animals. Barbiturate anesthesia is sufficiently disruptive of thermoregulation that  $\Delta T_s$  of colonic temperature yield energy dose values in several mammals that compare quite favorably with those based on whole-body calorimetry.

#### 1. INTRODUCTION

Some of the experimental results on absorption of RF energy that have been obtained from animals and from models of man have recently been evaluated in the light of numerical calculations on an improved model of man [Hagmann *et al.*, 1977]. Two new effects that were predicted by numerical solutions and were confirmed experimentally are part-body resonances and multibody effects. Both are described in this paper for the first time. New empirical equations for the SAR for  $E \parallel L$  orientation are also given along with test data obtained from several vertebrate species.

#### 2. PART-BODY RESONANCES

Figures 1 and 2 show part- and whole-body SARs calculated for the improved model of man at various frequencies in, respectively, free space and in electrical contact with ground, when the vector of the electric field is parallel with the model's long axis ( $E \parallel L$ ) and the direction of propagation ( $k$ ) is from the ventral to dorsal aspect. Fine structure in the whole-body SARs is due to part-body resonances.

In previously reported experiments (with figurines) on whole-body SARs for man, an anomalous increase in the rate of energy deposition was observed in the region of 470 MHz for  $E \parallel L$  and  $k \parallel L$  orientations [Gandhi *et al.*, 1977]. Theoretical studies of a 10-cm isolated spherical model of the human head have shown that its first geometrical resonance occurs near 450 MHz [Jones and Spiegel, 1974]. Our numerical calculations (Figures 1 and 2) for the improved model of man (Figure 3) with  $E \parallel L$  have shown that

resonance of the intact human head occurs at a frequency near 350 MHz. For head resonance, numerical solutions give the  $S$  parameter (ratio of absorptive cross section to physical cross section) of the intact human head as 3.00 for man in free space and 2.66 for man on a ground plane. The magnitude of resonant absorption of the intact human head is sufficient to cause the experimentally observed increase in whole-body SAR. The numerically obtained head-resonance frequency of 350 MHz is in agreement with the experimental data presented in this paper, but is somewhat lower than the 450- to 470-MHz values obtained from earlier experimental data and is also lower than the first geometrical resonance of the 10-cm isolated sphere. Further work is in progress to resolve these differences.

Joines and Spiegel [1974] calculate that the ratio of the absorptive cross section to the physical cross section of the isolated human head is approximately 1.1 at geometrical resonance near 450 MHz and 1.4 at a second resonant peak that occurs near 2.1 GHz, if appropriate allowance is made for the inhomogeneous structure of a multilayered model. The present studies indicate that the magnitude of the geometrical resonance of the intact human head is more than twice that of the isolated human head for either of the previously identified resonances.

Table 1 gives experimental values of SARs of figurines filled with biologically simulating materials with  $k \parallel L$ , propagation from head to toe. For these experiments, accurately scaled figurines, 25.4, 33.0, and 40.6 cm in length, were exposed in free space to radiation at 2450 MHz. The whole-body dose was obtained by a Thermonetics Model 2401-A gradient-layer calorimeter. The heads of the figurines were attached to torsos with a saline-soaked cloth (to maintain conductive contact), which permitted easy

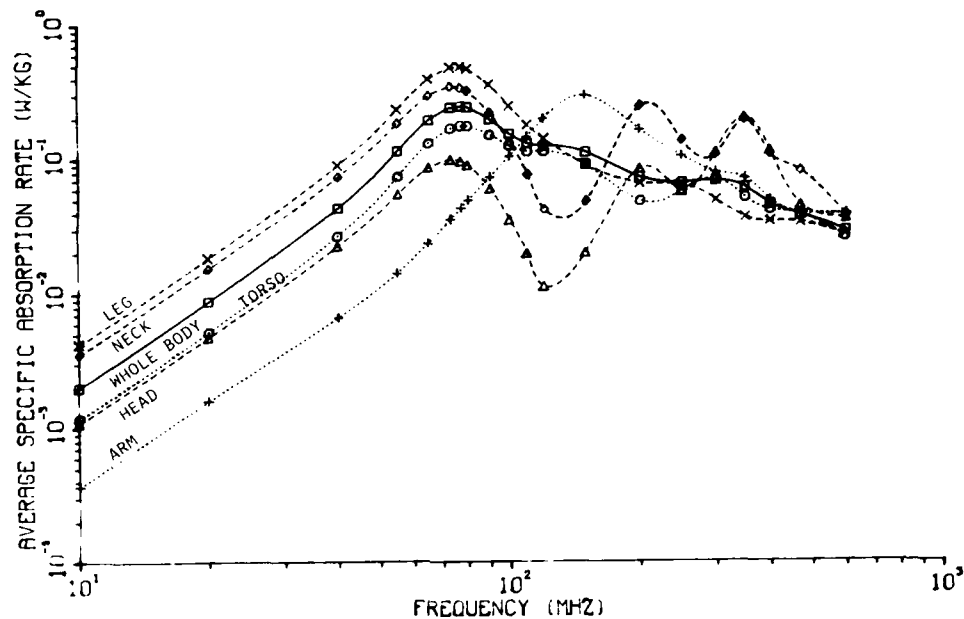


Fig. 1. Part-body SARs for a homogeneous model of man in free space;  $E \hat{H}$ ,  $\mathbf{k}$  ventral to dorsal, incident power density of  $1 \text{ mW cm}^{-2}$ .

separation during subsequent measurements of head SARs. To determine the energy dose in the head after separation, the part of the polyurethane mold that held the biologically simulated head was wrapped in Saran Wrap to prevent heat

loss by evaporation for the duration of its placement in the calorimeter.

We believe that the significance of the head's resonance, as shown in Table 1, should be extended to studies of

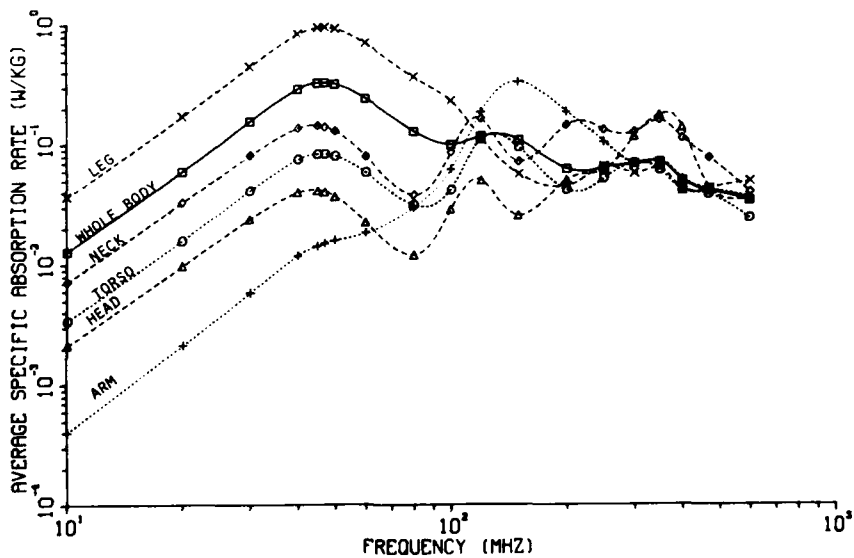


Fig. 2. Part-body SARs for homogeneous model of man in contact with a ground of infinite conductivity,  $E \hat{H}$ ,  $\mathbf{k}$  ventral to dorsal; incident power density of  $1 \text{ mW cm}^{-2}$ .

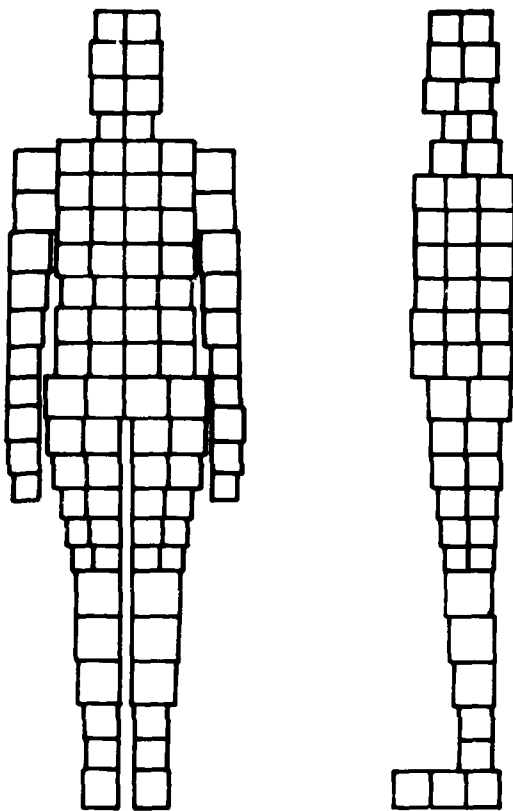


Fig. 3. An improved model of man

animals. For animals with a head similar in size to that of the laboratory rat, resonance is near the commercially significant frequency of 2450 MHz. The head's resonance was not obtained in earlier numerical solutions where the ratio of head to whole-body SAR was reported as 1.07 at 300 MHz and 1.09 at 400 MHz [Chen *et al.*, 1976].

The frequency of maximal energy deposition in the arms is approximately 150 MHz when the arm's length is nearly half a free-space wavelength. At resonance, the arm has an absorptive cross section that is 2.3 times the physical cross section.

### 3. MULTIBODY EFFECTS

It has been shown that the energy absorbed by man at resonance corresponds to the energy received by a half-wave dipole of length approximately equal to the height of the man [Gandhi *et al.*, 1976, 1977]. Antenna theory has been used to calculate the effective area (or gain) per dipole for a pair of thin dipoles in broadside (sagittal) configuration ( $\mathbf{E} \parallel \hat{\mathbf{l}}$ ,  $\mathbf{k}$  perpendicular to the line joining the dipole's centers). Figure 4 gives the variation of effective area as a

function of spacing for half-wave dipoles. Figure 5 gives the variation of effective area as a function of frequency for dipoles of length 1.75 meters at a fixed spacing of 0.65  $\lambda$ . Standard numerical procedures have been used to compute the required values of mutual impedance of dipoles [Baker *et al.*, 1962].

Figure 4 shows that if two thin half-wave dipoles are tangent, each will receive approximately one half the energy it would receive if isolated in free space. For separations greater than two or three free-space wavelengths, the antennas have little coupling so that each has an effective area approximating the isolated free-space value. At a spacing of 0.65  $\lambda$ , each dipole will receive about 50 percent more energy than it would if it were isolated. Figure 5 shows that at a fixed spacing of 0.65  $\lambda$ , two dipoles with lengths of 1.75 meters will have an enhancement of about 50 percent in received energy over a fairly wide band of frequencies rather than only at the frequency for which they are half-wave dipoles. A series of oscillations and then a roll-off are seen at the high-frequency end in Figure 5. Since antenna theory has been shown to predict accurate SARs for human models and for animals with and without nearby reflectors [Gandhi *et al.*, 1977], it is anticipated that the variation of SARs for the  $\mathbf{E} \parallel \hat{\mathbf{l}}$  orientation for near-resonant targets as a function of spacing will be given by the curve of Figure 4. The variation of SAR with frequency for biological targets that are separated a distance of 0.65  $\lambda$  would similarly be given by the curve in Figure 5.

Numerical solutions have been obtained for the multibody effect using the improved model of man [Hagmann *et al.*, 1977]. The solutions have been obtained for the configuration of two men standing side by side having  $\mathbf{E} \parallel \hat{\mathbf{l}}$  and  $\mathbf{k}$  directed ventrally. Lack of symmetry between the left and right sides in each model has necessitated the use of 180 independent cells in the formulation of the matrix. Since there are three unknown field components for each cell, the matrix is 540 by 540 complex, which corresponds to a system of 1080 simultaneous equations in 1080 real unknowns. Total computer time for each multibody problem was 19 hours, 25 minutes with dedicated usage of a PDP-10 digital computer. Weak diagonal dominance, which is inherent in the matrix, contributes to the conditioning to allow reasonable round-off errors with such a large matrix. Noniterative matrix solutions were required for convergence.

The data points in Figure 4 and 5 represent numerical solutions of calculated enhancement in SAR for human models due to two-body effects. The numerical solutions are reasonably consistent with antenna theory for man at resonance as is shown in Figure 4, but significant departure from antenna theory is seen at subresonant frequencies (Figure 5). All calculations based on antenna theory have been zero order; that is, they have no correction for non-sinusoidal current distributions. Significant first- and second-order corrections are required when the antennae

TABLE I. Experimental SAR for  $k/\lambda$  propagation from head to toe. Phantom models of man. Incident power density =  $10 \text{ mW cm}^{-2}$ .

Unmodulated Frequency MHz		Whole-Body Average SAR in $\text{mW/g}$	Average SAR* In $\text{mW/g}$	Percentage of Whole- Body Energy Deposited In the Head	R/SAR Ratio
35.6	E from ventral to dorsal	0.62	1.80	20.6	2.88
	E from arm to arm	0.69	1.50	15.6	2.27
67.3	E from ventral to dorsal	0.57	1.48	20.4	2.59
	E from arm to arm	0.56	1.24	16.9	2.23
569.0	E from ventral to dorsal	0.28	0.75	15.6	1.57
	E from arm to arm	0.39	0.79	17.1	1.78

R/SAR = Ratio of head average SAR (whole-body average SAR).

SAR = absorption coefficient/physical cross section.

\* = These values may be somewhat lower than actual numbers because of a heat loss by convection to the torso.

are not very thin and the half length is much different from  $\lambda/4$  [King, 1956]. Thus, the sizeable lateral extent of the model of man is thought to be responsible for the difference between numerical solutions and antenna theory at low frequencies.

Some asymmetry is present in the distribution of absorbed-energy density between the two body halves in all numerical solutions obtained for the two-body effect. Figure 6 illustrates the calculated local SAR values for one of two models of man when the separation between the models is  $0.65\lambda = 2.53\text{ m}$  at the resonant frequency of 77

MHz. The whole-body SAR is 45.4 percent greater than that for man in free space. In general the body halves closest to each other have somewhat less enhancement than the more distant body halves, but the asymmetry is reversed in the arms.

A greater enhancement in the SAR by a factor as large as 2.5 is anticipated for the inner targets from antenna theory for three or more bodies, each of which is separated  $0.65\lambda$  from the closest neighbors. Table 2 gives the results of preliminary experimental tests of the multibody effect with anesthetized Long-Evans rats. The configurations used in

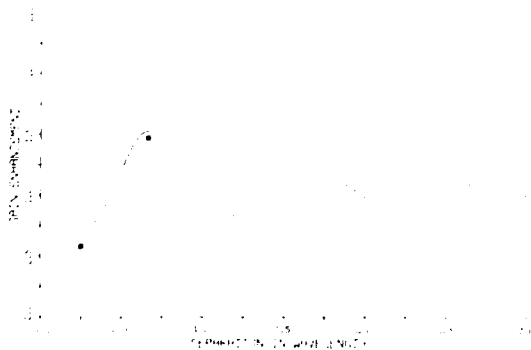


Fig. 4. Variation of gain enhancement as a function of spacing of a pair of half-wave dipoles in broadside (sagittal) configuration. Data points represent calculated enhancements of SARs in human models due to two-body effect.

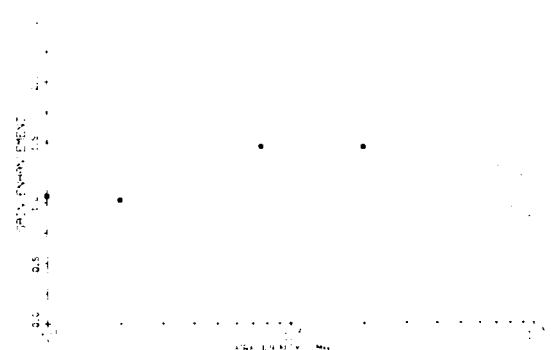


Fig. 5. Variation of gain enhancement with frequency for a pair of 1.75-meter dipoles in broadside (sagittal) configuration at a spacing of  $0.65\lambda$ . Data points represent calculated enhancements of SARs in human models due to two-body effect.

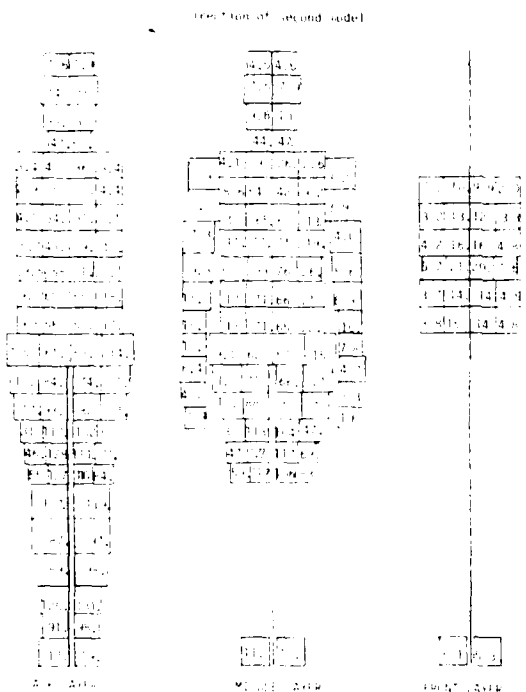


Fig. 6. Local SAR values ( $\text{mW g}^{-1}$  per  $\text{mW cm}^{-2}$ )  $\times 100$  for one of two homogeneous models of man having a center-to-center spacing of  $0.65 \lambda$  at 77 MHz. Incident power density of  $1 \text{ mW cm}^{-2}$ , distance between closest arms of the two models =  $0.51 \lambda$ .

the tests are shown in Figure 7. Note that for each of the animals, an experimental frequency considerably higher than its resonant frequency was used, confirming the fairly wide-band nature of the multibody effect. Note also that the central animal in a three-animal ensemble has ap-

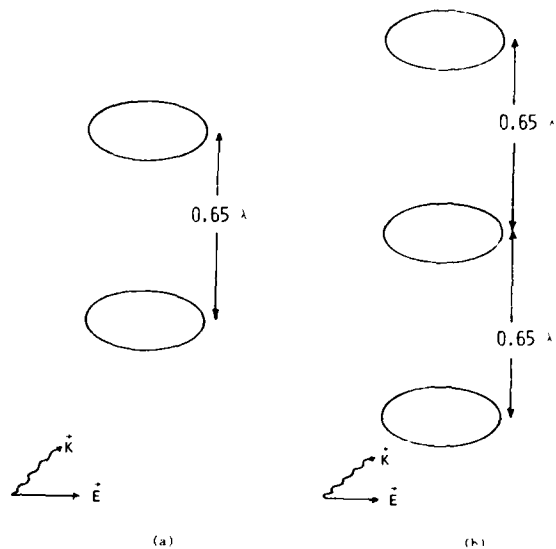


Fig. 7. Geometry used in measurement of enhancement of SARs due to proximity of other biological bodies. (a) two-animal exposure; (b) three-animal exposure.

preciable greater enhancement in SAR than is obtained in either animal of a two-animal exposure. Experiments at several frequencies with varying interanimal spacing need to be done before the full implications of multibody effects on the SAR are understood.

#### 4. EMPIRICAL EQUATIONS FOR WHOLE-BODY AVERAGE SAR UNDER FREE-SPACE IRRADIATION

The subresonant frequency dependence [Gandhi et al., 1977] and observed  $1/f$  dependence in the supraresonant region have been used to develop the empirical equa-

TABLE 2. Experimental enhancement in SAR due to proximity to other biological bodies. Anesthetized Long-Evans rats with  $\text{EML}$  at 2450 MHz. Center-to-center interanimal separation =  $0.65 \lambda$  ( $\approx 7.96 \text{ cm}$ ).

Mass of Animal Grams	Anticipated Resonant Frequency (MHz)	Enhancement Factor for Two-Animal Exposure	Enhancement Factor for Three-Animal Exposure	
			Side Animal	Central Animal
191 ± 6	987	1.22 ± 0.046 N = 4	1.30 ± 0.0507 N = 4	1.24 ± 0.0585 N = 3
248 ± 23	7.00	1.07 ± 0.118 N = 4	1.50 ± 0.0917 N = 3	1.80 ± 0.148 N = 3
1 - 234 ± 45	755	1.97 0.166 N = 9	1.92 ± 0.113 N = 6	1.77 ± 0.0611 N = 3

\* Anticipated resonant frequencies were calculated from an equation given by Gandhi et al. [1977].

TABLE 3. Empirical equations for SARs in human models and in laboratory animals. Free-space irradiation, E||, polarization, resonant frequency,  $f_r = 11.4 \text{ L}_{\text{cm}}^{-1} \text{ GHz}$ .

	For Man Models	For Laboratory Animals
For subresonant region ( $\approx 0.1 f_r < f < f_r$ )		
SAR in $\text{mW/cm}^2$ for 1 $\text{mW/cm}^2$ incident plane wave field	$0.52 \frac{\text{L}_{\text{cm}}^2}{\text{mass}} \frac{1}{f_r} - 2.75$	$0.8 \frac{\text{L}_{\text{cm}}^2}{\text{mass}} \frac{1}{f_r} - 2.75$
For supraresonant region ( $\approx f_r < f < 1.6 S_{\text{res}} f_r$ )		
SAR in $\text{mW/cm}^2$ for 1 $\text{mW/cm}^2$ incident plane wave field	$0.95 \frac{\text{L}_{\text{cm}}^2}{\text{mass}} \frac{1}{f_{\text{GHz}}} - 1.0$	$0.2 \frac{\text{L}_{\text{cm}}^2}{\text{mass}} \frac{1}{f_{\text{GHz}}} - 1.0$

where  $L_{\text{cm}}$  is the long dimension of the target in centimeters, and

$$S_{\text{res}} = \frac{1}{0.35 \text{ mass}} \quad \text{and} \quad \frac{1}{0.16 \text{ mass}} \text{ for birds}$$

tions in Table 3 for the whole-body average SAR for human models and for laboratory animals with  $E$  polarization. While the numbers of biologically simulating models of man are the same as those reported earlier [Gandhi *et al.*, 1977], the coefficients for  $S_{\text{res}}$  and SARs of laboratory animals are 59 percent higher and are derivable from antenna theory for the capture cross section of 0.38  $\lambda$  dipoles by a procedure similar to that of Gandhi *et al.* [1976]. The revised higher values for SARs are in good agreement with experimentally determined values (Table 4) for several animal species. For the data in Table 4, the animals were anesthetized (sodium pentobarbital, 45 mg  $\text{kg}^{-1}$ ) to prevent movement and to maintain thereby a fixed orientation and also to limit pharmacologically the normal thermoregulatory functions of the animal [Putthoff *et al.*, 1977]. The experimental SAR was calculated from the increase in colonic temperature (cloacal temperature in the case of lizards and birds) after three minutes of free-space irradiation at 100  $\text{mW cm}^{-2}$ . For the 500-g rat and the 120.3-g dove, freshly euthanized animals were used and the calorimeter was employed to determine the whole-body dose; the procedure was similar to that outlined by Phillips *et al.* [1975]. The points to note in Table 4 are: (1) The SARs from the empirical equations for laboratory animals (for the supraresonant region shown in Table 3) correlate well with experimental measurements on several species that range in mass from 18.8 to 2245 g, and in length, from 8 to 44 cm. For these animals, a whole-body SAR varying by a factor of 36.1:1 is observed at 50  $\text{mW cm}^{-2}$  for 2450-MHz irradiation. (2) For ring doves there is a significant difference between experimental values of SARs and those calculated using the empirical equation. The reason

for this discrepancy is not clear. Subtracting the mass of the plumage from the whole-body mass of the birds increases the values calculated via the empirical equation by a few percent but does not explain the observed difference for this avian. (3) Reliable correlations between whole-body calorimetric values on freshly killed animals and SARs based on measurements of colonic temperature of anesthetized animals confirm the rapid hemodynamic dispersion of heat in living animals. Previous measurements of field intensities needed for comparable times to convolution [Gandhi and Hunt, in preparation] at different frequencies has also demonstrated that whole-body integral dose and dose rates are important parameters in the study of living animals.

## 5 CONCLUSIONS

Numerical solutions based on an improved model of man have demonstrated that the deposition of energy at supraresonant frequencies has a fine structure that is ascribable to resonance of body parts. Failure to allow for the detailed structure of the body of man through use of prolate spheroidal, ellipsoidal, and other idealized models would cause the part-body resonances to be overlooked. The enhancement of electromagnetic energy deposition in the head at head-resonant frequencies may be important in future studies of the blood-brain barrier and of animal behavior. Numerical solutions, antenna theory, and experimental results with animals have shown that energy deposition is altered by multibody effects. A maximum of about 50 percent enhancement in SAR is found with two bodies, but significantly greater enhancement is possible with three or more bodies, interbody spacing being critical.

TABLE 4. Whole body SARs in  $\text{mW/g}$  for EIL orientation of several species of laboratory animals irradiated by 2450 MHz energy in free space. Freshly euthanized animals and a Thermoetics Model 2401-A gradient-layer calorimeter were used to measure the 500-g rat and the 120.3-g dove. Other measurements are based on anesthetized animals.

Animal	Length cm	SAR in $\text{mW/g}$ from 2450 MHz fields	Percent Error		
			From Measurements	From Empirical Equation	
<b>Long Evans rat (adult, New Zealand)</b>					
355	25	11.72	11.83	+ 2.5	
440	25	8.47	9.48	+14.1	
499	26	9.41	10.07	+ 6.5	
506	26	9.41	9.92	+ 5.1	
508	25	8.47	9.51	+10.9	
550	26	7.53	9.13	+17.5	
500	--	9.48	--	--	
<b>Rabbit (New Zealand white)</b>					
2091	44	3.80	4.25	+10.6	
2090	44	4.27	4.25	+ 0.5	
2245	43	3.90	3.71	+ 5.1	
<b>Dove (Columba livia, male, adult)</b>					
24	9	68.61	72.48	+ 5.3	
22	8.5	72.94	74.67	+ 2.3	
23	8.5	70.40	71.43	+ 1.4	
<b>Deer mouse (Peromyscus maniculatus)</b>					
24	6.5	58.90	58.63	+ 4.0	
24	8	68.61	67.41	+ 6.5	
<b>Ring dove (Columba livia, male)</b>					
141.5	14	36.11	19.12	--	
143.2	15.5	37.66	26.92	--	
144	13	29.03	17.45	--	
144	13	28.60	17.43	--	
120.3	--	29.76	--	--	
<b>White-tailed deer (Odocoileus virginianus)</b>					
24	9.5 + 21 cm tail	124.55	15.46		
23	9.5 + 9 cm tail	133.95	15.95		
20.5	8.5 + 22 cm tail	124.77	13.26		
18.8	9.5 + 10 cm tail	92.15	8.95		

The length of the animals was measured from snout to posterior portion of animal body excluding the tail.

Antenna theory and the observed  $1/f$  dependence at supraresonant frequencies have been used to develop empirical equations for the whole-body SAR for models of

man and for laboratory animals with the vector of the  $E$  field parallel to the body's long axis. The empirical SAR values are shown to be in good agreement with the experimental values obtained for several animal species.

**Acknowledgments.** The authors wish to acknowledge the assistance of A. Riazi, I. Chatterjee, and T. Thimakis in obtaining parts of the experimental data. This work was supported in part by the US Army Medical Research and Development Command, Washington, D.C., under Contract DAMD 17-74-C-4092, and in part by the National Aeronautics and Space Administration under Contract NAS 2-9555.

## REFERENCES

- Baker, H. C., and A. H. Lagrone (1962), Digital computation of the mutual impedance between thin dipoles, *IRE Trans. Antennas Propagat.*, AP-10, 172-178.
- Chen, K. M., and B. S. Guru (1976), Induced EM field and absorbed power density inside human torsos by 1 to 500 MHz EM waves, *Tech. Rep. No. 1*, NSF Grant ENG 74-12603, Michigan State Univ., E. Lansing, MI.
- Gandhi, O. P., and E. L. Hunt, Enhancement in electromagnetic power deposition for man and animals in the presence of reflecting surfaces, in preparation.
- Gandhi, O. P., E. L. Hunt, and J. A. D'Andrea (1977), Deposition of electromagnetic energy in animals and in models of man with and without grounding and reflector effects, *Radio Sci.*, 12(6S), 39-47.
- Gandhi, O. P., K. Sedigh, G. S. Beck, and E. L. Hunt (1976), Distribution of electromagnetic energy deposition in models of man with frequencies near resonance, in *Biological Effects of Electromagnetic Waves, Selected Papers of the USNC/URSI Annual Meeting, Boulder, Colorado, October 20-23, 1975, Vol. II*, edited by C. C. Johnson and M. L. Shore, 44-67, HEW Publ. (FDA) 77-8011, US Government Printing Office, Washington, D.C. 20402.
- Hagmann, M. J., O. P. Gandhi, and C. H. Durney (1977), Numerical calculation of electromagnetic energy deposition in a realistic model of man, accepted for publication in *IEEE Trans. Microwave Theory Tech.*
- Joines, W. T., and R. J. Spiegel (1974), Resonance absorption of microwaves by the human skull, *IEEE Trans. Biomed. Eng.*, BME-21, 46-48.
- King, R. W. P. (1956), *The Theory of Linear Antennas*, Harvard University Press, Cambridge, MA, 944 pp.
- Phillips, R. D., E. L. Hunt, and N. W. King (1975), Field measurements, absorbed dose, and biologic dosimetry of microwaves, *Ann. N. Y. Acad. Sci.*, 247, 499-509.
- Putthoff, D. L., D. R. Justesen, L. B. Ward, and D. M. Levinson (1977), Drug-induced ectothermia in small mammals: The quest for a biological microwave dosimeter, *Radio Sci.*, 12(6S), 73-80.

## APPENDIX D

*Radio Science* Volume 14, Number 6S, pages 23-29, November-December 1979

### Numerical calculation of electromagnetic energy deposition in models of man with grounding and reflector effects

*M. J. Hagmann and O. P. Gandhi*

*Departments of Electrical Engineering and Bioengineering, University of Utah, Salt Lake City, Utah 84112*

(Received November 4, 1977)

Image theory has been used to obtain moment-method solutions of the deposition of electromagnetic energy in standard man as a function of grounding and reflector effects. The calculated values are in good agreement with experimental data. For the **EH** orientation, the resonant frequency of standard man shifts from 77 MHz in free space to 47 MHz when standing on a ground plane. The dependence of reflector effects on spacing and frequency are in agreement with the gain enhancement calculated by dipole by antenna theory.

#### 1. INTRODUCTION

Experimental observations of grounding and reflector effects have been reported previously, but numerical methods have not been available to confirm the observations [Gandhi *et al.*, 1977b]. We have used image theory to reduce the problem of man either grounded or in front of reflectors to that of a multibody target in free space. Moment-method solutions of the electric-field integral equation have a pulse-function basis and delta functions for testing. A 180-cell model of the 50th-percentile standard man was used in the calculations [Hagmann *et al.*, 1977].

#### 2. APPLICATION OF IMAGE THEORY WITH COMPRESSION

If all reflectors and ground planes are assumed to be perfect conductors and infinite in extent, then they may be ignored if suitable images of the scattering body are included. Since polarization currents in the images contribute to the scattering, it is necessary to treat all parts of the scattering body and the images as discrete cells. If pulse functions are used as a basis, it is necessary that each subvolume be small enough that the electric field that it contains may be assumed constant.

A moment method solution with pulse functions will relate the column matrix  $E$ , which contains the unknown electric-field values in each cell, to the column matrix  $I$ , which contains values of the incident electric field in each cell, through a square matrix  $A$  by the equation

$$AE = E \quad (1)$$

Equation 1 may be solved directly, but a reduction of matrix size will allow the solution to be found with greater

economy, or alternately, more cells may be used for greater accuracy. A reduction in matrix size is possible by the use of "compression," which is described next.

The geometry involved when images are used causes the fields to have symmetry. Let  $m$  be the number of unique values of  $E$  that are repeated in the  $n^3$  possible sign changes. We say index the cells so that all cells from 1 to  $m$  correspond to the unique  $E$  values, and for any integer  $1 \leq i \leq m$ , then  $I_{i,1}, I_{i,2}, \dots, I_{i,n}$  are correct and values related to  $E_i$  by symmetry.

The relationship of all  $n^3 \times n^3$  of the  $E$  values to the unique  $E$  values may be expressed in matrix form:

$$\begin{bmatrix} E_1 \\ E_2 \\ \vdots \\ E_m \end{bmatrix} = \begin{bmatrix} I_{1,1} & I_{1,2} & E_1 \\ I_{2,1} & I_{2,2} & E_2 \\ \vdots & \vdots & \vdots \\ I_{m,1} & I_{m,2} & E_m \end{bmatrix} \quad (2)$$

where  $I_{i,j}$ ,  $I_{i,k}$ , ...,  $I_{i,n}$  are  $m$  by  $m$  matrices with one in the diagonal and zero elsewhere, and  $I_{i,1}$  is the unity matrix.

Compression may be obtained by noting that only the first  $m$  simultaneous equations need to be used in equation (1); substituting (2) in (1) will give  $m$  sets of  $m$  simultaneous equations in the  $m$  unknowns  $E_i$ ,  $i = 1, 2, \dots, m$ .

$$A \begin{bmatrix} I_{1,1} & I_{1,2} & E_1 \\ I_{2,1} & I_{2,2} & E_2 \\ \vdots & \vdots & \vdots \\ I_{m,1} & I_{m,2} & E_m \end{bmatrix} = \begin{bmatrix} E_1 \\ E_2 \\ \vdots \\ E_m \end{bmatrix} \quad (3)$$

$$A' \begin{bmatrix} E_1 \\ E_2 \\ \dots \\ E_m \end{bmatrix} = \begin{bmatrix} E'_1 \\ E'_2 \\ \dots \\ E'_m \end{bmatrix} \quad (4)$$

where  $A'$  is an  $m$  by  $m$  matrix formally defined by  $A'$  = first  $m$  rows of:

$$A \begin{bmatrix} I_1 \\ I_2 \\ \dots \\ I_n \end{bmatrix} \quad (5)$$

In implementing compression, the computation of matrix  $A'$  is made by making  $n$  modified passes through the loops that would normally be used to accumulate the scattering matrix.

We have used compression with image theory to treat a body with one plane of symmetry above a ground plane, as is shown in Figure 1. The field relationships used for a body with one plane of symmetry in front of a flat reflector are shown in Figure 2. It is also possible to use compression with image theory to treat a body in a corner reflector, if the corner reflector has a dihedral angle equal to  $180^\circ/N$

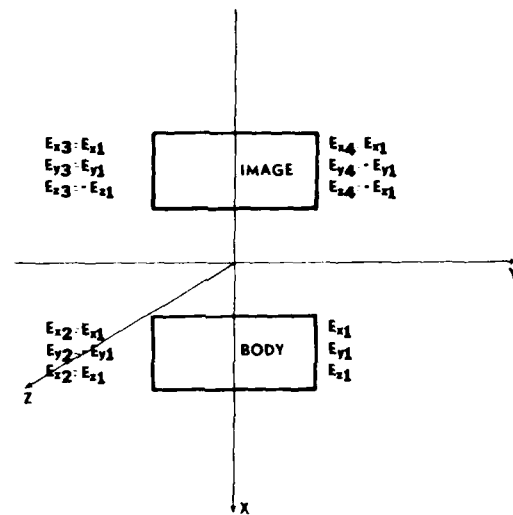
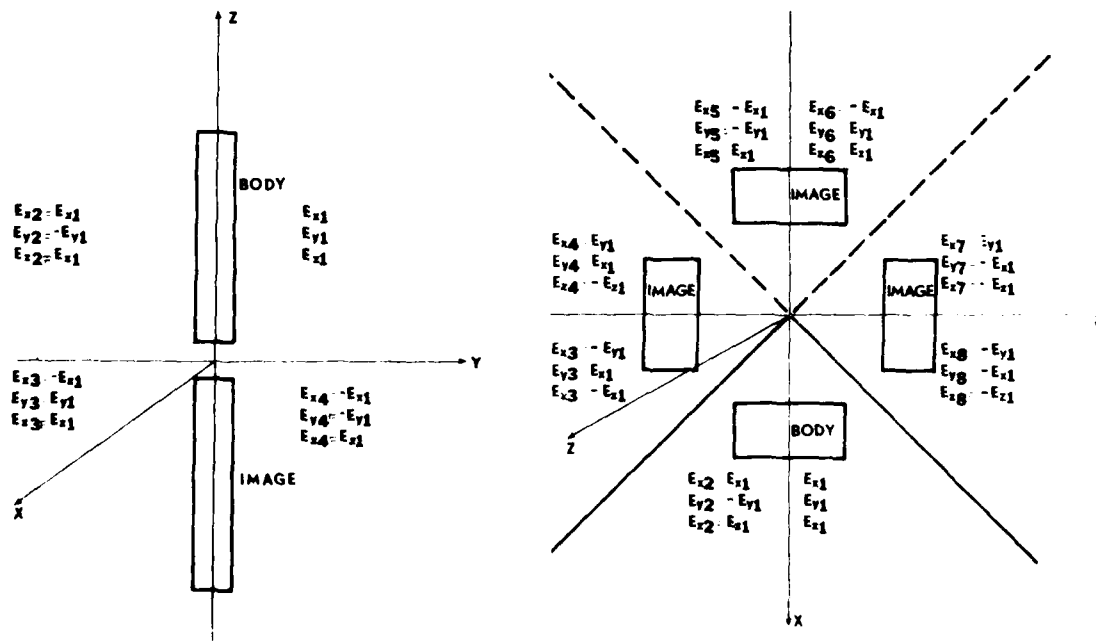


Fig. 2. Field relationships for a body with one plane of symmetry in front of a flat reflector.  $\mathbf{E}(\mathbf{f}, \mathbf{k})$ .

where  $N$  is an integer. Field relationships used for a body with one plane of symmetry in front of a  $90^\circ$  corner reflector are shown in Figure 3.



There are two types of symmetry relationships used for  $E$  values in the three figures: (1) Two points located symmetrically in respect to a plane of symmetry of the body that contains both  $k$  and  $E$  will necessarily have  $E$  values that are mirror images so that the two halves are indistinguishable under reflection. (2) Two points located symmetrically in respect to a plane of symmetry of the body that contains  $k$  and is perpendicular to  $E$  will necessarily have  $E$  values that are negated mirror images, so that if the values are exchanged, they will correspond to the solution for oppositely directed  $E$ . This relationship is also found for two points located symmetrically in respect to a ground plane or to a flat reflector as required for symmetrical motion of a charge and its image.

An alternative to the use of image theory with compression is to use special Green's functions in place of the free-space Green's function. Special Green's functions are available that could be used to account for scattering objects located near targets having various shapes and even finite conductivities [Tai, 1971; Baños, 1966]. We have not yet pursued the use of such Green's functions.

The results of calculations for grounding and reflector effects are described in the next sections.

### 3. GROUND EFFECTS

All calculations of grounding effects have assumed that a man is standing on or above a perfectly conducting ground plane that is infinite in extent. The incident field is vertically polarized with  $k$  directed from the ventral to the dorsal aspect of the man. Internal fields in the model are the same as those in one-half of a double-man, which consists of the model and its image in free space. A 180-cell model of the 50th-percentile standard man has been used for the calculations [Hagmann *et al.*, 1977].

The calculated resonant frequency of man standing on a ground plane is 47 MHz as compared to 77 MHz for man in free space. The specific absorption rate (SAR) of man on the ground plane at the reduced resonant frequency is 32.5 percent greater than the SAR for man in free space at the free-space resonant frequency. At lower frequencies, the SAR of man standing on a ground plane may be increased considerably from that of the same model in free space. This increase results from these frequencies being closer to resonance for the grounded man. For example, at 10 MHz the SAR of man standing on a ground plane is 0.0163 W kg<sup>-1</sup> per mW cm<sup>-2</sup>, which is about seven times that found for the same model in free space.

Figures 4 and 5 illustrate, respectively, the distribution of absorbed energy in man at 10 MHz in free space and in contact with the ground plane. The enhancement of local energy deposition due to the grounding effect is approximately a factor of 60 in the area of the heel.

Figure 6 shows the part-body and whole-body SAR for the model of man with different spacings from the ground

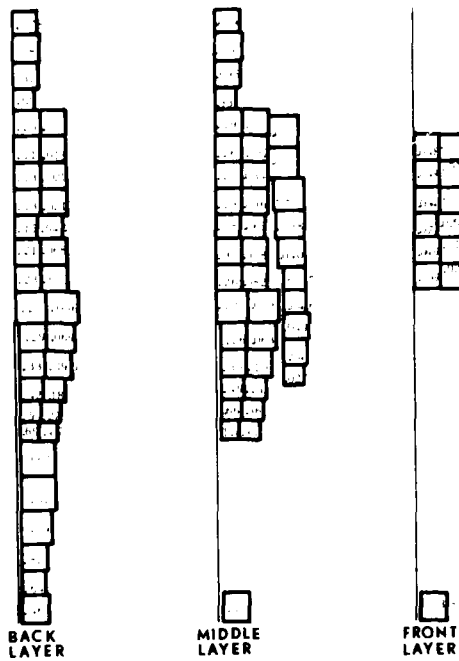


Fig. 4. Local SAR values ( $\text{W kg}^{-1}$  per  $\text{mW cm}^{-2}$ )  $\times 100$  for inhomogeneous model of man in free space at 10 MHz.

plane at 10 MHz. Figure 6 is consistent with the experimental observation on models that a small separation that breaks electrical contact with the ground plane is sufficient to eliminate much of the grounding effect [Gandhi *et al.*, 1975]. Several calculations made for the grounded resonant frequency of 47 MHz show a fall-off in magnitude of grounding effects with increasing distance from the ground plane, which is similar to the results at 10 MHz (Figure 6). A model composed of 292 cells was made by dividing each of the six lowest cells in each leg of the 180-cell model into eight identical cubical cells. Six solutions made for the 292-cell model and duplicated with the 180-cell model suggest that the fall-off of the grounding effect with increasing distance from the ground plane may be slightly slower than is found with the 180-cell model.

Figure 7 shows part- and whole-body SARs for the model of man standing on a ground plane at various frequencies. The part-body resonances shown in Figure 7 have also been observed in calculations for the same model of man in free space [Gandhi *et al.*, 1977a]. The enhancement in absorption of energy due to the presence of a ground plane is greatest in the leg and least in the head. Figure 8 shows whole-body SARs for the model of man both in free space and when standing on a ground plane at various frequencies. Grounding effects are most prominent at low frequencies.

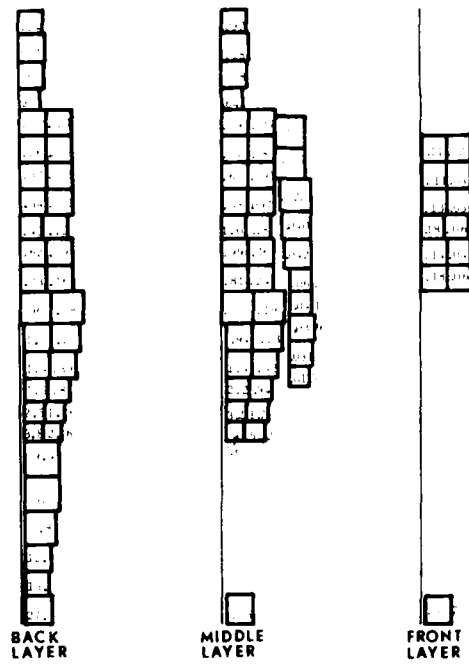


Fig. 5. Local SAR values ( $\text{W kg}^{-1}$  per  $\text{mW cm}^{-2}$ )  $\times 100$  for inhomogeneous model of man standing on a ground plane at 10 MHz.

cies. Above a frequency of about 200 MHz, part- and whole-body SAR values show little dependence on the presence of a ground plane.

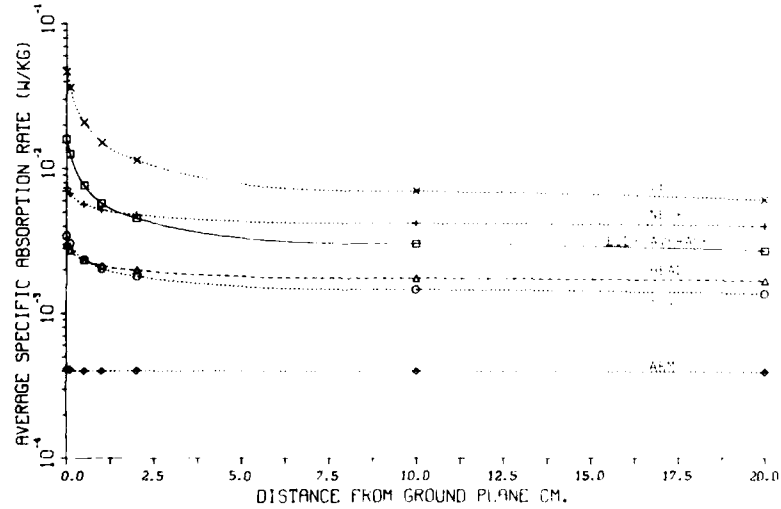


Fig. 6. Whole-body SARs in man for different spacings from the ground at 10 MHz;  $\mathbf{E} \parallel \mathbf{k}$ ,  $\mathbf{k}$  ventral to dorsal, incident power density of  $1 \text{ mW cm}^{-2}$ .

#### 4. REFLECTOR EFFECTS

All calculations of reflector effects have assumed that a man is standing in front of a reflector that is perfectly conducting and infinite in extent. The incident field is vertically polarized with  $\mathbf{k}$  directed from the ventral to the dorsal aspect of the man. One image is required for a flat reflector and three are needed for a 90° corner reflector.

The enhancement of SAR due to reflector effects is approximately the same as the ratio of effective area of a half-wave dipole with a reflector to that of an isolated dipole in free space [Gandhi et al., 1977b]. Antenna theory has been used to perform numerical calculations made for the model of man. Standard procedures have been used for computation of the required values of mutual impedance of dipoles [Baker and LaGrone, 1962].

Figures 9-12 show the enhancement of energy absorption as calculated for the model of man with reflector effects and the corresponding gain-enhancement factors calculated for thin dipoles from antenna theory. Values of enhancement for the whole-body average SAR have been used in preparing Figures 9-12, but the curves for part-body energy absorption are nearly identical, which indicates that the distribution of energy through the model is almost independent of the presence of a reflector. Experimental values in Figures 9-12 are for models of man and were reported earlier [Gandhi et al., 1977b].

Figures 9 and 10 show the variation of enhancement of energy absorption as a function of spacing from a reflector at the free-space resonant frequency of 77 MHz. In Figure 9 the numerical values for the model of man are markedly below the curve for thin dipoles at small values of separation.

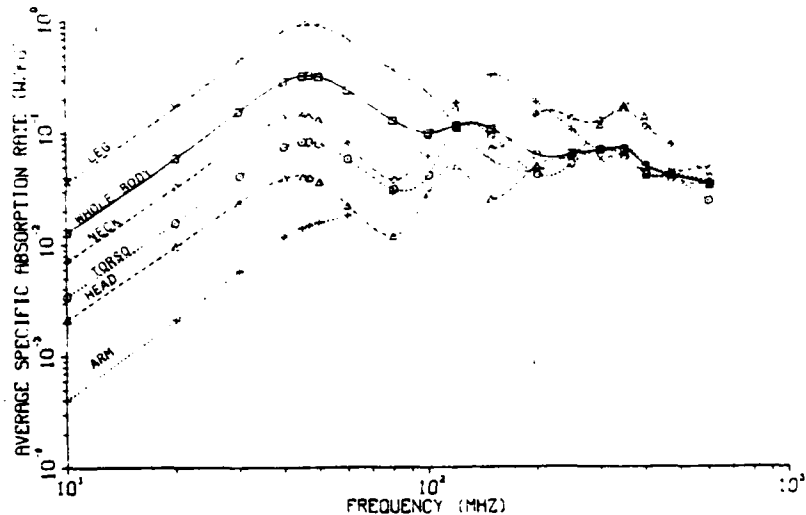


Fig. 7. Part-body SARs for a homogeneous model of man on a ground plane; EIL, k ventral to dorsal, incident power density of  $1 \text{ mW cm}^{-2}$ .

tion. Antenna theory requires that the gain be small when the spacing is not much greater than the thickness of the dipole, but such variation is missed in the thin dipole approximation.

Figures 11 and 12 show the variation of enhancement of energy absorption as a function of frequency for fixed ratios of spacing to wavelength. The antenna-theory calculations were made for a thin dipole with a length of 1.75 meters, which is identical to the height of the model. Figures 11 and 12 show that the reflector effects are found over a wide range of frequencies. Values for the model of man have a pronounced roll-off at higher frequencies, which is not seen in calculations for the thin dipoles. In Figures 11 and 12 it can be seen that the rate of roll-off of the SAR at high frequencies is consistent with experimental

results that are obtained from models of man. Antenna theory requires that the gain decrease at higher frequencies when the effective area of the dipole images is blocked by the physical cross section of the dipole, but such variation is missed in the thin-dipole approximation.

All gain calculations have been based on zero-order antenna theory; that is, they have no correction for non-sinusoidal current distributions. Significant first- and second-order corrections are required when the antennae are not very thin and the half-length is much different from  $\lambda/4$  [King, 1956]. The sizable lateral extent of the model of man is thought to be responsible for the difference between

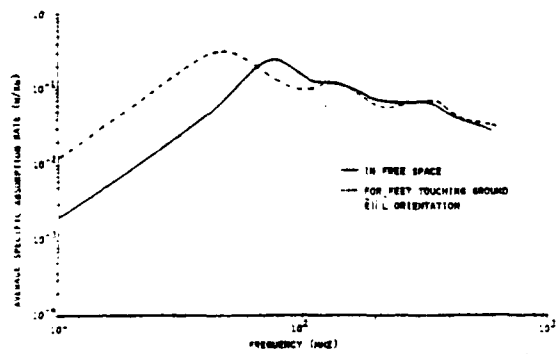


Fig. 8. Whole-body SARs for homogeneous model of man; EIL, k ventral to dorsal, incident power density of  $1 \text{ mW cm}^{-2}$ .

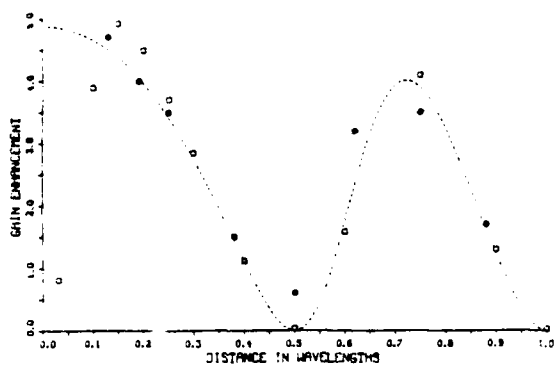


Fig. 9. Variation of gain enhancement with spacing for a half-wave dipole in front of a flat reflector. Squares represent numerical solutions for enhancement of SARs in man at 77 MHz ( $L/\lambda = 0.45$ ). Solid circles represent experimental values for anatomically scaled figurines at  $L/\lambda = 0.417$ .

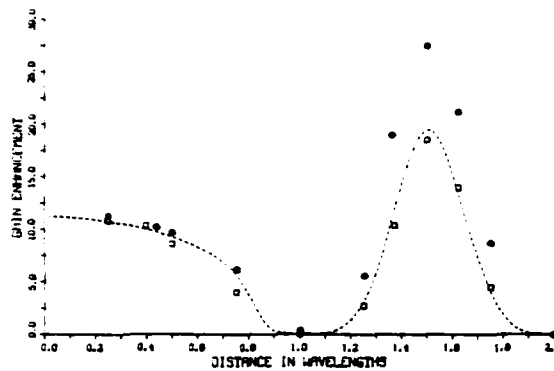


Fig. 10. Variation of gain enhancement with spacing for a half-wave dipole in front of a  $90^\circ$  corner reflector. Squares represent numerical solutions for enhancement of the SAR in man at 77 MHz ( $L/\lambda = 0.45$ ). Solid circles represent experimental values for anatomically scaled figurines at  $L/\lambda = 0.417$ .

numerical solutions and antenna theory at low frequencies in Figure 12.

The numerical solutions indicate that for frequencies near resonance, the enhancement in SAR due to a reflector is approximately equal to the enhancement in gain of a half-wave dipole with the same reflector configuration. Experimental studies on models of man have also shown that the enhancement of SAR is equal to the enhancement in gain of a dipole, but the gain must be calculated for the finite experimental reflector rather than for an infinite reflector having the same dihedral angle. For certain combinations of length and width of the reflecting sheets, a finite corner reflector may exhibit supergain — a gain significantly greater than that for infinite reflecting planes [Cottany and Wilson, 1958; Schelkunoff and Friis, 1952].

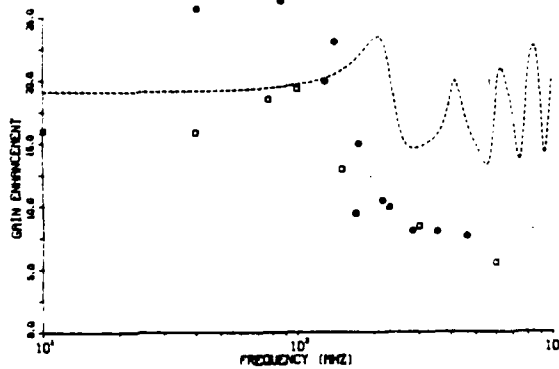


Fig. 11. Variation of gain enhancement with frequency for a 1.75-meter dipole  $0.75\lambda$  from a flat reflector. Squares represent numerical solutions for enhancement of SARs in man. Solid circles represent experimental values for anatomically scaled figurines.

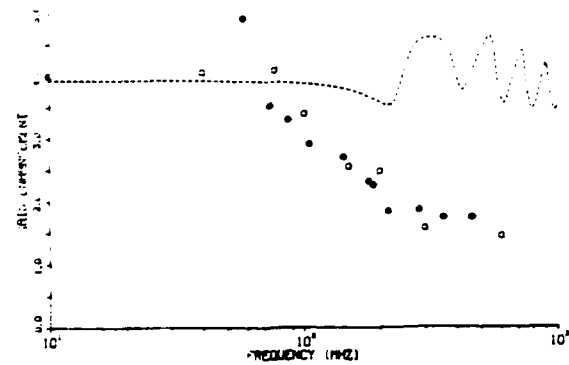


Fig. 12. Variation of gain enhancement with frequency for a 1.75-meter dipole  $1.5\lambda$  from a  $90^\circ$  corner reflector. Squares represent numerical solutions for enhancement of SARs in man. Solid circles represent experimental values for anatomically scaled figurines.

Examples of the effect of such supergain combinations are seen in the experimental values in Figures 10-12.

Figures 13 and 14 were copied from an experimental study of finite-size corner reflectors [Cottany and Wilson, 1958]. In both figures the angle of the aperture was adjusted for maximum gain at a particular distance of the dipole from the reflector. For reflector lengths greater than about  $0.5\lambda$  (Figure 13), the aperture angle is  $90^\circ$  and distance of the dipole from the reflector is  $1.5\lambda$ . For reflector lengths greater than  $1.0\lambda$  (Figure 14), the aperture angle

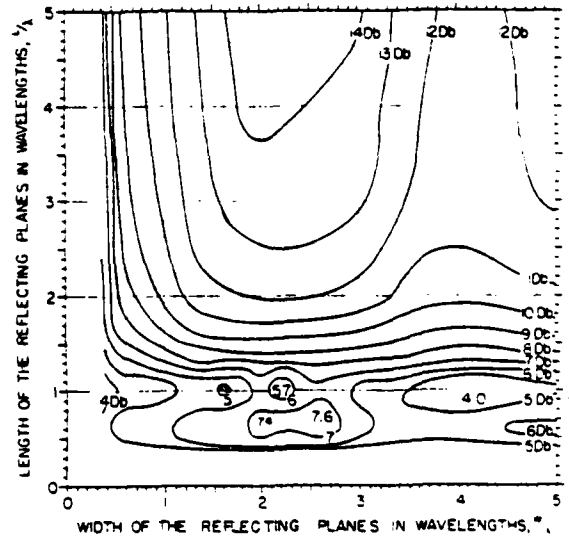


Fig. 13. Contours of constant gain for a corner-reflector antenna with the dipole in third position for various reflector sizes. For lengths greater than  $-0.5\lambda$ , the aperture angle is  $90^\circ$  and the distance of the dipole from the reflector is  $1.5\lambda$  [Cottany and Wilson, 1958].

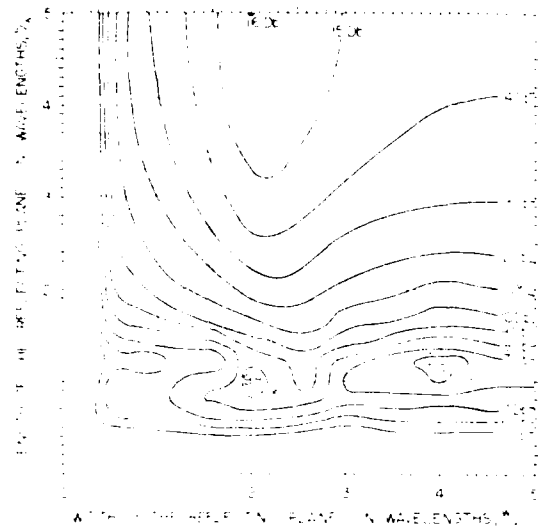


Fig. 14. Contours of constant gain for a corner-reflector antenna with the dipole in second position for various reflector sizes. For lengths greater than  $1.0 \lambda$ , the aperture angle is  $65^\circ$  and the distance of the dipole from the reflector is  $1.2 \lambda$  [Cottany and Wilson, 1958].

is  $65^\circ$  and distance of the dipole from the reflector is  $1.2 \lambda$ .

Note in Figure 13 that for proper combinations of length and widths of the reflecting planes, the enhancement in SAR over the free-space value may be 30 to 45 percent greater than that for infinite reflectors. For such supergain combinations the SAR may be enhanced (see Figure 13) by as much as 14 to 14.5 dB (a factor of 25 to 28) rather than 12.9 dB (19.5) anticipated for infinite reflectors, or the factor of 16 that is projected from consideration of the local  $E$  fields in the standing-wave pattern of a  $90^\circ$  corner reflector. As is shown in Figure 13, the dimensions  $2\lambda \times 3.5\lambda$  of the reflectors used for the experimental results of Figures 10 and 12 correspond to one of the supergain combinations.

Supergain combinations of length and width are also presented for a  $65^\circ$  corner reflector (see Figure 14). Antenna calculations with image theory are restricted to corner reflectors having dihedral angles of  $(N+1)^\circ$  where  $N$  is an integer. As seen in Figure 14, gain enhancement is not limited to such special angles, and we expect that significant enhancements of the SAR will occur for a wide variety of reflectors.

## 5. CONCLUSIONS

Image theory has been used to treat grounding and reflector effects so that all calculations are limited to a perfectly conducting ground plane, or to reflectors with an infinite extent. Experimental results suggest that reflectors of finite size may provide significantly more or less

enhancement in energy deposition than that calculated for infinite reflectors. The effect of finite conductivity on grounding or reflector effects with models of man has not yet been evaluated either theoretically or experimentally.

The decrease in resonant frequency and alteration in energy deposition due to grounding may be explained by considering a double-length man in free space. If the model of man had a cross section independent of height and a complex permittivity independent of frequency, the grounded resonant frequency would be one-half the free-space resonant frequency, but a ratio of 0.610 is obtained for the model that has been used.

The dependence of reflector effects on spacing and frequency are in agreement with the gain enhancement calculated for dipoles by antenna theory. The enhancement in energy deposition due to reflector effects becomes small for small values of separation or for high frequencies, which effects agree with antenna theory only if finite width of the dipole is considered.

**Acknowledgment.** This work was supported by US Army Medical Research and Development Command, Washington, D. C., under Contract DAMD 17-74-C-4092.

## REFERENCES

- Baker, H. C., and A. H. LaGrone (1962), Digital computation of the mutual impedance between thin dipoles, *IRE Trans. Antenna Propagat.*, AP-10, 172-178.
- Baños, A., Jr. (1966), *Dipole Radiation in the Presence of a Conducting Half-Space*, 245 pp., Pergamon Press, Oxford.
- Cottany, H. V., and A. C. Wilson (1958), Gains of finite-size corner reflector antennas, *IRE Trans. Antenna Propagat.*, AP-6, 366-369.
- Gandhi, O. P., J. A. D'Andrea, B. K. Jenkins, J. L. Lords, J. R. Mijanovich, and K. Sedigh (1975), Behavioral and biological effects of resonant electromagnetic absorption in rats, *Tech. Rep. UTEC MD-75-174* under Contract No. DAMD 17-74-C-4092, 29 pp., Microwave Device and Physical Electronics Laboratory, University of Utah, Salt Lake City, UT 84112.
- Gandhi, O. P., M. J. Hagmann, and J. A. D'Andrea (1977a), Some recent results on deposition of electromagnetic energy in animals and models of man, paper presented at the 1977 USNC URSI meeting, Airlie, VA.
- Gandhi, O. P., E. L. Hunt, and J. A. D'Andrea (1977b), Deposition of electromagnetic energy in animals and in models of man with and without grounding and reflector effects, *Radio Sci.*, 12(6S), 39-47.
- Hagmann, M. J., O. P. Gandhi, and C. H. Durney (1977), Numerical calculation of electromagnetic energy deposition for a realistic model of man, paper presented at the 1977 USNC URSI meeting, Airlie, VA, accepted for publication in *IEEE Trans. Microwave Theory and Tech.*
- King, R. W. P. (1956), *The Theory of Linear Antennas*, 944 pp., Harvard University Press, Cambridge, MA.
- Schelkunoff, S. A., and H. T. Friis (1952), *Antennas. Theory and Practice*, 639 pp., John Wiley and Sons, New York.
- Tai, C. T. (1971), *Dyadic Green's Functions in Electromagnetic Theory*, 246 pp., Intext Educational Publishers, Scranton, PA.

APPENDIX E

SOME RECENT RESULTS ON THE DEPOSITION OF ELECTROMAGNETIC  
ENERGY IN ANIMALS AND MODELS OF MAN !

O. P. Gandhi and M. J. Hagmann

Departments of Electrical Engineering and Bioengineering  
University of Utah, Salt Lake City, Utah 84112

ABSTRACT

A realistic human model and improved numerical methods have been used for calculation of deposition of electromagnetic energy. Unlike earlier solutions both the average absorption and the distribution of absorbed energy within the model are in good agreement with experimental measurements made using phantom models. The distribution of absorbed energy is frequency-dependent and may be explained in terms of resonance of the various body parts. Numerical solutions for man near a ground plane and near reflectors are presented for the first time. At 10 MHz the specific absorption rate (SAR) of man standing on a ground plane is about seven times that for man in free space. Multibody effects have been predicted from antenna theory and observed with experiments using anesthetized rats. For two resonant targets separated by  $0.65 \lambda$  an increased SAR, 170 percent of the free-space value, has been observed.

*Proceedings of the Workshop on Physical Basis of Electromagnetic Interactions with Biological Systems, University of Maryland, June 15-17, 1977 (Editors: L. S. Taylor and A. Y. Cheung)*

## DESCRIPTION OF MODEL AND NUMERICAL TECHNIQUES

Solutions in electromagnetics are facilitated by choosing a model of simple geometry. Then an exact analytical solution may be possible, or a numerical solution may be expressed in terms of easily constructed whole-domain basis functions. We have rejected such methods since emphasis was placed on a realistic model of man. When simple geometries are not possible, one can always attempt a solution by "brute-force" using moment methods with a subsectional basis. We have used moment method solution of the electric field integral equation with a pulse function basis and delta functions for testing<sup>1</sup>.

A total of 180 cubical cells of various sizes were used to obtain a best fit of the contour on diagrams of the 50th percentile standard man<sup>2</sup>. Sizes and placement of the cells is shown in Fig. 1. Anatomical cross section<sup>3,4</sup> were used in partitioning bone, fat, skin, muscle, lung tissue, air, heart, brain, kidney, liver, and spleen through the cells. Whole-body volume fractions of each tissue type are in agreement with published values. Properties reported in the literature for the tissue types<sup>5-7</sup> have been used to calculate the volume-weighted complex permittivity of each cell.

Previously reported solutions for models of man have a ratio of 239.1 for energy deposition in one pair of adjacent cells at 10 MHz<sup>8</sup>. The arrangement and different sizes of cells in the present model cause the maximum ratio of energy deposition for a pair of adjacent cells to be 8:1 at the same frequency. The pulse function approximation is invalid if conditions force significant variation of  $\vec{E}$  within the cells and a large difference between calculated energy deposition in adjacent cells suggests the existence of such variations.

If  $\Delta$  is the side of a cubical cell and  $k$  represents the magnitude of the complex propagation vector within the cell, then substantial variation of the electric field must occur within the cell if  $k\Delta > \sqrt{6}$ <sup>9</sup>. Thus the pulse function approximation may not be justified at frequencies above 200 MHz with the new model suggesting an increasing error at higher frequencies. Volume

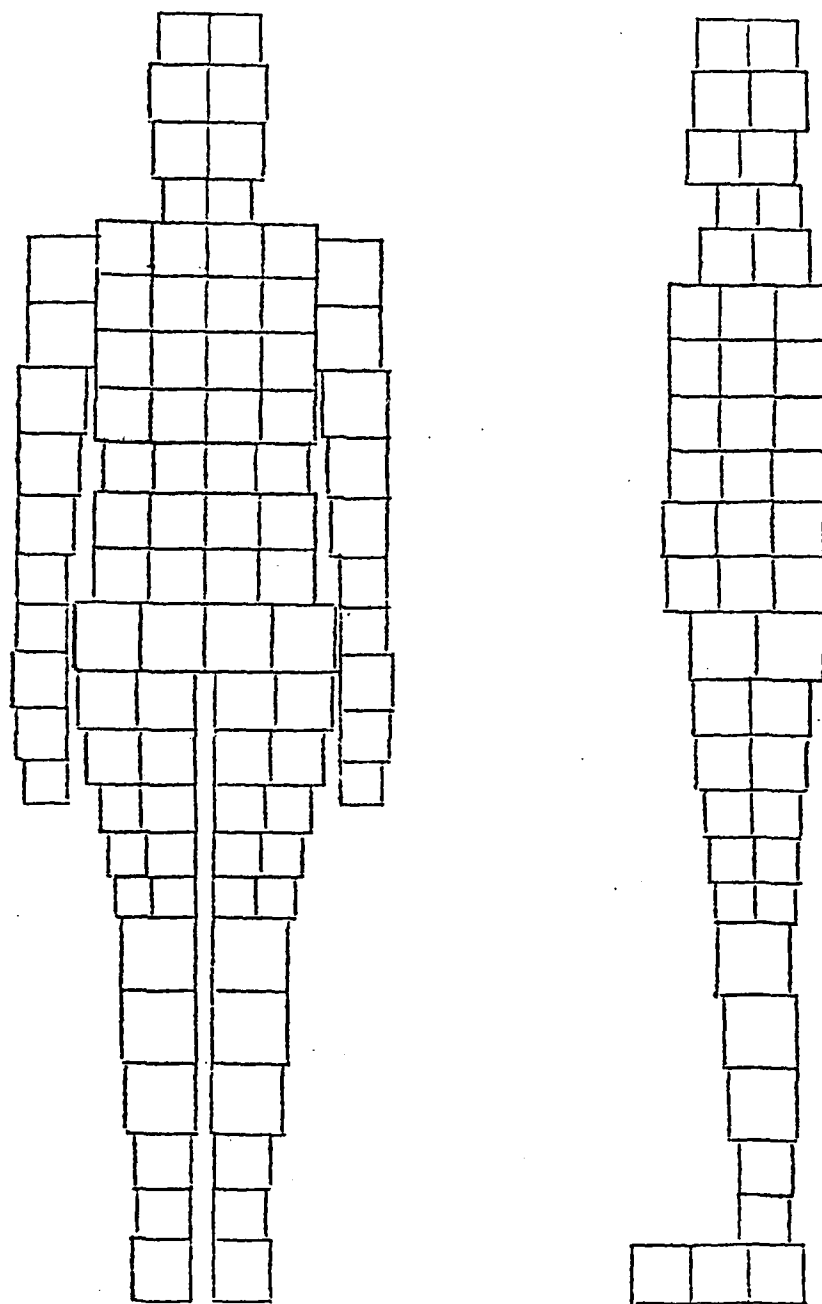


Figure 1.  
An improved model of man for numerical calculations.

weighting of the complex permittivity within each cell may also be unjustified at frequencies above 200 MHz though the results appear reasonable to at least 500 MHz.

A numerical solution using a pulse function basis results in a single value representing  $\vec{E}$  within each cell. It is possible to use the  $\vec{E}$  values to calculate  $1/2 \sigma E \cdot \vec{E}^*$  for each cell and use a volume average to estimate the specific absorption rate (SAR)<sup>8</sup>. Large numbers of cells must be used in order to find accurate values of SAR by such a procedure. For example, our calculations of the SAR of a 12cm muscle cube at 1 MHz show an error of 37% with eight cells, 26% with twenty seven cells, and 20% with sixty four cells. The delta functions used for testing enforce the integral equation at the center of each cell so that the calculated  $\vec{E}$  values are most representative of the cell centers. Inspection of the solutions suggests that the local values of  $\vec{E}$  have appreciably less error than occurs in the SAR. If there is much variation of  $\vec{E}$  within a scattering body then even if we have exact values of  $\vec{E}$  at the cell centers appreciable error would be expected in the calculated SAR. We have found that accuracy is improved by using a three-dimensional interpolant<sup>10</sup> with the  $\vec{E}$  values initially calculated for each cell to account for some of the variation of  $E$  within each cell. Trilinear and triquadratic interpolants have both been used to estimate the variation of  $\vec{E}$  between the cell centers. The interpolant is integrated in calculating the SAR. For the 12cm muscle cube at 1 MHz, the SAR found, using twenty seven cells with the triquadratic interpolant, has error comparable with the calculation using sixty four cells without the interpolant. The increase in cost due to use of the interpolant is about one percent. All values of energy absorption in this paper have been calculated using interpolants.

#### DISTRIBUTION OF ABSORBED ENERGY -- PART BODY RESONANCES

The principal contribution from the free space calculations is the distribution in energy deposition. Figure 2 shows the part-body and whole-body SAR for the homogeneous model of man with two-thirds the complex permittivity of muscle with  $\vec{E} \parallel \hat{L}$  and  $\vec{k}$  directed front-to-back. Calculated values of

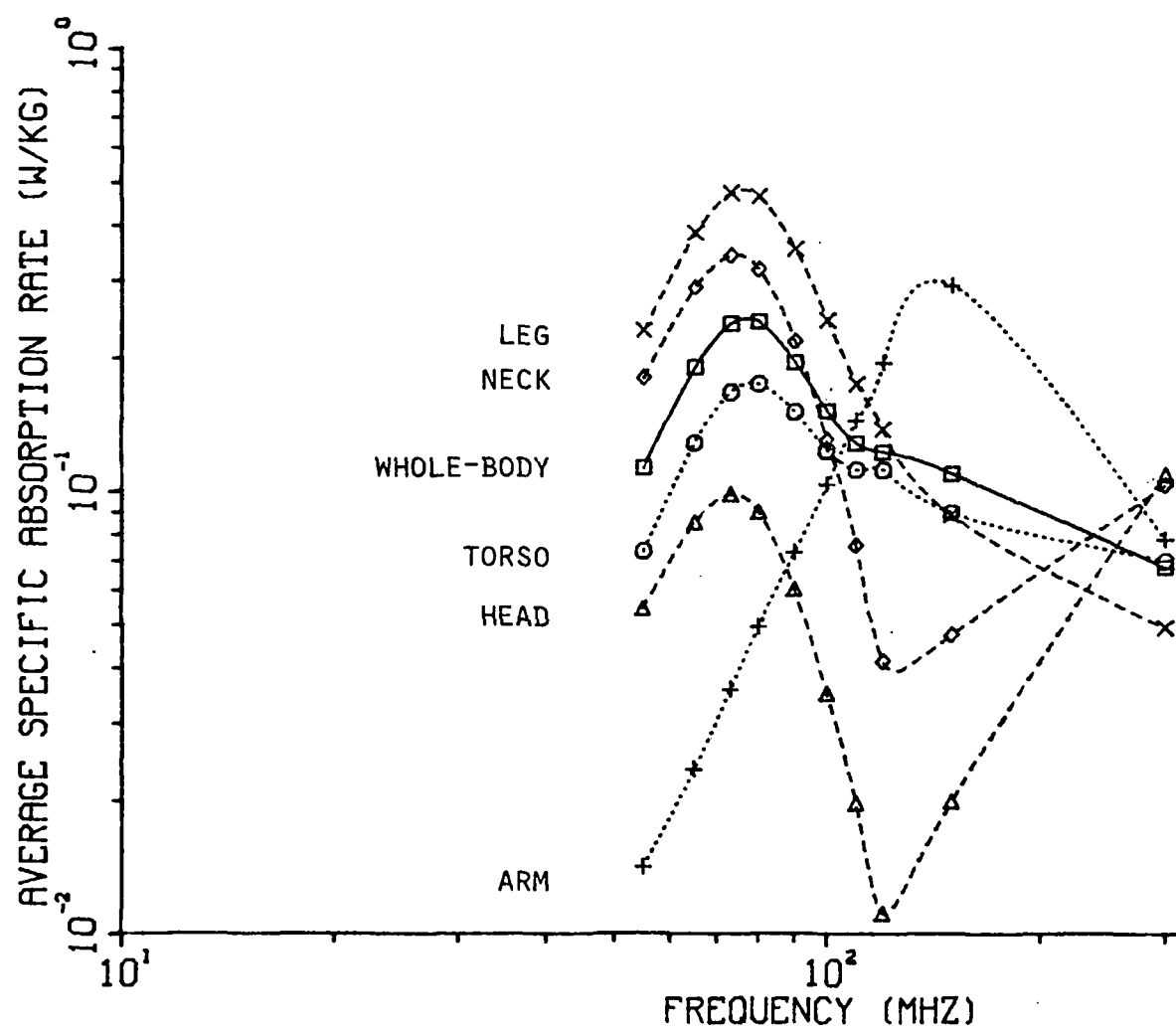


Figure 2.  
Part-body SAR for homogeneous model of man. Incident intensity =  $1 \text{ mW.cm}^2$ .

whole-body SAR are typically within 20% of values found for prolate-spheroidal and ellipsoidal models<sup>11</sup>. Unlike earlier numerical models the distribution of absorbed energy within the model is in good agreement with that found experimentally for homogeneous phantom models<sup>12</sup>. For free space irradiation with this polarization near resonance, the local absorption in the legs and neck is considerably higher than the whole-body average while the torso has less than average absorption.

When the inhomogeneous complex permittivities are used with the model, a change of less than two percent occurs typically in the whole-body SAR, but a more significant change occurs in the distribution of energy deposition. Figures 3 and 4 illustrate the distribution of absorbed energy in man at 80 MHz in free space for the homogeneous and inhomogeneous models, respectively. One difference is that the inhomogeneous model has reduced absorption in regions with high bone content.

In previously reported experimental<sup>13</sup> results on whole body SAR for man, an anomalous increase in the rate of energy deposition was observed in the region of 470 MHz for  $\vec{k} \parallel \hat{L}$  and  $\vec{E} \parallel \hat{L}$  orientations. This has now been identified as the first (geometrical) resonance frequency of the head. Continuing experiments have given the absorption cross section for the head region as large as 3.1 times the physical cross section, perhaps on account of reflections from the nearby torso. At the head resonance frequency, an SAR 4.5 times the average value for the rest of the body has been experimentally observed.

Higher order resonances based on a multilayer formulation may exist for the head region at higher frequencies. Initial numerical results show one such resonance at frequencies of the order of 2000 MHz. It is, however, anticipated that the overall absorption cross section at these frequencies may not be as large as that for the first resonance, where an enhancement factor of 3.1 has been observed for the head region.

The frequency for maximum energy deposition in the arms is approximately 150 MHz (see Fig. 2) with an absorption cross section that is 2.3 times the physical cross section.

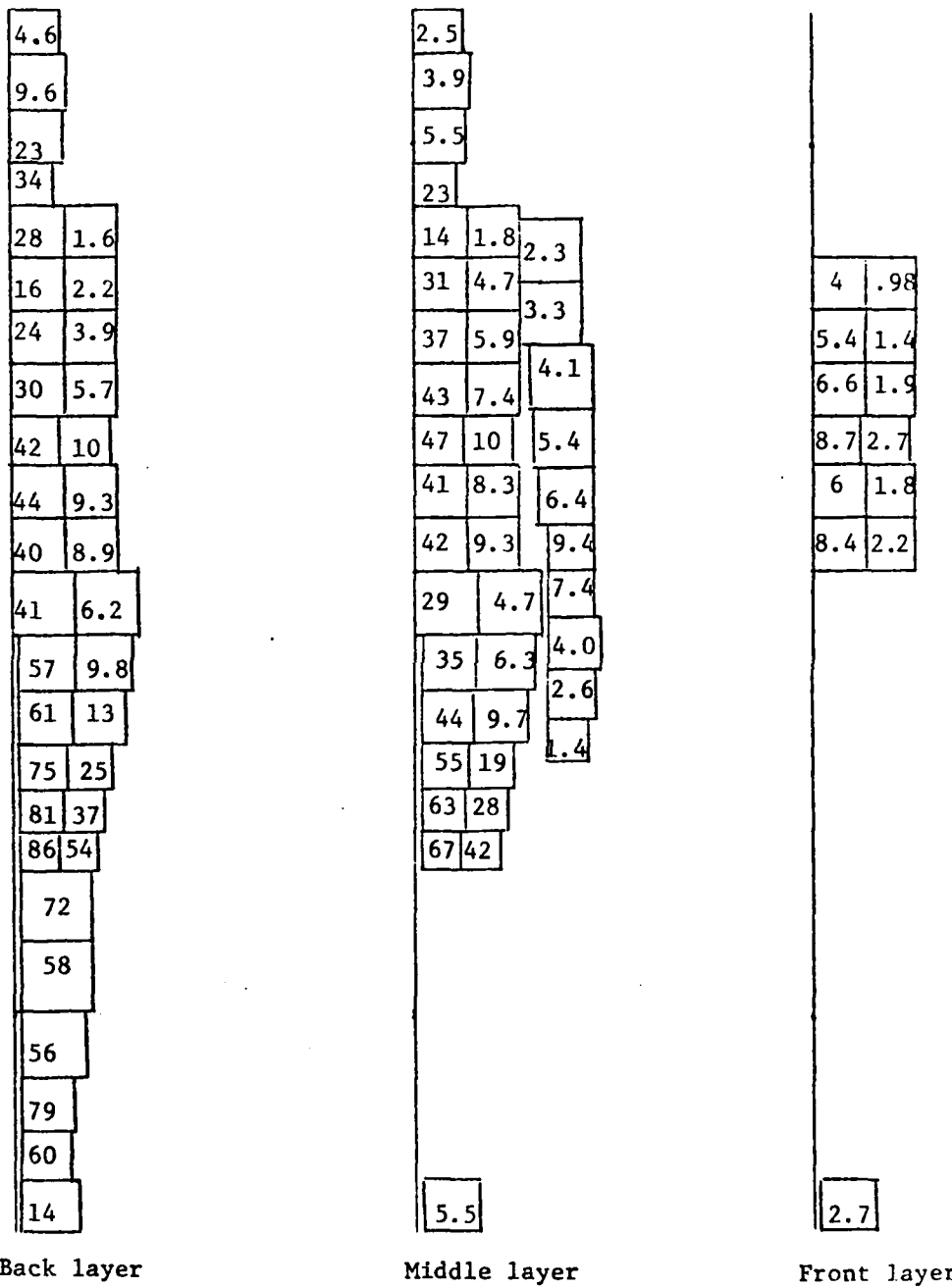


**Figure 3.**  
 Local SAR values (watts/kg per  $\text{mW/cm}^2$ )  $\times 100$  for homogeneous model of man  
 with vertical polarization at 80 MHz.

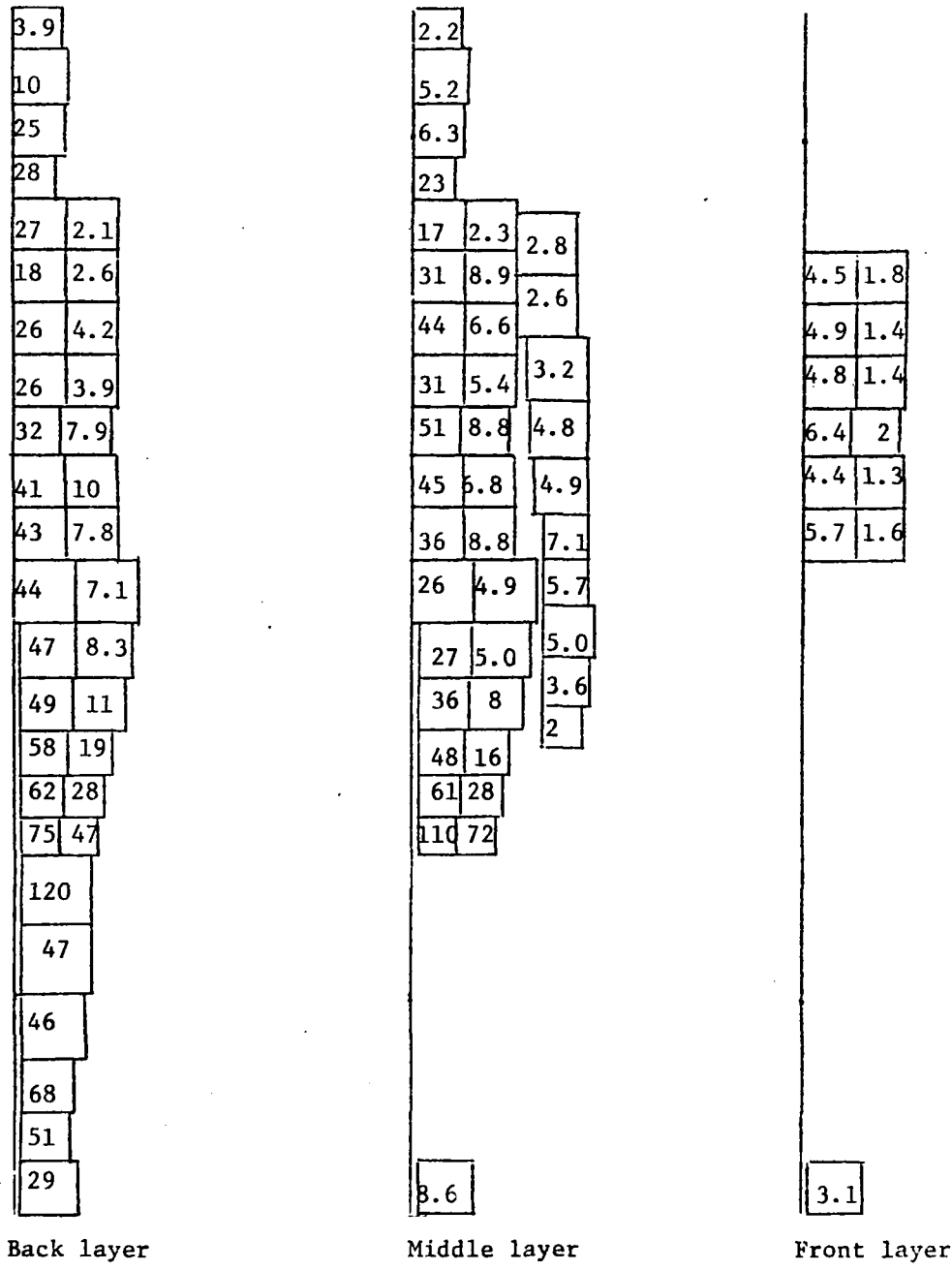


Figure 4. Local SAR values (watts/kg per  $\text{mW/cm}^2$ )  $\times 100$  for inhomogeneous model of man with vertical polarization at 80 MHz.

## GROUND EFFECTS

Experimental observations of ground and reflector effects<sup>13</sup> have been reported previously but numerical methods have not been available to explain the observations. We have used image theory to reduce the problem of man above ground or in front of reflectors to a multibody problem in free space. Symmetries have been used to reduce the matrix size.

All calculations of ground effects have assumed that man is standing on or above a perfectly conducting ground plane that is infinite in extent. The incident field is vertically polarized with  $k$  directed front-to-back on the man. Internal fields in the model are the same as those in one half of a double-man consisting of the model and its image in free space.

The resonance frequency of man standing on a ground plane is one half that for man in free space. The SAR of man on the ground plane at the reduced resonant frequency is within 2 percent of the SAR for man in free space at the free-space resonance frequency.

At 10 MHz the SAR of man standing on a ground plane is 0.0163 watts/kg per  $\text{mW/cm}^2$ , which is about seven times that found for the same model in free space. The enhancement in SAR due to the ground effect is found since the frequency of 10 MHz is much closer to the grounded man resonance frequency ( $\approx 35$  MHz) than to the free-space resonance frequency ( $\approx 70$  MHz).

Figures 5 and 6 illustrate the distribution of absorbed energy in man at 10 MHz in free space and in contact with the ground plane, respectively. The enhancement factor in local energy deposition due to the ground effect is about 60 in the heel area.

Figure 7 shows the part body and whole body SAR for the inhomogeneous model of man with different spacings from the ground plane at 10 MHz. A small separation that breaks electrical contact with the ground plane is sufficient to eliminate much of the ground effect.

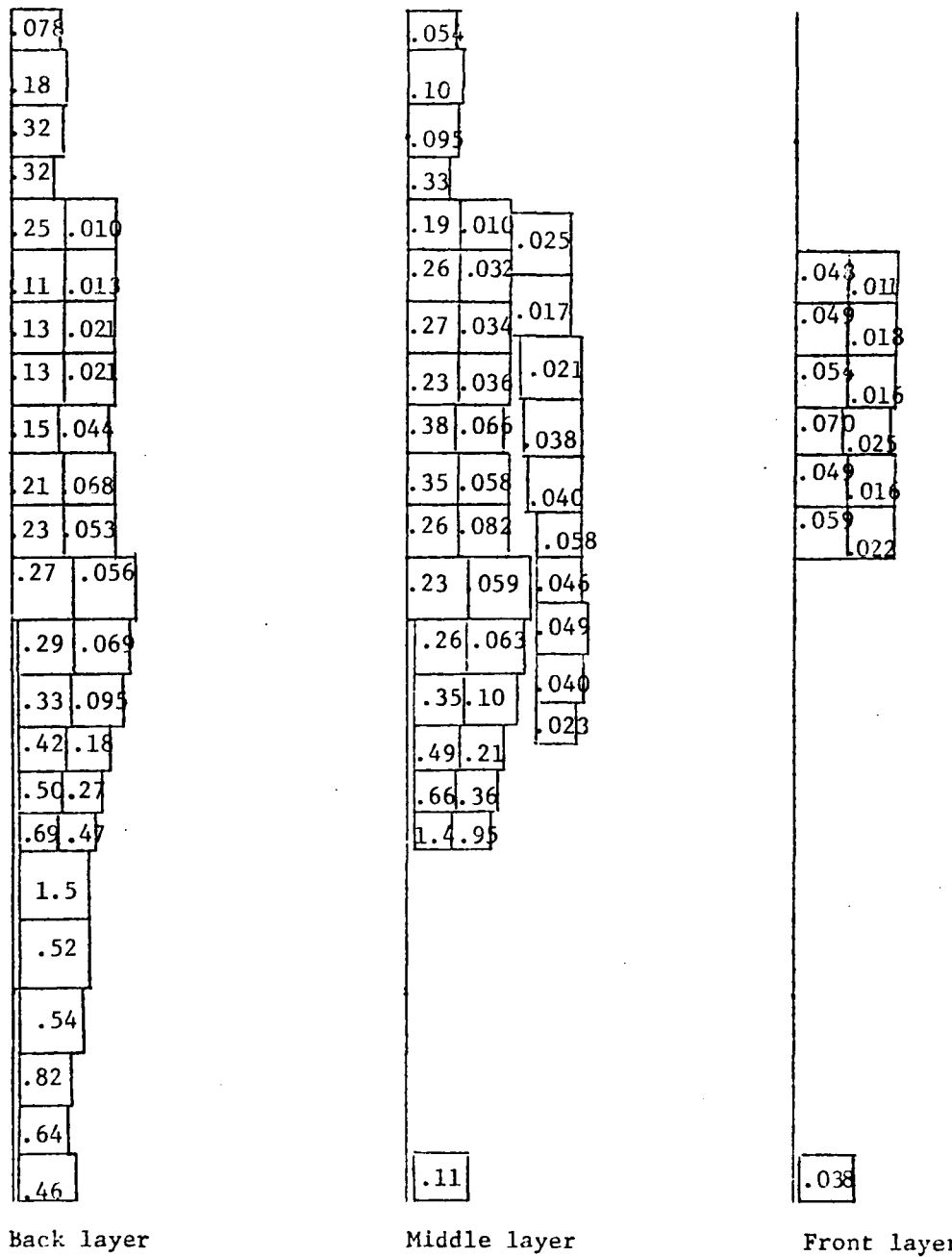


Figure 5.  
Local SAR values (watts/kg per  $\text{mW/cm}^2$ )  $\times 100$  for inhomogeneous model of man in free space at 10 MHz.

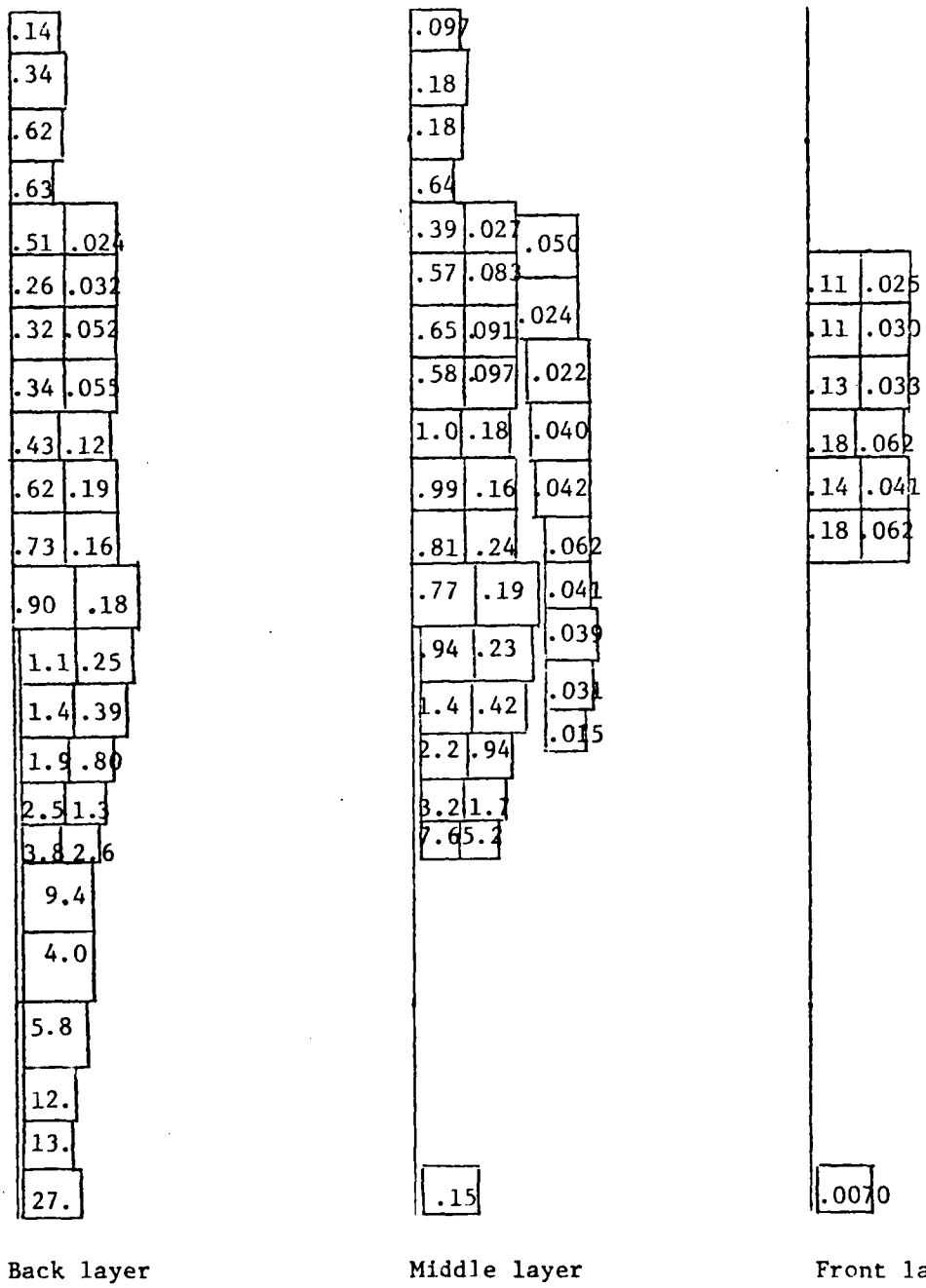


Figure 6.  
 Local SAR values (watts/kg per  $\text{mW/cm}^2$ )  $\times 100$  for inhomogeneous model of man standing on a ground plane at 10 MHz.

## REFLECTOR EFFECTS

All calculations of reflector effects have assumed that man is standing in front of a reflector that is perfectly conducting and infinite in extent. The incident field is vertically polarized with  $\vec{k}$  directed front-to-back on the man. One image is required for a flat reflector and three are needed for a  $90^\circ$  corner reflector.

At 65 MHz the computed SAR is 4.87 times the free-space value when man is  $0.1875 \lambda$  in front of a flat reflector and 16.6 times the free-space value when man is  $1.5 \lambda$  in front of the axis of a  $90^\circ$  corner reflector.

Antenna theory may be used<sup>13</sup> to calculate the ratio of effective area of a half-wave dipole with a reflector to that of the dipole in free space. Such ratios are within 16% of the above calculated factors of enhancement of SAR due to reflector effects.

For certain length-to-width ratios, the experimentally<sup>13</sup> observed enhancement in energy deposition is 30 to 40% higher than that anticipated from antenna theory and calculated numerically for reflectors of infinite dimensions. This phenomenon is, once again, in agreement with experimentally obtained antenna gains for finite size<sup>14</sup> corner reflector antennas. Significantly enhanced rates of energy deposition are projected for all kinds of corner angles (not just the values corresponding to  $180^\circ/n$ , where  $n$  is an integer) and for reflector lengths and widths that are no more than a fraction of a wavelength at the resonance frequency.

## MULTIBODY EFFECTS

Driving point impedance values for a broadside array of two half-wave dipoles<sup>15</sup> have been used to prepare Fig. 8 which shows the variation of effective area per dipole with spacing. If the two dipoles are tangent, each will receive approximately one half the energy it would receive if isolated in free space. For separations greater than two or three free space wavelengths, the antennas have little coupling so that each has an effective area approximating the isolated free space value. At a spacing of  $0.65 \lambda$ , each dipole will receive about 56% more energy than it would if it were isolated.

Figure 7.  
SAR in man for different spacings from the ground; frequency = 10 MHz.  
Incident intensity = 1 mW/cm.

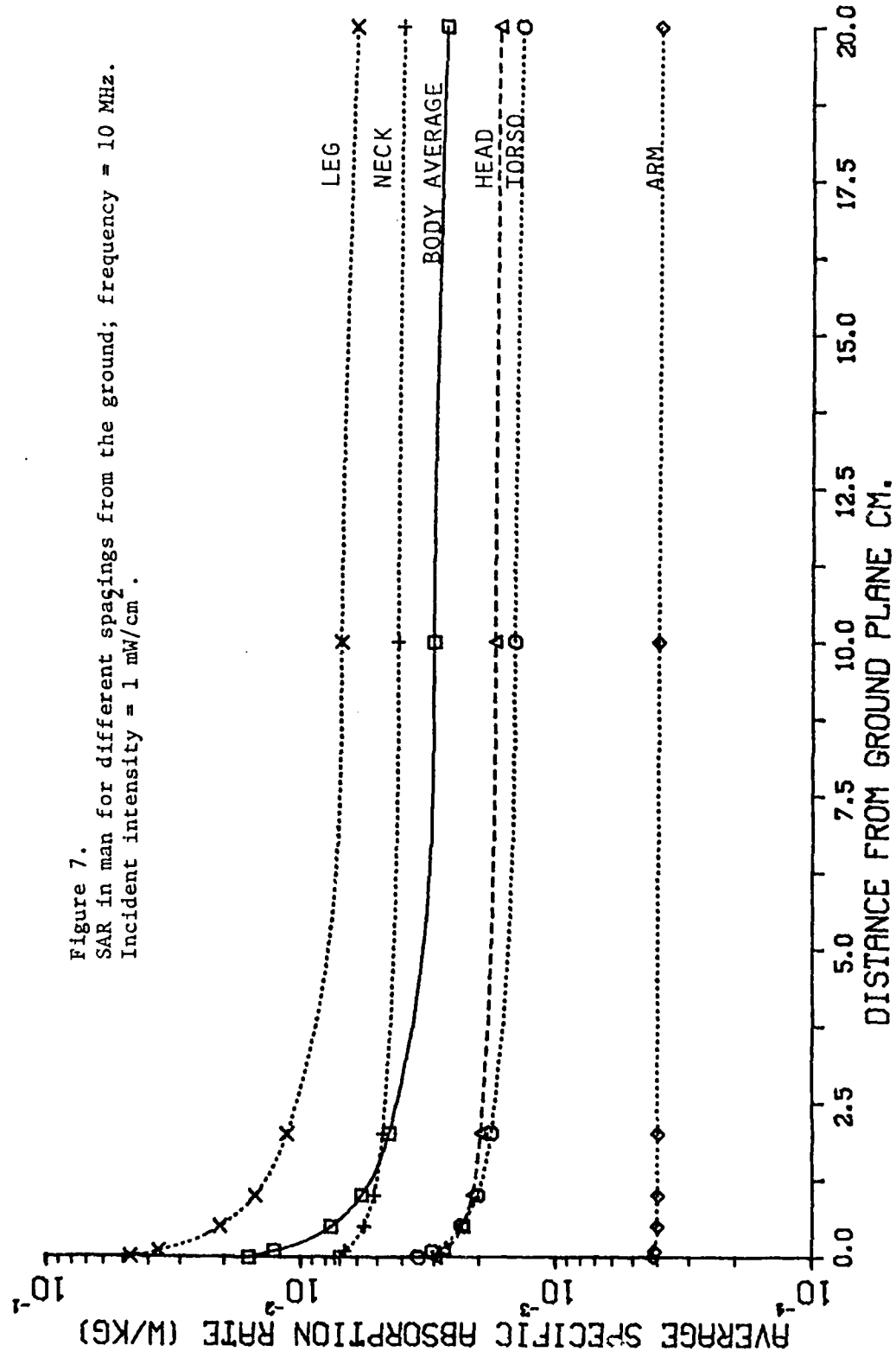
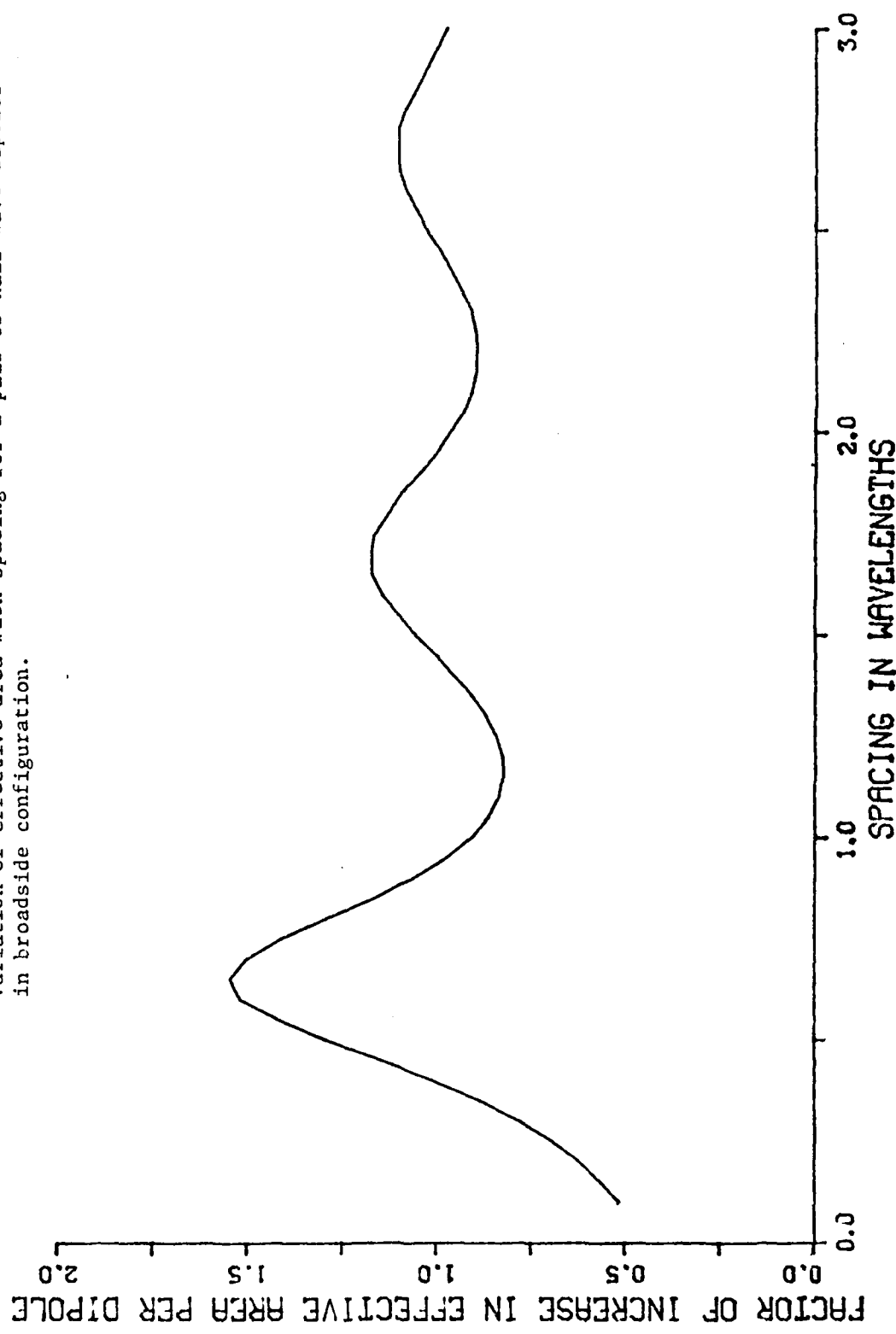


Figure 8.  
Variation of effective area with spacing for a pair of half-wave dipoles  
in broadside configuration.



It has been shown<sup>13</sup> that the energy absorbed by man at resonance corresponds to the energy received by a half-wave dipole of length approximately equal to the height of the man. Mutual impedance, and hence driving point impedance, values are dependent upon the shape of the antenna elements, but we may expect that the variation of SAR with spacing for two men near resonance is similar to Fig. 8.

Preliminary experiments using animals have confirmed the existence of multibody effects. We have used anesthetized adult rats with  $\vec{E} \parallel \hat{L}$  orientation and frontal (broadside) incidence. In tests with 480 ± 50 gram rats at 600 MHz with an incident intensity of  $100 \text{ mW/cm}^2$ , isolated animals had an average temperature increase of  $0.675^\circ \text{ C/min}$ . For two animals placed  $0.65 \lambda$  apart, the monitored animals had an average temperature increase of  $1.14^\circ \text{ C/min}$ . A 70 percent increase in SAR was caused by the presence of the second animal.

Antenna theory suggests similar enhancements in SAR for targets in the subresonance and supraresonance regions, also for spacing on the order of  $0.65\text{--}0.7 \lambda$ . Furthermore, a greater enhancement in the SAR by a factor as large as 2.5 is anticipated for the inner targets with three or more elements.

## REFERENCES

1. G. W. Hohmann, *Geophys.* 40, 309 (1975).
2. N. Diffrient, A. R. Tilley and J. C. Bardagjy, *Humanscale 1/2/3*, MIT Press, Cambridge, 1974.
3. D. J. Morton, *Manual of Human Cross Section Anatomy*, Williams and Wilkins, Baltimore, Second Edition, 1944.
4. A. C. Eycleshymer and D. M. Schoemaker, *A Cross-Section Anatomy*, D. Appleton and Company, New York 1911.
5. C. C. Johnson and A. W. Guy, *Proc. IEEE* 60, 692 (1972).
6. C. C. Johnson, C. H. Durney and H. Massoudi, *IEEE Trans. MTT-23*, 739 (1975).
7. H. P. Schwan, *Advances in Biological and Medical Physics*, Vol. V, (ed. by J. H. Lawrence and C. A. Tobias) Academic Press, 1957.
8. K. M. Chen and B. S. Guru, *Induced EM Field and Absorbed Power Density Inside Human Torso by 1 to 500 MHz EM Waves*, Technical Report No. 1, NSF Grant ENG 74-12603, April 1976.
9. M. J. Hagmann, O. P. Gandhi and C. H. Durney, *IEEE Trans. MTT-25*, (1977).
10. M. J. Hagmann, O. P. Gandhi and C. H. Durney, *Improvement of Convergence in Moment-Method Solutions by the Use of Interpolants*, *IEEE Transactions*, to be published.
11. C. C. Johnson, C. H. Durney, P. W. Barber, H. Massoudi, S. J. Allen and J. C. Mitchell, *Radio Frequency Radiation Dosimetry Handbook*, USAF Report SAM-TR-76-35, September 1976.
12. O. P. Gandhi, K. Sedigh, G. S. Beck and E. L. Hunt, *USNC/URSI Meeting Summary of Papers*, 201 (1975).
13. O. P. Gandhi, E. L. Hunt and J. A. D'Andrea, *Deposition of Electromagnetic Energy in Animals and Models of Man*, USNC/URSI Meeting, Amherst, Massachusetts (1976).
14. H. V. Cottany and A. C. Wilson, *IRE Trans. AP-6*, 366 (1958).
15. R. W. P. King, *Tables of Antenna Characteristics*, IFI/Plenum, New York, 1971.

## APPENDIX F

IEEE TRANSACTIONS ON MICROWAVE THEORY AND TECHNIQUES, VOL. MTT-27, NO. 9, SEPTEMBER 1979

809

# Head Resonance: Numerical Solutions and Experimental Results

MARK J. HAGMANN, MEMBER, IEEE, OM P. GANDHI, FELLOW, IEEE, JOHN A. D'ANDREA, AND  
INDIRA CHATTERJEE, STUDENT MEMBER, IEEE

**Abstract**—We have used numerical solutions and experiments with phantom models of man, and experiments with the Long Evans rat to show the existence of head resonance. Greatest absorption in the head region of man occurs at a frequency of about 375 MHz. Absorption is stronger for wave propagation from head to toe than it is when the electric field is parallel to the long axis. The highest absorption cross section for the human head is projected to be approximately 3.5 times its physical cross section.

### I. INTRODUCTION

WE HAVE previously reported numerical solutions for the deposition of electromagnetic energy in a realistic model of man which showed the existence of

resonances for body parts such as the head and arms, as well as for the whole body [1]. Further work has been done regarding head resonance, since we believe the phenomenon may be important in the study of behavioral effects, blood-brain barrier permeability, cataractogenesis, and other microwave bioeffects.

Our results show that the first resonance of the intact human head occurs at a frequency of about 375 MHz and has an *S* parameter (ratio of absorption cross section to physical cross section) of about 3.5 for incident plane waves propagating from head to toe. Earlier calculations for a spherical model of the isolated human head showed a geometrical resonance with *S* = 1.1 near 450 MHz, and a second resonance with *S* = 1.4 occurring near 2.1 GHz when allowance is made for the inhomogeneous structure by using a multilayered model [2]. The results of our study

Manuscript received October 16, 1978; revised February 23, 1979.  
The authors are with the Departments of Electrical Engineering and Bioengineering, University of Utah, Salt Lake City, UT 84112.

suggest that the absorption in the head region is strongly dependent on the presence of the rest of the body.

In the following sections of this paper we present new data regarding resonance of the intact human head obtained using both numerical solutions and phantom models for man, as well as experimental results for the Long Evans rat.

## II. NUMERICAL SOLUTIONS

Fig. 1 illustrates a realistic model of man which we used in earlier computations showing head resonance [1]. The model was obtained by using a total of 180 cubical cells of various sizes to obtain a best fit of the contour on diagrams of the 50th percentile standard man [3]. All numerical solutions reported in this paper are for a model having more detailed modeling of the neck and head, as shown in Figs. 2 and 3. Representation of the rest of the body is as shown in Fig. 1. Note that the number of cells has been increased from 12 to 144 in the head region, and from 4 to 32 in the neck region for a whole body total of 340 cells.

We have used a moment-method solution of the electric field integral equation with a pulse function basis and delta functions for testing [1] and an interpolant follow-up for improvement of convergence [4]. Since there are three unknown field components per cell, even using one plane of symmetry of the model the matrix is  $510 \times 510$  complex, which corresponds to a system of 1020 simultaneous equations in 1020 real unknowns. Noniterative matrix solutions are required since the matrix has at least one complex eigenvalue having a real part with magnitude exceeding unity [5]. A total of 17 h of dedicated usage of a PDP-10 digital computer was required for each solution. Fortunately, weak diagonal dominance which is inherent in the matrix formulation contributes to the conditioning to allow reasonable round-off errors with such a large matrix size.

Figs. 4 and 5 show the head and whole-body specific absorption rate (SAR) calculated for the new model of man in free space with an incident plane wave having two different polarizations. Note that head resonance is more pronounced when the propagation vector is parallel to the body axis ( $\hat{k} \parallel \hat{L}$ ) with propagation from head to toe than it is when the electric field is parallel to the long axis ( $\hat{E} \parallel \hat{L}$ ). Experimental data for the Long Evans rat, described in Section IV of this paper, also suggest that head resonance is stronger for  $\hat{k} \parallel \hat{L}$  than for  $\hat{E} \parallel \hat{L}$  polarization. Some experimental data obtained using biological phantom models of man are presented for comparison in the next section of this paper.

Figs. 6 and 7 illustrate the distribution of absorbed energy in the head region near head resonance. The presence of a hot spot exists near the center of the head which is also seen in the distribution at the geometrical resonance for a sphere [2]. The distribution shown in Figs. 6 and 7 is only approximate since a homogeneous model was used in all calculations.

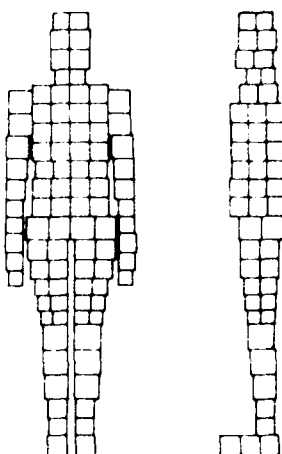


Fig. 1. Realistic model of man.



Fig. 2. Detailed modeling of the neck and head, front view.

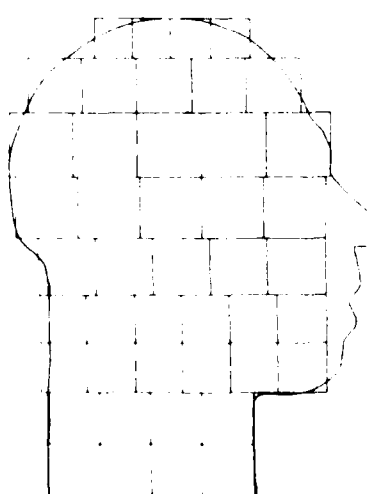


Fig. 3. Detailed modeling of the neck and head, side view.



Fig. 4. Head and whole-body absorption for  $E_{\parallel}$ , propagation from front to back, incident intensity =  $10 \text{ mW/cm}^2$ .



Fig. 5. Head and whole-body absorption for wave propagation from head to toe,  $E$  front to back, incident intensity =  $10 \text{ mW/cm}^2$ . Open markers are for numerical solutions and solid markers are for phantom models of man.

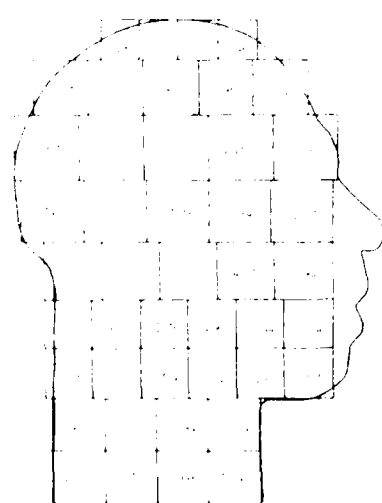


Fig. 6. Local SAR values, watts per kilogram for  $10 \text{ mW/cm}^2$  incident fields, Inner layer of cells, 350 MHz,  $E$  head to toe,  $E$  front to back, whole-body average = 0.6132, head average = 2.014.

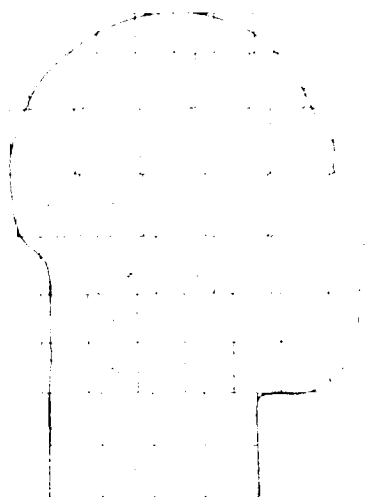


Fig. 7. Local SAR values, watts per kilogram for  $10 \text{ mW/cm}^2$  incident fields, Outer layer of cells, 350 MHz,  $E$  head to toe,  $E$  front to back, whole-body average = 0.6132, head average = 2.014.

### III. EXPERIMENTAL RESULTS FOR PHANTOM MODELS OF MAN

We have used accurately scaled figurines [6] of 20.3-, 25.4-, 33.0-, and 40.6-cm length, with biological phantom mixtures [7], described in Table I, to model the exposure of man to plane waves in free space. All values of absorbed dose were measured using a Thermonetics model 2401-A gradient layer calorimeter. Each figurine had the head attached to the torso by a layer of saline-soaked cloth, thus maintaining conductive contact but allowing easy separability for measurement of energy deposition in the head. For determination of the absorbed dose in the head, after separation, the part of the polyurethane mold holding the biological phantom material shaped in the form of the head was wrapped in Saran Wrap to limit loss of water by evaporation.

Table II gives the experimental values of SAR for figurines containing biological phantom mixtures and irradiated with propagation from head to toe. A plot of data from Table II on Fig. 5 shows good agreement between the numerical solutions and experiments with phantom models of man. The values in Table II suggest that for propagation from head to toe, the magnitude of absorption in the head region near head resonance is not strongly dependent on orientation of the  $E$  vector.

Both the numerical solutions in Section II and the phantom figurines have used homogeneous models. The next section of this paper presents experimental data obtained with the Long Evans rat.

### IV. EXPERIMENTAL RESULTS FOR THE LONG EVANS RAT

Table III gives the experimental values of SAR for several tests made with both freshly killed and anesthetized Long Evans rats. The number of measurements ( $n$ )

**TABLE I**  
COMPOSITIONS AND PROPERTIES OF PHANTOM MIXTURES, EXPERIMENTAL FREQUENCY = 2450 MHz

Experimental Orientation Design Frequency (MHz)	Normalized Whole-Body Absorbed Heat Content*		Composition of Phantom Mixture (%)		Measured Resonance Heat Content (%)	Relative Intensity (%)
	Water	Whole Body	H <sub>2</sub> O	CH <sub>3</sub> Cl		
Head to toe	1.000	1.000	1.00	0.00	1.000	100.0
Head to tail	0.716	0.716	0.71	0.29	0.716	100.0
Head to side	0.716	0.716	0.71	0.29	0.716	100.0
Head to side	0.716	0.716	0.71	0.29	0.716	100.0
Head to side	0.716	0.716	0.71	0.29	0.716	100.0

\* Average absorption coefficient of 0.0016 percent was used, except for the head-to-side orientation which had a value of 0.0014 percent. The absorption path length was constant using either the average of the two values for the head-to-tail and head-to-side orientations or the mean of the two values for the head-to-toe orientation.

† Measured at 2450 MHz. Attenuation from 2450 to 1000 MHz was taken as 0.001 dB/decade.

**TABLE II**  
SAR\* OF PHANTOM MODELS OF MAN FOR WAVE PROPAGATION  
FROM HEAD TO TOE

Orientation	Head Absorbed Heat Content (%)	Whole- Body Absorbed Heat Content (%)	SAR	
			Head Absorbed Heat Content (%)	Whole- Body Absorbed Heat Content (%)
Head to toe	1.000	1.000	1.000	1.000
Head to tail	0.716	0.716	0.716	0.716
Head to side	0.716	0.716	0.716	0.716
Head to side	0.716	0.716	0.716	0.716
Head to side	0.716	0.716	0.716	0.716

\* With  $E_0 = 10 \text{ mW/cm}^2$ , incident at 2450 MHz.

and calculated standard errors in the measurements (SEM) are also given in the Table. Scaling suggests that head resonance for a medium-sized rat should occur near the test frequency of 2450 MHz.

The anesthetized rats were given a 45-mg/kg dose of sodium pentobarbital to facilitate use of a fixed orientation and limit thermo-regulatory functions. Calorimetric measurements were used to determine the absorbed dose in the freshly killed rats. These measurements were made using a Thermonetics model 2401-A Seebeck envelope gradient layer calorimeter. The dose was also determined by measurement of the rate of increase in rat colonic temperature and brain temperature, using liquid crystal temperature optical fiber (LCOF) probes, in the anesthetized rats. For brain temperature the LCOF probe was implanted in a tracheal hole 3 mm posterior to the Bregma cranial suture, 2 mm lateral to the midline cranial suture, and 6–8 mm below the top surface of the cortex.

The results in Table III show that head resonance is more pronounced for  $k \parallel E$  than for  $E \parallel k$  orientation which was also noted with the numerical solutions. Note that the ratio of head-to-whole-body heat content is less for the anesthetized rat than for the dead rat. Blood circulation may be reducing the relative magnitude of heating in the head region.

**TABLE III**  
SAR\* VALUES FOR THE LONG EVANS RAT

Orientation	Head Absorbed Heat Content (%)	Whole-Body Absorbed Heat Content (%)	SAR		
			With $E_0 = 10 \text{ mW/cm}^2$ , Incident at 2450 MHz		
			n = 2	n = 4	n = 8
Anesthetized rat	25.11	25.07	25.07	24.80	24.80
Dead rat	21.49	21.58	21.58	21.69	21.69

\* With  $E_0 = 10 \text{ mW/cm}^2$ , Incident at 2450 MHz.

## V. SUMMARY AND CONCLUSIONS

We have used three methods to study head resonance: numerical solutions, experiments with phantom models of man, and experiments with the Long Evans rat. All three approaches show the existence of head resonance. The phenomenon appears to have a greater magnitude for wave propagation from head to toe than for  $E \parallel k$  orientation. For the former orientation the head absorption cross section as high as 3.5 times the physical cross section is projected.

The numerical solutions, which are supported by the experimental results for phantom models of man, suggest that the absorption is much stronger than would be predicted using a sphere to model the isolated head. The strong dependence on polarization would, of course, also be missed using a spherical model.

We believe that the enhanced absorption in the head region may make head resonance significant in the study of behavioral effects, blood-brain barrier permeability, cataractogenesis, and other microwave bioeffects.

## REFERENCES

- [1] O. P. Gandhi and M. J. Hagmann, "Some recent results on deposition of electromagnetic energy in animals and in models of man,"

- presented at the USNC/URSI meeting, Airlie, VA, Oct. 30–Nov. 4, 1977. To be published in a special issue of *Radio Sci.* based on selected papers of the meeting.
- [2] W. T. Jones and R. J. Spiegel, "Resonance absorption of microwaves by the human skull," *IEEE Trans Biomed Eng.*, vol. BME-21, Jan. 1974, pp. 46–48.
  - [3] N. Diffrient, A. R. Tilley, and J. C. Bardaggy, *Humanscale 1–2–3*, Cambridge, MA: M.I.T. Press, 1974.
  - [4] M. J. Hagmann, O. P. Gandhi, and C. H. Durney, "Improvement of Convergence in moment-method solutions by the use of interpolants," *IEEE Transactions on Microwave Theory and Techniques*, Vol. MTT-26, No. 11, November 1978, pp. 904–908.
  - [5] D. M. Young, *Iterative Solution of Large Linear Systems*, New York: Academic, 1971.
  - [6] O. P. Gandhi, E. L. Hunt, and J. A. D'Andrea, "Deposition of electromagnetic energy in animals and in models of man with and without grounding and reflector effects," *Radio Science*, vol. 12, no. 6(S), 1977, pp. 39–48, special issue based on selected papers of the 1976 USNC/URSI meeting in Amherst, MA.
  - [7] O. P. Gandhi and K. Sedigh, "Biological phantom materials for simulation at different frequencies," presented at the USNC/URSI meeting, Amherst, MA, Oct. 11–15, 1976.

## APPENDIX G

400

IEEE TRANSACTIONS ON BIOMEDICAL ENGINEERING, VOL. BME-26, NO. 7, JULY 1979

# Electromagnetic Absorption in a Multilayered Model of Man

PETER W. BARBER, MEMBER, IEEE, OM P. GANDHI, FELLOW, IEEE, MARK J. HAGMANN,  
MEMBER, IEEE, AND INDIRA CHATTERJEE, STUDENT MEMBER, IEEE

**Abstract**—A multilayered planar model is used to examine the dependence of whole-body power absorption on the configuration of surface layers, e.g., skin, fat, and muscle which normally occur in biological bodies. It is found that the layering resonance for three-dimensional bodies (as opposed to the geometrical resonance) can be predicted quite accurately by a planar model. Calculations for a multilayered prolate spheroidal model of man predict a whole-body layering resonance at 1.8 GHz with a power absorption 34 percent greater than that predicted by a homogeneous model.

## INTRODUCTION

RECENT interest in quantifying both the hazardous and potentially beneficial effects of nonionizing electromagnetic (EM) radiation on man has been the impetus for a great deal of experimental and theoretical research. Of particular interest are calculations to determine the relationship between incident power density and the resulting absorbed power due to whole-body irradiation of man. Recent theoretical methods that have been used include a perturbation approach [1] useful for analyzing homogeneous ellipsoidal models and an integral equation method [2] for analyzing homogeneous prolate spheroidal models. The absorption characteristics of inhomogeneous irregular shaped models constructed of cubical sub-volumes have been studied by volume integral moment method techniques [3], [4]. In these whole-body irradiation studies, the power absorption is determined as a function of the angle of incidence, polarization, and frequency of the incident EM wave. Usually the results are shown as a plot of specific absorption rate in watts/kilogram versus frequency, where an incident power density of 1 mW/cm<sup>2</sup> is assumed. Typically, for a given angle of incidence and polarization, the power absorption increases relatively rapidly with frequency to a resonant peak and then slowly decreases to an asymptotic high-frequency limit.

There is another interaction which takes place which has not been considered in recent whole-body calculations. Both homogeneous and inhomogeneous models have not accounted for the EM interaction due to the surface layering of biological

Manuscript received March 13, 1978; revised February 1979. This work was supported in part by the United States Army Medical Research and Development Command under Contract DAMD-17-74-C-4092.

The authors are with the Department of Electrical Engineering and the Department of Bioengineering, University of Utah, Salt Lake City, UT 84112.

bodies, e.g., the layers of skin, fat, and muscle. An investigation of these effects is the subject of this paper.

## ABSORPTION EFFECTS DUE TO LAYERING

Early calculations to assess the biological significance of EM radiation used planar models consisting of skin, fat, and semi-infinite muscle layers [5]. Later a two-layered (fat and muscle) spherical model was used [6]. These earlier investigations are summarized in [7]. Both studies showed that the absorption characteristics are critically dependent on the number and thickness of the surface layers. More recent whole-body calculations have not considered the effect of surface layers. One reason for this is due to the unavailability of multilayered analytical solutions for any geometry other than the plane, infinite circular or elliptical cylinder, and sphere. In the case of numerical approaches, such as the volume moment method technique, practical limitations on the number of cells which may be used prohibit consideration of layering effects.

A six-layered sphere has recently been used to model the isolated head [8]–[10]. Of particular interest are results in [9] and [10] which compare the frequency dependent absorption in six-layered spheres with that in corresponding homogeneous spheres. One of the power absorption results in [9] has been recalculated and is shown in Fig. 1 as a plot of absorption efficiency versus frequency. This and subsequent multilayered sphere calculations were made using a Mie theory computer program based on the mathematical development in [8]. The absorption efficiency is the total power absorbed divided by the power incident on the geometrical cross section. An absorption efficiency greater than unity indicates that the influence of the body on the incident wave extends beyond the geometrical boundary. The absorption efficiency for the homogeneous brain tissue sphere increases with frequency until the maximum is reached and then slowly decreases. The amplitude and frequency of the resonance are dependent upon the size, shape, and dielectric characteristics of the model. This maximum absorption condition can be called the *geometrical resonance*. The absorption efficiency for the six-layered model has an additional resonance which is due to the impedance matching effects of the surface layers and at this resonance the absorption efficiency is almost 30 percent greater than that at the geometrical resonance. This second maximum absorption condition can be called the *layering resonance*.

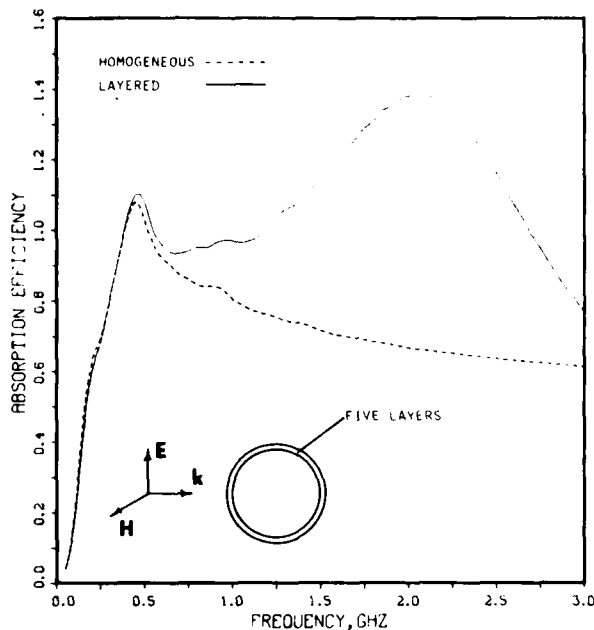


Fig. 1. Absorption characteristics of the six-layered 10-cm radius spherical head model of Joines and Spiegel [9]. The five outside layers (and thickness) are skin (0.15 cm), fat (0.12 cm), bone (0.43 cm), dura (0.1 cm), and CSF (0.3 cm). The radius of the inner brain sphere is 8.9 cm.

The most interesting feature shown in Fig. 1 is that the presence of layering enhances the absorption of the spherical model. Another feature is that the geometrical and layering resonances appear to be independent of one another, i.e., the geometrical resonances of the homogeneous and layered spheres are almost identical, while the layering resonance of the six-layered sphere appears merely as an enhancement of the absorption over that of the homogeneous sphere.

Calculations for a homogeneous and six-layered planar model have been made for the same tissue thicknesses and dielectric characteristics as were used to obtain the results in Fig. 1. The calculations were made using conventional planar techniques [11]. The brain tissue core in the spherical model was assumed to extend to infinity in the planar model. These results are shown in Fig. 2. The planar model, which does not exhibit a geometrical resonance, does however show the same layering resonance as is observed in Fig. 1 for the layered spherical model. The location of the layering resonance and the enhancement of the absorption efficiency due to the layering are almost identical for the planar and spherical models. Taking the ratio of the layered to homogeneous absorption efficiencies for the planar model in Fig. 2 and multiplying by the homogeneous sphere result in Fig. 1 gives the dashed curve in Fig. 3, a predicted absorption for the layered sphere. Comparing this predicted absorption to the actual absorption shows that the layering enhancement of the planar model can be applied to the homogeneous sphere solution to predict the absorption in the layered sphere to within 5 percent, both in absorption efficiency at a given frequency and in the location of the resonant peaks.

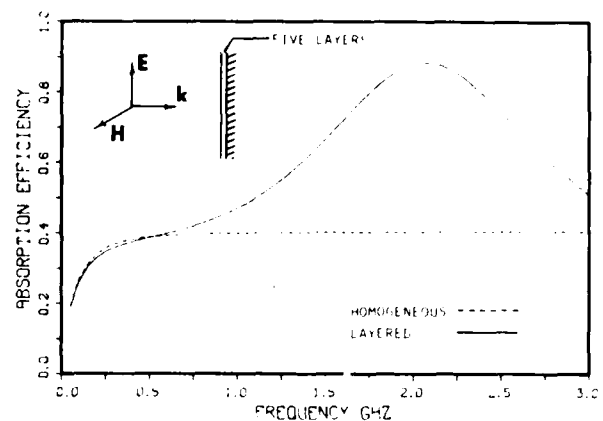


Fig. 2. Absorption characteristics of a six-layer planar model. The five outside layers are the same as those in Fig. 1. The innermost layer is semi-infinite brain material.

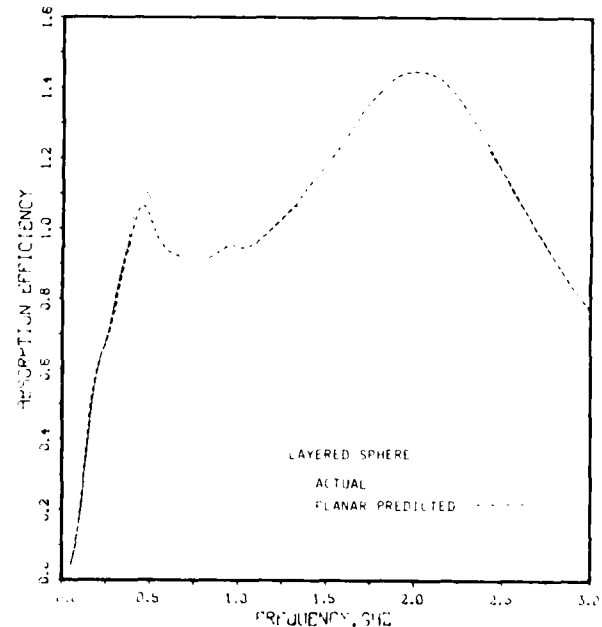


Fig. 3. Actual and planar predicted absorption characteristics of the six-layered spherical head model of Fig. 1.

There are two obvious questions that need to be answered: Why are the geometrical and layering resonances essentially independent in Fig. 1, and why does the planar model predict the layering resonance of the head model with such accuracy?

To answer the first question, consider the geometrical resonance of the head model in Fig. 1. The resonance of the homogeneous sphere is dependent on the radius and constitutive makeup of the sphere. For high-loss dielectric bodies of the type considered here, the peak absorption occurs when the ratio of circumference to free-space wavelength ( $2\pi a/\lambda = ka$ ) is about unity. For the homogeneous sphere in Fig. 1, resonance occurs when  $ka = 0.94$ . Referring to the scale drawing of the sphere in Fig. 1, it is clear that the surface layers repre-

sent a small fraction of the total sphere radius (about 10 percent). One would expect then that replacing the outer portion of the homogeneous sphere by a layered segment which on the average has similar dielectric characteristics and whose thickness is much less than a wavelength in the material will have little effect on the geometrical resonant frequency. This is the case as noted in Fig. 1. The layers have an independent resonant frequency, which in this case is approximately four times the geometrical resonant frequency. The frequency at which the layers resonate is a function of their thickness and constitutive parameters. Given the electrical characteristics of the layers, the layering resonant frequency is inversely proportional to the thickness of the layers. The fact that the layering resonant frequency is well removed from the geometrical resonant frequency of the homogeneous sphere accounts for the independence of the two resonances. Numerical calculations show that when the layers are a larger fraction of the sphere radius, i.e., the frequency of surface layer resonance approaches the geometric resonance frequency of the homogeneous sphere, then the geometrical resonance of the inhomogeneous sphere is no longer the same as the geometrical resonance of the homogeneous sphere.

Now consider the second question as to why the planar models can predict both the resonant frequency and enhancement over the homogeneous case for the layered sphere. Looking first at the resonant frequency, we note that in the planar case the incident and transmitted waves are normal to the surface. In the case of the sphere, the only statement that can be made with certainty is that the incident wave is in general not normal to the surface. However, the absorption is due to an internal interaction and the behavior of the fields transmitted into the sphere must be considered.

Snell's law can be used to relate the angle of the transmitted wave to the angle of the incident wave at local regions on the surface. Snell's law for a wave propagating from free space with permittivity  $\epsilon_0$  into a region with permittivity  $\epsilon$  is given by

$$\sin \theta_t = (\epsilon_0 / \epsilon)^{1/2} \sin \theta_i$$

where  $\theta_i$  and  $\theta_t$  are the angles of incidence and transmission, respectively, both angles being measured from the local normal to the surface. The dielectric characteristics of biological tissue are characterized by a relatively large complex permittivity. For example, at the layering resonant frequency of 2.06 GHz, the dielectric constant of the outer skin layer is 47.5-j11.4. Substituting this into Snell's law for  $\theta_i = 90^\circ$  (grazing incidence), it is found that the angle of transmission is only  $8^\circ$  from the normal. Since the angle of transmission will be even smaller for other angles of incidence, it is clear that the transmitted wave propagates almost normally into the tissue regardless of the angle of incidence, i.e., the wave transmitted into the sphere interacts with the surface layers in essentially the same manner as it does in the planar model, as shown in Fig. 4. Therefore, the resonant frequency resulting from this interaction should be the same whether the layers reside on the surface of a sphere or on the surface of a plane.

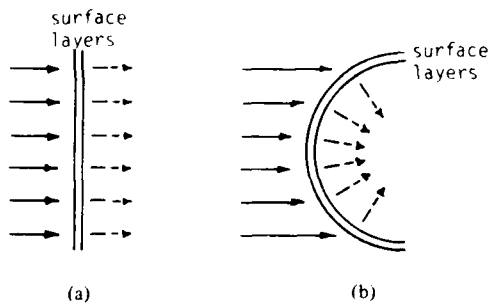


Fig. 4. The local behavior of the transmitted wave is almost identical, i.e., normal to the surface, at (a) planar and (b) nonplanar interfaces for materials with a high dielectric constant.

The fractional enhancement of the absorption due to the layering can best be understood by considering the surface layers as a frequency-dependent impedance matching device. At frequencies well removed from the layering resonant frequency (either far above or far below), the surface impedance of the layered model is the same as for the homogeneous model, i.e., at the lower frequencies the layers are so thin as to have a negligible effect and at very high frequencies the depth of penetration is so low that the transmitted power is all absorbed in the surface skin layer which has electrical characteristics almost identical to those of the brain material of the homogeneous model. In the region of the layering resonant frequency, an enhanced power transmission occurs, and this enhancement is dependent only on the surface layering configuration, and therefore the fractional enhancement in power transmission will be the same for both spherical and planar models. In the layered planar model, the power transmitted into the innermost layer is completely absorbed. The fractional power absorption enhancement in the sphere can only be the same if all the transmitted power is also absorbed. This will occur if the diameter of the innermost brain material is many skin depths thick. A calculation at the layering resonant frequency of 2.06 GHz shows that the diameter of the inner brain sphere is greater than six skin depths, insuring almost total absorption.

The planar-prediction procedure which has been outlined here for the spherical head model is equally applicable to arbitrary nonspherical bodies, because the mechanism of absorption enhancement depends only on the transmitted wave being nearly perpendicular to the surface layers, a phenomenon which is independent of the body shape. Extensive calculations for other spherical bodies and infinite cylinders (H. Massoudi, private communication) have verified the validity of the planar-prediction method. Summarizing:

- 1) The layering and geometrical absorption resonances for a layered three-dimensional object will be independent if the layering resonant frequency is well above the geometrical resonance, i.e., the surface layers responsible for the layering resonance are a small fraction of the overall size of the object.
- 2) If the resonances are independent (a condition which can be tested by comparing the geometric resonance of the homogeneous three-dimensional object with the layering resonance

of a semiinfinite planar model), then a planar model can be used to predict the absorption layering resonance for nonplanar geometries provided that the complex dielectric constant of the object is large so that the transmitted fields are normal to the layers and the skin depth in the material is small enough that the power transmitted into the interior of the three-dimensional object can be assumed to be completely absorbed. Note that 1) must be satisfied before 2) can be applied, i.e., the geometric resonance must be independent of the layering because the planar model cannot predict changes in the geometric resonance, only in the layering resonance. Conditions 1) and 2) may appear to be so restrictive as to have little application; however, they are in fact satisfied by most biological models.

#### LAYERING ABSORPTION RESONANCE IN MAN

It has been shown that a semiinfinite planar model can accurately predict the layering resonance in a nonplanar biological model. The interest here is in determining the effect of layering on the whole-body absorption of EM waves by man. This will be done by using a planar model to determine the absorption enhancement due to surface layering and then applying the resulting enhancement factor to whole-body absorption results previously obtained for a homogeneous prolate spheroidal model of man.

In the numerical calculations which follow, the dielectric characteristics of the various tissue types are taken from [12] for frequencies up to and including 10 GHz. Above 10 GHz, the permittivity and conductivity are based on the characteristics of electrically polarizable molecules [10], modified to provide continuity at 10 GHz with the lower frequency dielectric characteristics.

The surface layers of man in general consist of skin-fat-muscle or skin-fat-muscle-bone-muscle arrangements. The surface layering information required for the multilayered planar model was obtained from published anatomical cross-sectional data [13], [14]. Tissue thicknesses were examined in 79 horizontal cross sections of man. Average thickness of the surface layers of skin, fat, muscle, and bone were calculated over the front half of each cross section. It was found that the surface characteristics could be represented by three-layer skin-fat-muscle configurations in 37 of the cross sections, while the remaining 42 cross sections were better represented by a five-layer skin-fat-muscle-bone-muscle configuration. The mean thickness (and standard deviation) of the skin and fat layers for 79 cross sections are 2.25 mm (0.73mm) and 2.62 mm (1.47 mm), respectively. Corresponding values for the muscle and bone layers for 42 cross sections are 9.74 mm (4.32 mm) and 9.01 mm (4.81 mm), respectively. Calculations similar to those shown in Fig. 2 were made for each of the 79 cross sections. The results were weighted by the fractional frontal surface area which they represented and then averaged to obtain the layered curve in Fig. 5. Note that there is an absorption enhancement over homogeneous muscle tissue of 34 percent at 1.8 GHz and a reduction of 24 percent at 5.7 GHz.

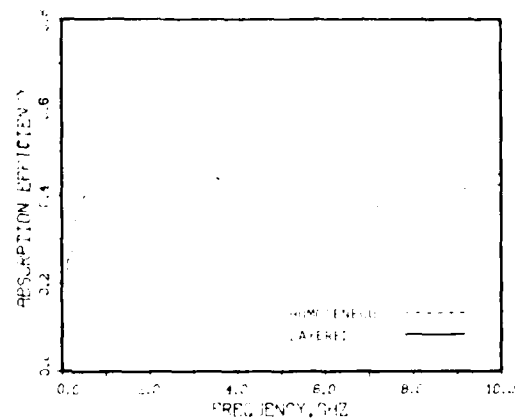


Fig. 5. Predicted whole-body layering resonance in man utilizing a planar model.

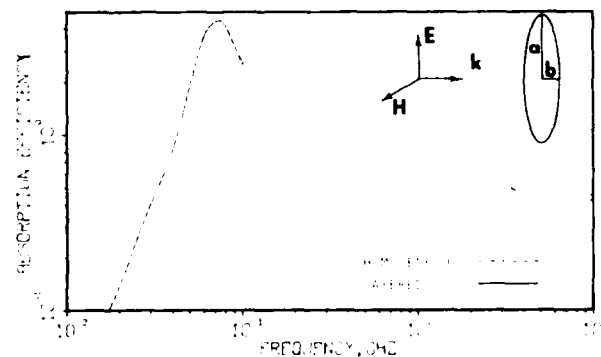


Fig. 6. Whole-body absorption versus frequency for a model of man exposed to a broadside incident plane wave polarized parallel to the long axis of the model. The dashed curve was calculated using homogeneous prolate spheroidal and circular cylindrical models ( $a/b = 6.34$ ,  $a = 0.875$  m). The solid curve is the planar-predicted absorption in a corresponding multilayered model of man.

Fig. 6 shows the whole-body absorption efficiency for both a homogeneous and a multilayered model of man. The homogeneous result was obtained using a combination of prolate spheroidal and cylindrical models [15]. The specific result shown is for the maximum absorption case which occurs when the model is illuminated broadside by a wave polarized parallel to the long axis of the model. The homogeneous results in [15] were obtained using the dielectric characteristics for a homogenized mixture of fat, bone, and muscle rather than muscle tissue alone. Homogeneous calculations for muscle tissue alone would result in a more accurate multilayered prediction; however, these results are not presently available. The multilayered result was obtained by taking the ratio of the layered to homogeneous absorption efficiencies for the planar model in Fig. 5 and multiplying the layering enhancement factor by the homogeneous result in Fig. 6. Inasmuch as the multilayered data used to generate Fig. 5 were obtained over the front surface of the cross sections of man, the multilayered curve in Fig. 6 is applicable to frontal illumination of a man model. The net effect of the surface layering is generally to increase the absorption in the postresonance region. The

layering enhancement at 1.8 GHz and reduction at 5.7 GHz represents the greatest deviation from the homogeneous result. Calculations beyond 10 GHz show that the two results merge when the depth of penetration becomes so small that the total absorption in the multilayered model occurs in the muscle-like skin tissue.

Comparing Fig. 6 to Fig. 1, it is clear that the enhancement of the absorption due to layering is not nearly as great for the whole-body model as it is for the isolated head model. There are two reasons for this. First, for the polarization of the incident wave shown here, the long slender shape of the prolate spheroidal whole-body model results in much greater absorption at the geometrical resonance (absorption efficiency = 4.43) as compared to the spherical head model (absorption efficiency = 1.08). Second, the layering enhancement for the whole-body case is much less than for the spherical head model because of the averaging over many different layering combinations in the whole-body calculations rather than using a single layering configuration as was done for the spherical head model. If an averaging scheme were used in the head model calculations, a reduction in the layering enhancement would occur there also.

### CONCLUSIONS

It has been shown that a planar model can accurately predict the layering resonance for a nonplanar geometry. Specifically, results for multilayered and homogeneous semiinfinite planar models determine a layering enhancement factor which can be applied to whole-body absorption results obtained from non-layered three-dimensional geometries to predict the absorption characteristics of three-dimensional layered geometries. The technique has been used to predict the power absorption characteristics of a multilayered model of man.

### ACKNOWLEDGMENT

The authors wish to thank Dr. L. Larsen of Walter Reed Army Institute of Research for pointing out the importance of surface layering on the EM absorption characteristics of man.

### REFERENCES

- [1] H. Massoudi, C. H. Durney, and C. C. Johnson, "Long-wavelength electromagnetic power absorption in ellipsoidal models of man and animals," *IEEE Trans. Microwave Theory Tech.*, vol. MTT-25, pp. 47-52, Jan. 1977.
- [2] P. W. Barber, "Electromagnetic power deposition in prolate spheroid models of man and animals at resonance," *IEEE Trans. Biomed. Eng.*, vol. BME-24, pp. 513-521, Nov. 1977.
- [3] K. M. Chen and B. S. Guru, "Internal EM field and absorbed power density in human torsos induced by 1-500 MHz EM waves," *IEEE Trans. Microwave Theory Tech.*, vol. MTT-25, pp. 746-756, Sept. 1977.
- [4] M. J. Hagmann, O. P. Gandhi, and C. H. Durney, "Numerical calculation of electromagnetic energy deposition for a realistic model of man," *Radio Sci.*, submitted in Nov. 1977.
- [5] H. P. Schwan and K. Li, "Hazards due to total body irradiation by radar," *Proc. IRE*, vol. 44, pp. 1572-1581, Nov. 1956.
- [6] A. Anne, "Scattering and absorption of microwaves by dissipative dielectric objects: The biological significance and hazards to mankind," Ph.D. dissertation, University of Pennsylvania, Philadelphia, PA, July 1963.
- [7] H. P. Schwan, "Radiation biology, medical applications, and radiation hazards," in *Microwave Power Engineering*, vol. 2, E. C. Okress, Ed., New York: Academic, pp. 213-243, 1968.
- [8] A. R. Shapiro, R. J. Lutomirski, and H. T. Yura, "Induced fields and heating within a cranial structure irradiated by an electromagnetic plane wave," *IEEE Trans. Microwave Theory Tech.*, vol. MTT-19, pp. 187-196, Feb. 1971.
- [9] W. L. Joines and R. J. Spiegel, "Resonance absorption of microwaves by the human skull," *IEEE Trans. Biomed. Eng.*, vol. BME-21, pp. 46-48, Jan. 1974.
- [10] C. M. Weil, "Absorption characteristics of multilayered sphere models exposed to UHF/microwave radiation," *IEEE Trans. Biomed. Eng.*, vol. BME-22, pp. 468-476, Nov. 1975.
- [11] C. T. A. Johnk, *Engineering Electromagnetic Fields and Waves*. New York: Wiley, 1975.
- [12] C. C. Johnson and A. W. Guy, "Nonionizing electromagnetic wave effects in biological materials and systems," *Proc. IEEE*, vol. 60, pp. 692-718, June 1972.
- [13] A. C. Fycleshymer and D. M. Schoemaker, *A Cross-Section Anatomy*. New York: Appleton, 1911.
- [14] D. J. Morton, *Manual of Human Cross Section Anatomy*. Baltimore, MD: Williams and Wilkins, 1944.
- [15] C. H. Durney, C. C. Johnson, P. W. Barber, H. Massoudi, M. Iskander, S. J. Allen, and J. C. Mitchell, "Radiofrequency radiation dosimetry handbook: 2nd ed.," Dep. Bioeng., Univ. Utah, Salt Lake City, UT, 1978.

**Peter W. Barber** (M'74) was born in Anchorage, AK, on September 5, 1942. He received the B.S. degree in electrical engineering from Washington State University, Pullman, in 1964, and the M.S. and Ph.D. degrees in engineering from the University of California, Los Angeles, in 1967 and 1973, respectively.

From 1964 to 1974 he was employed as an Electrical Engineer by the McDonnell Douglas Corporation, Long Beach, CA, where he was primarily engaged in the design of aircraft antennas. Since July 1974, he has been associated with the University of Utah, Salt Lake City, where he is presently Assistant Professor of Bioengineering and Research Assistant Professor of Electrical Engineering. He is currently engaged in teaching and research in electromagnetic theory.

Dr. Barber is a member of Sigma Tau and Tau Beta Pi.



**Om P. Gandhi** (S'57-M'58-SM'65-I'79) was born in Multan, West Pakistan, on September 23, 1934. He received the B.Sc. (Honors) degree in physics from Delhi University in 1952, the Diploma in electrical communication engineering from the Indian Institute of Science, Bangalore, India, in 1955, and the M.S.E. and Sc.D. degrees in electrical engineering from the University of Michigan, Ann Arbor, in 1957 and 1960, respectively.

Subsequently, he worked at Philco Scientific Laboratory, Blue Bell, PA, on semiconductor plasmas. From 1962 to 1966 he worked at Central Electronics Engineering Research Institute, Pilani, India, first as Assistant Director and then as Deputy Director in charge of the Microwave Devices group. Since 1967, he has been with the University of Utah, Salt Lake City, where he is a Professor of Electrical Engineering and Research Professor of Bioengineering. His re-

search interests include electromagnetic biological effects and biomedical applications of microwaves.

Dr. Gandhi is a member of Sigma Xi, Phi Kappa Phi, and Eta Kappa Nu.



**Mark J. Hagmann** (S'75-M'79) was born in Philadelphia, PA, on February 14, 1939. He received the B.S. degree in physics from Brigham Young University, Provo, UT, in 1960, and the M.Sc.Ed. and Ph.D. degrees in electrical engineering from the University of Utah, Salt Lake City, in 1966 and 1978, respectively.

From 1961 to 1964 he worked as a Physics and Mathematics Teacher. He did additional graduate studies in physics at Brigham Young University, Provo, UT, during 1965-1967.

During 1968-1975, he worked in the research and development of explosives for IRI-CO Chemicals, West Jordan, UT. Since 1978 he has been a Research Associate at the Department of Electrical Engineering and the Department of Bioengineering, University of Utah. His main research interests are electromagnetics and microwave biological effects.



**Indira Chatterjee** (S'78) was born in Bangalore, India, on April 2, 1954. She received the B.Sc. Honors and M.Sc. degrees in physics from Bangalore University, Bangalore, India, in 1972 and 1975, respectively, and the M.S. degree in physics from Case Western Reserve University, Cleveland, OH, in 1977.

She is currently working towards the Ph.D. degree in the Department of Electrical Engineering, University of Utah, Salt Lake City. The emphasis of her degree is on the interaction of electromagnetic radiation with biological systems.

## APPENDIX H

### BEHAVIORAL EFFECTS OF RESONANT ELECTROMAGNETIC POWER ABSORPTION IN RATS

John A. D'Andrea and Om P. Gandhi  
Departments of Electrical Engineering and Bioengineering

Raymond P. Kesner  
Department of Psychology

University of Utah  
Salt Lake City, Utah 84112

#### ABSTRACT

The factors of microwave radiation frequency and orientation of an animal in the microwave beam are important parameters in determining dose rate. During microwave irradiation these factors may, on the one hand, account for differential temperature rise in the rat and, on the other hand, produce differential disruption of behavioral performance. Fifteen male Long Evans rats, in Experiment I, were exposed to continuous wave (CW) microwave energy in the 220-500 MHz region in three body orientations to determine the most absorbant frequency and body orientation within the microwave field as evidenced by colonic temperature rise. The most absorbant orientation was found with the animal length aligned parallel to the electric field. In Experiment II, six male Long Evans rats were trained to lever press for dry food pellets. Each animal was then randomly exposed while lever pressing to three microwave frequencies (360, 480, and 500 MHz) in two body orientations (parallel to the electric field or parallel to the direction of microwave travel). The differential absorption rates due to the systematic manipulation of frequency and orientation variables did selectively disrupt behavioral performance of the rat. Greatest disruption of behavioral performance occurred when exposures were made with the animal aligned parallel to the electric field at 500 MHz. Less disruption of performance occurred at 360 or 480 MHz in this orientation. Little disruption of performance was observed when the animal was aligned parallel to the direction of the microwave travel at 360, 480, or 500 MHz.

#### INTRODUCTION

In recent years the relationship between electromagnetic phenomena and biological systems has generated considerable interest. Of particular interest have been the variables which determine the dose rate on the biological target. A variety of investigators [1, 2, 3, 4] have noted that the dose rate for the biological organism depends strongly on such factors as: (1) average and instantaneous field intensity, (2) duration of exposure, (3) size and shape of the organism, (4) dielectric properties of the organism, (5) wavelength of radiation, and (6) orientation of the organism in microwave fields. Recently Gandhi [5, 6] has noted a strong resonance phenomena based on animal size, wavelength of radiation, and animal orientation in microwave fields. Since these factors should account for differential absorption and temperature rise

*Biological Effects of Electromagnetic Waves*, Vol. I, Selected Papers of the 1975 USNC/URSI Meeting, Boulder, Colorado [HEW Publication (FDA) 77-8011]

in the rat during irradiation, these conditions should also produce differential disruption of behavioral performance in the rat during irradiation. To investigate these factors further, two experiments were conducted to determine the effect of these factors on rat heating and behavioral performance during irradiation.

## EXPERIMENT I: MATERIALS AND METHOD

### Subjects

Fifteen male Long Evans rats 350-380 grams in body weight were used. All rats were deprived of food to 85 percent of their free-feeding weights.

### Microwave Irradiation Apparatus

The microwave radiation chamber consisted of two parallel copper plates. The lower plate was 2 mm in thickness and measured 120 cm x 198.2 cm. The upper plate was 1 mm in thickness and measured 63.5 cm x 198.2 cm. Both plates were enclosed in a rectangular plywood box 215 cm x 88 cm x 150 cm. The interior of the box was lined with sheets of microwave absorbing material (11.8 cm thick Eccosorb). A ventilating fan was placed at one end of the chamber to remove air from the chamber at the rate of 310 cubic feet per minute. Additional ventilation openings were placed near the position of the animal to allow entry of fresh air. Two small doors (63 x 63 cm) were constructed in each side of the chamber.

A block diagram of the exposure apparatus is shown in Fig. 1. Microwave power was obtained from an Epsco signal source operating in the 200-500 MHz band with a minimum output of 100 watts power. A Philco model 164B bidirectional power meter was used to monitor power delivered to and reflected from the parallel plate chamber. Power leaving the parallel plate radiation chamber was monitored by a Hewlett-Packard No. 434A calorimetric power meter. A Heathkit cantenna was used for final dissipation of power from the parallel plate chamber. A Weinschell No. 109L double stub tuner was used to balance the irradiation system and reduce reflected power to a minimum. Frequency of the microwave energy delivered to the parallel plate chamber was monitored by a Hewlett-Packard No. 5253B frequency counter. Interconnection of the various components of the irradiation system utilized UG58/U coaxial cable.

### Determination of Absorbed Microwave Power

The intensity of the microwave field within the parallel plate chamber at the position of the rat was measured as mW/cm<sup>2</sup> by a General Microwave Corporation Raham model 1 (300-18,000 MHz) field intensity probe.

A calorimetric method [2] was used to determine how much of the microwave power was actually absorbed by the animal during each exposure. The amount of absorbed power was expressed as

$$\text{mW/gm} = 4180 \times \frac{\Delta T}{t}$$

where

$\Delta T$  = rectal temperature increase of rat in degrees Celsius during microwave exposure

t = time of exposure in seconds

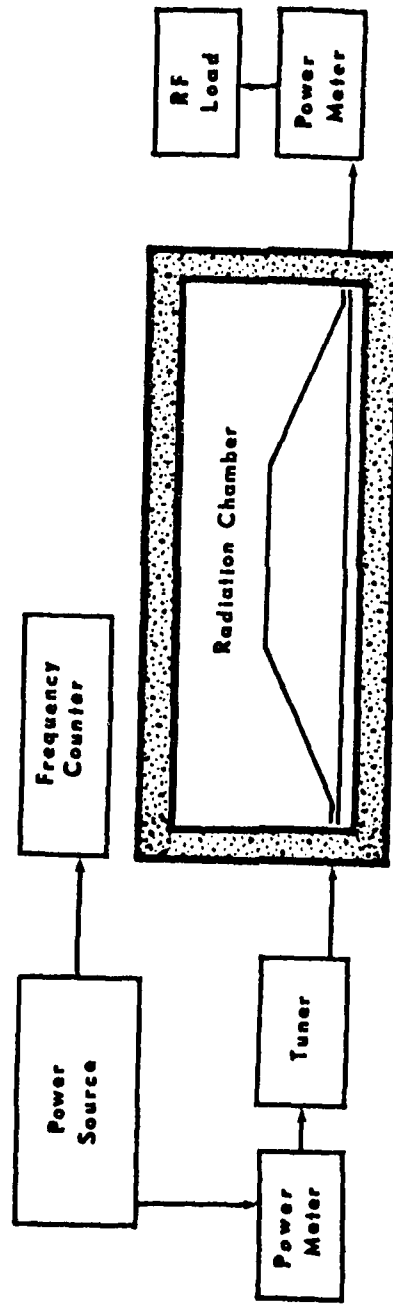


Figure 1. Radiation exposure apparatus.

4180 = conversion constant

### Procedure

Each rat was habituated for thirty minutes a day over a four-day period to a cylindrical Plexiglas rat holder (.32 cm x 6.5 cm x 24 cm). The holder was constructed with 1.27 cm slots on both upper and lower surfaces to interfere little with normal heat dissipation by the animal and to ensure release of urine and fecal material. On exposure days a microwave transparent liquid crystal fiber optic temperature probe [7] was inserted colonically (4 cm) and held in place by masking tape applied to the rat's tail. Each rat was then placed in the rat holder and set inside the radiation chamber such that the length of the rat body was parallel to the electric component of the microwave field ( $E \parallel L$ ). Each rat was allowed approximately twenty minutes before microwave exposure to allow for colonic thermal equilibrium. Exposure to microwave irradiation commenced when colonic temperature had stabilized. In each case microwave power was gradually increased over a 5-second period to the established field density of  $25 \text{ mW/cm}^2$ . This was done to avoid peak surges of power above  $25 \text{ mW/cm}^2$  at radiation onset. Each rat was then exposed to ten minutes of microwave radiation at one of twenty frequencies in the 220-500 MHz range. The microwave field intensity,  $\text{mW/cm}^2$ , and amount of power absorbed by the animal,  $\text{mW/gm}$ , were recorded for each exposure. All rats were exposed randomly to the twenty frequencies. This procedure was repeated four times. Some of the rats were additionally exposed to microwave radiation at 360, 480, and 500 MHz with the length of the rat body parallel to the magnetic field ( $H \parallel L$ ) and the direction of microwave propagation through the chamber ( $C \parallel L$ ). Relative humidity during the radiation exposures varied between 12 percent and 40 percent. Ambient temperature of the radiation chamber was controlled by room temperature (70-72° F). All exposures were CW radiation.

### EXPERIMENT I: RESULTS

Figure 2 shows the mean relative absorption of microwave power  $((\text{mW/gm}) / (\text{mW/cm}^2))$  and a scale indicating the animal rise in body temperature (centigrade) per minute from 220-500 MHz for animals aligned with the long axis of the body parallel to the electric field ( $E \parallel L$ ). Also shown are the mean  $((\text{mW/gm}) / (\text{mW/cm}^2))$  values of absorbed power for animals aligned parallel to either the magnetic field ( $H \parallel L$ ) or with the direction of wave propagation through the chamber ( $C \parallel L$ ) at 360, 480, and 500 MHz. The most microwave power-absorbant animal orientation in this frequency range clearly was with the long axis of the animal parallel to the electric field ( $E \parallel L$ ). In this orientation 500 MHz appears to be the most absorbant frequency. Analysis of variance techniques [8] indicates that there is a differential absorption of power in the electric orientation depending on frequency ( $p < .01$ ). Use of Newman Kuels multiple comparison techniques further indicates that exposures to 500 MHz irradiation in the electric orientation were clearly different from all other exposure frequencies in this orientation ( $p < .05$ ) except 360 and 440 MHz. Exposure of rats to 360 MHz radiation in this orientation was also different from other frequency exposures ( $p < .05$ ) except at 260, 440, 460, 480, and 500 MHz. These results indicate that for the passive rat, simple body heating as measured by a change in colonic temperature is dependent on both frequency ( $p < .01$ ) and body orientation relative to the microwave fields within the radiation chamber.

### EXPERIMENT II: MATERIALS AND METHOD

#### Subjects

Six male Long-Evans rats 350-380 grams in body weight were used as

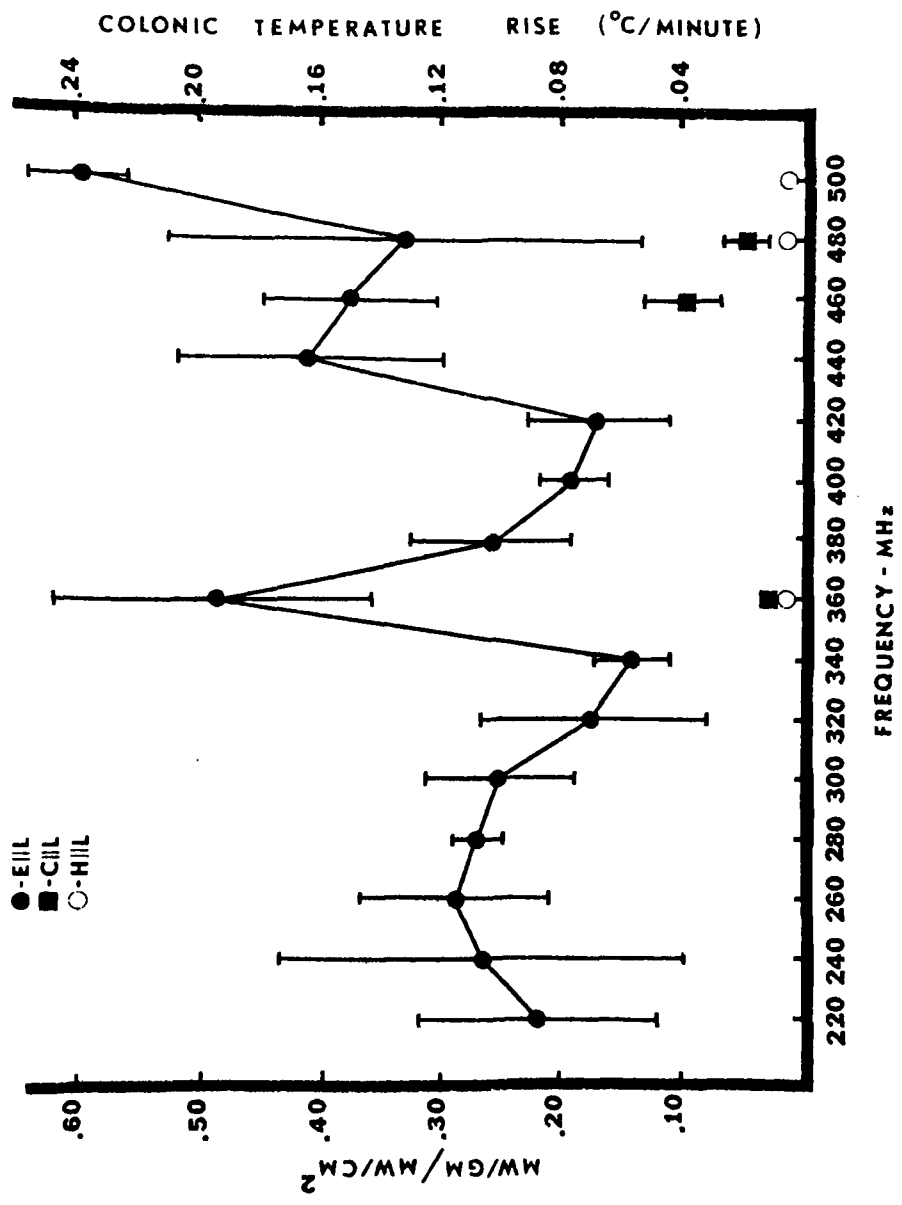


Figure 2. Mean frequency and body orientation dependent microwave absorption and colonic temperature rise in the Long Evans rat.

subjects. All animals were deprived of food to, and maintained at, 85 percent of free-feeding body weights.

#### Apparatus

The parallel plate irradiation system and rat holder were identical to that of Experiment I. The rat holder was modified by attaching a small Plexiglas response lever and small 1.25 cm diameter glass food cup. Since standard metallic microswitches cannot be used in a microwave field, an alternate system of monitoring lever-pressing behavior was devised. This was accomplished by passing a concentrated light beam through 47 mil plastic Dupont Crofon fiber optics. The fiber optics were arranged in such a way that each lever press made by the rat interrupted the passage of the light beam. A sensitive photocell arrangement outside of the radiation chamber could then detect each interruption of the light beam and consequently each lever press. A Lehigh Valley Electronics Corporation pellet feeder was mounted outside the radiation chamber and delivered 45 mg Noyes food pellets to the glass cup of the rat holder inside the radiation chamber via a 1.27 cm x 1 m section of Tygon flexible plastic tubing. Scheduling and recording of behavioral test sessions was accomplished via a system of relay circuitry, digital printing counters, and cumulative response recorders.

#### Procedure

All six rats were trained to lever press for food pellets on a random interval thirty-second schedule of reinforcement. The clock time used for the scheduling was three seconds, with a probability of .10 food-pellet delivery. With this arrangement a food pellet could be delivered from three seconds to every 180 seconds, with the average time of each food-pellet delivery being every thirty seconds. Each rat was given daily thirty-minute lever-pressing sessions until a stable rate of responding was achieved. Lever-pressing behavior was considered stable when the number of lever presses during the first five minutes of a session varied less than 10 percent from a similar measure of the previous daily session. On the average, approximately twenty daily lever-pressing sessions were required to achieve stable response rates.

Once stable responding rates were achieved, all animals were repeatedly and randomly exposed to different conditions of microwave radiation. For all microwave exposures, the field density within the chamber at the position of the rat was maintained at 25 mW/cm<sup>2</sup> as measured by the field intensity meter. All rats were exposed randomly to 360, 480, and 500 MHz microwave radiation, with both the length of the rat body parallel to the electric field ( $E \parallel L$ ) and direction of wave propagation through the microwave chamber ( $C \parallel L$ ). In this fashion each rat was exposed to the six possible combinations of three frequencies and two body orientations of microwave exposure while performing a stable lever-pressing task. Radiation exposures with the rat body parallel to the magnetic field were not done due to the difficulty in rotating the radiation chamber. Retraining sessions were given each rat after each microwave exposure to maintain stable rates of responding before the next microwave exposure and to check for possible carryover effects. Microwave irradiation began at the beginning of the sixth minute of each exposure session and terminated at the end of the first one-minute interval during which responding fell below one-third of the rat's normal response rate per minute determined from the previous daily session. If the rat responded throughout the session at a rate above one-third the baseline, irradiation ceased at the end of the thirty-minute session, resulting in a maximum exposure of 25 minutes. The primary measure of lever-pressing disruption was time to work stoppage defined as the time from radiation onset until the end of the minute during which responding fell below one-third

of the baseline rate. Each rat was removed from the radiation chamber and animal holder at work stoppage or at the end of the session.

Colonic temperature measurements were made at the beginning of the radiation sessions and again at work stoppage or the end of an exposure session to determine the amount of microwave-induced heating for each of the exposure conditions. Water intake during the 24-hour period between each daily session while each animal was in its home cage was measured and recorded. Relative humidity during the radiation sessions varied between 12 percent and 40 percent. Ambient temperature of the radiation chamber was controlled by room temperature (70-72° F).

Because of a lack of closed circuit television equipment, visual observation of the animal's performance during microwave radiation was not possible.

## EXPERIMENT II: RESULTS

Frequency of the microwave radiation and orientation in the microwave field both proved to be of major importance in determining disruption of lever-pressing behavior. Figure 3 shows the time to work stoppage from radiation onset for the frequency and body orientation parameters. For microwave exposure sessions with the animal's length aligned parallel to the direction of wave propagation through the chamber ( $C \parallel L$ ), nearly all animals lever pressed at near normal rates throughout the session. Only one animal, and this at 500 MHz radiation in the  $C \parallel L$  orientation, reduced responding to the work-stoppage criterion. With the length of the rat body aligned parallel to the electric field ( $E \parallel L$ ), however, time to work stoppage was much shorter. Average values of time to work stoppage and standard deviations are shown in Fig. 3. Animals exposed to 360 and 480 MHz radiation in the  $E \parallel L$  orientation appeared nearly normal upon removal from the microwave chamber.

Animals exposed to 500 MHz radiation in the  $E \parallel L$  orientation appeared flushed and remained in a prone position with the body extended. The condition of the animal appeared similar to the description of what Justesen and King [9] termed "flaccid paralysis". Four of the animals exposed under these conditions had urinated profusely in the animal holder. The fur on the underside of the animal's body was wet in spite of the slots made in the holder to release urine from the holder and away from the microwave fields. The rats were clearly heat stressed. Each animal, however, quickly regained its upright position within minutes after removal from the radiation chamber. A randomized block factorial analysis of variance [8] was used to evaluate the effects of the treatments. This test indicated a significant difference between the frequency of radiation during exposure ( $F = 17.68$ ,  $df = 2/25$ ,  $p < .001$ ), the animal orientation in the microwave field ( $F = 119.24$ ,  $df = 1/25$ ,  $p < .001$ ), and a frequency by orientation interaction ( $F = 12.37$ ,  $df = 2/25$ ,  $p < .001$ ).

A Newman Kuels test found no difference in the times to work stoppage for the exposures with the length of the animal aligned parallel to the direction of the microwave propagation through the chamber ( $C \parallel L$ ) at 360, 480, and 500 MHz. Each of these exposure conditions was, however, different ( $p < .05$  or greater) from the exposures with the animal aligned with the length of the body parallel to the electric field ( $E \parallel L$ ) at 360, 480, and 500 MHz. With the animal aligned parallel to the electric field, times to work stoppage at 360 and 480 MHz were not significantly different. Exposure to 500 MHz radiation in this orientation was, however, different ( $p < .01$ ) from all other exposure conditions.

The amounts of body heating, as measured by colonic temperature change during irradiation, paralleled the behavioral effects. Figure 4 shows the

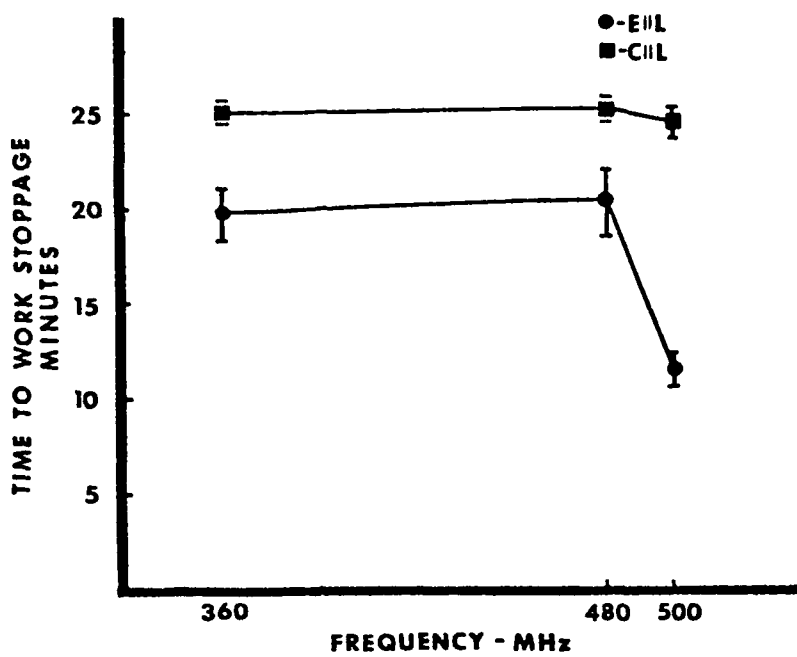


Figure 3. Time to work stoppage from radiation onset.

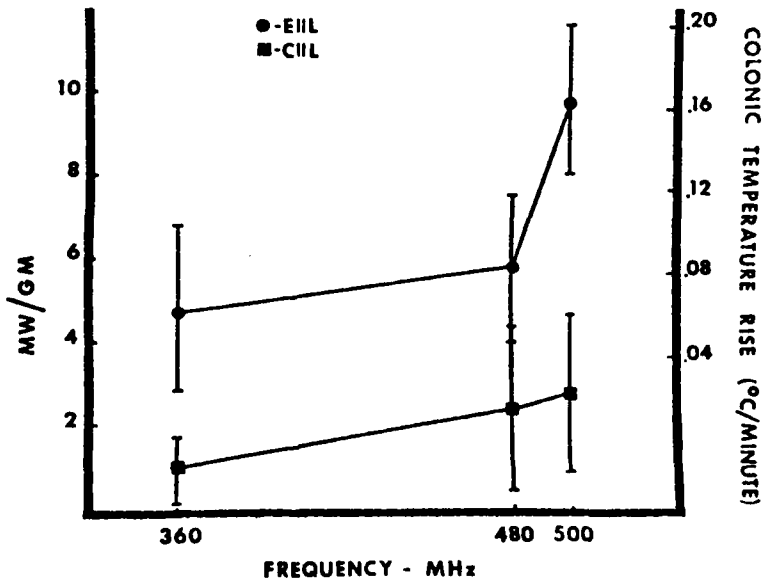


Figure 4. Mean frequency and body orientation dependent microwave absorption and colonic temperature rise in the Long Evans rat.

relative absorption of microwave energy as determined calorimetrically and given as mW/gm. Also shown in Fig. 4 is a scale showing the animal body temperature rise (centigrade per minute). For animals aligned parallel to the wave propagation ( $C \parallel L$ ), body heating was minimal. For animals aligned parallel to the electric field ( $E \parallel L$ ), however, heating was significant and increased as the frequency of radiation increased. A randomized block factorial analysis of variance [8] was used to evaluate the effect of the treatments on rat whole body heating as measured rectally. This test indicated a difference between the frequency of radiation during exposure ( $F = 21.70$ ,  $df = 2/25$ ,  $p < .01$ ), the animal's orientation in the microwave field ( $F = 129.81$ ,  $df = 1/25$ ,  $p < .01$ ), and a frequency of radiation by animal orientation interaction ( $F = 8.92$ ,  $df = 2/25$ ,  $p < .01$ ).

A Newman Kuels test indicated that rat body heating during exposure was not different at 360, 480, or 500 MHz when the rat body was parallel to direction of wave propagation ( $C \parallel L$ ) through the radiation chamber. With the rat aligned parallel to the electric field ( $E \parallel L$ ), however, 500 MHz exposures were different ( $p < .01$ ) from 360 and 480 MHz and also from the exposures in the wave propagation orientation at all frequencies. In the electric field orientation, rat body heating at 360 and 480 MHz were not different from each other but were clearly different from exposures in the wave of propagation orientation ( $p < .05$ ).

The measures of time to work stoppage and rat body heating expressed as mW/gm followed each other very closely in a reverse fashion. As body heating increased, time to work stoppage became much shorter. The correlation coefficient between the time to work stoppage and mW/gm measures for all animal radiation exposures was  $-.79$  ( $p < .01$ ).

Individual records of response rate are shown in Figs. 5 and 6. Responding during radiation in the  $E \parallel L$  orientation at 500 MHz is shown in Fig. 5 with comparable baseline performance and recovery responding the day following radiation exposure shown. Responding for the same animal during radiation in the  $C \parallel L$  orientation at 500 MHz is shown in Fig. 6. In both figures radiation onset is shown ( $RF_{on}$ ) as well as time to work stoppage and radiation termination ( $RF_{off}$ ).

An examination of the average number of responses per minute during microwave irradiation revealed an interesting finding. A comparison of each animal's average response rate during microwave irradiation until time to work stoppage or the end of the exposure session with a similar measure from the previous day's baseline performance showed no difference. Figure 7 shows this finding. Total lever-press rates for all exposure conditions were transformed into suppression of responding ratios. The suppression ratios were used as an index of the effect of microwave radiation exposure on responding. Each suppression ratio was indexed by the ratio of  $B/A + B$  where  $A$  represents the total number of lever presses during baseline performance. The score  $B$  represents the total number of lever presses during the period in radiation. Thus a ratio of 0.50 would indicate no relative change of lever presses during microwave irradiation compared to the same measure from baseline responding with no microwave irradiation present. A ratio of 0.00 would indicate a complete cessation of lever pressing during microwave radiation exposure. At each of the microwave exposure conditions, responding remained fairly stable with an abrupt drop or cessation of responding during the one-minute interval when the work stoppage criterion was met. A randomized block factorial analysis of variance [8] revealed that suppression of responding up until the work stoppage criterion was not different for either the frequency of microwave radiation ( $p > .10$ ) or the orientation of the animal in the microwave field ( $p > .10$ ).

Similarly a measure of the amount of water consumed by the rat between

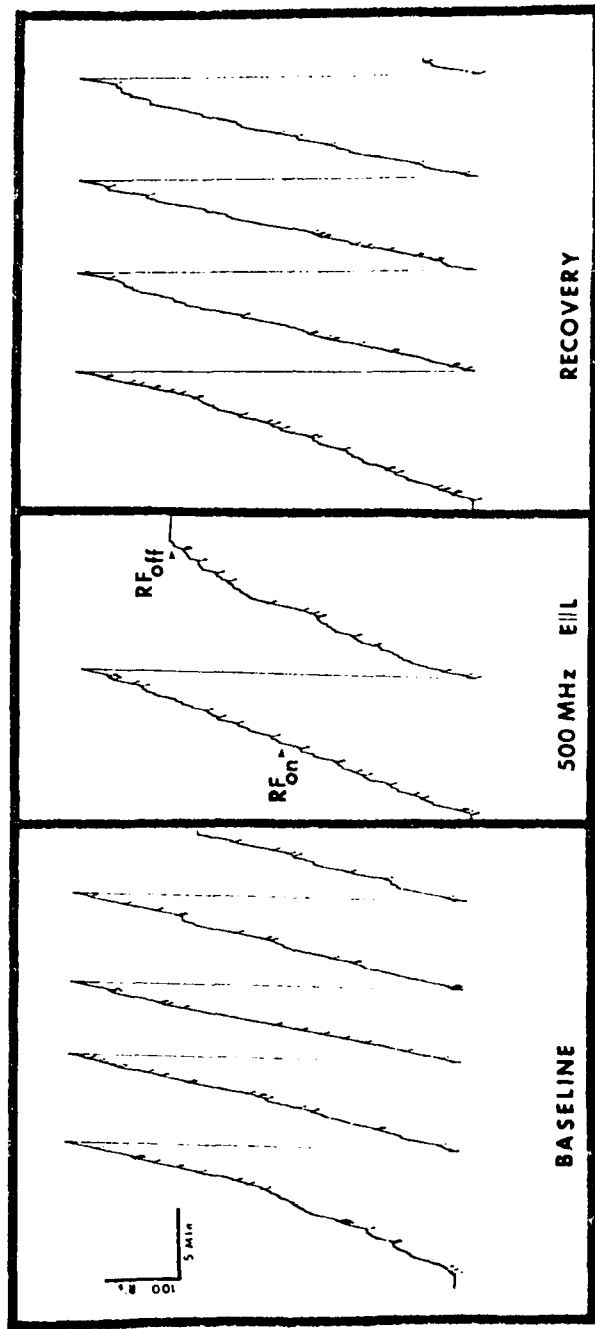


Figure 5. Cumulative response record of rat ---  
MW-20, 500 MHz,  $E \parallel L$ , radiation exposure.

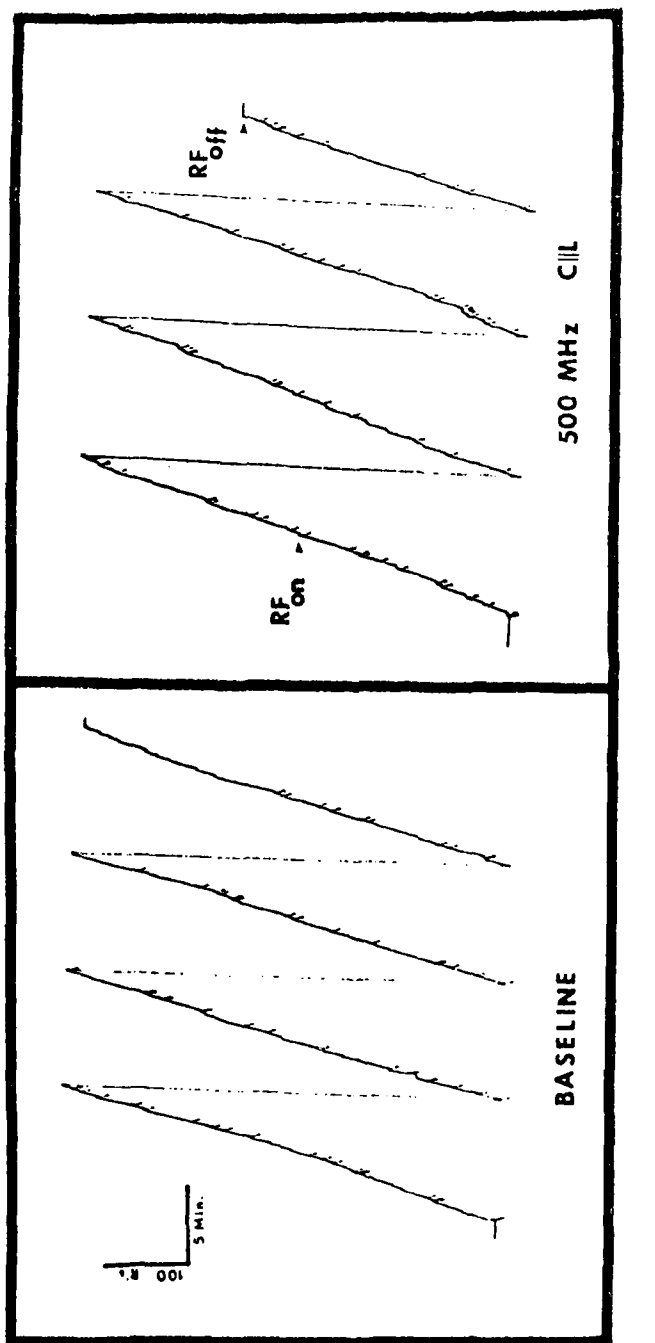


Figure 6. Cumulative response record of rat ---  
MW-20, 500 MHz,  $C \parallel L$ , radiation exposure.

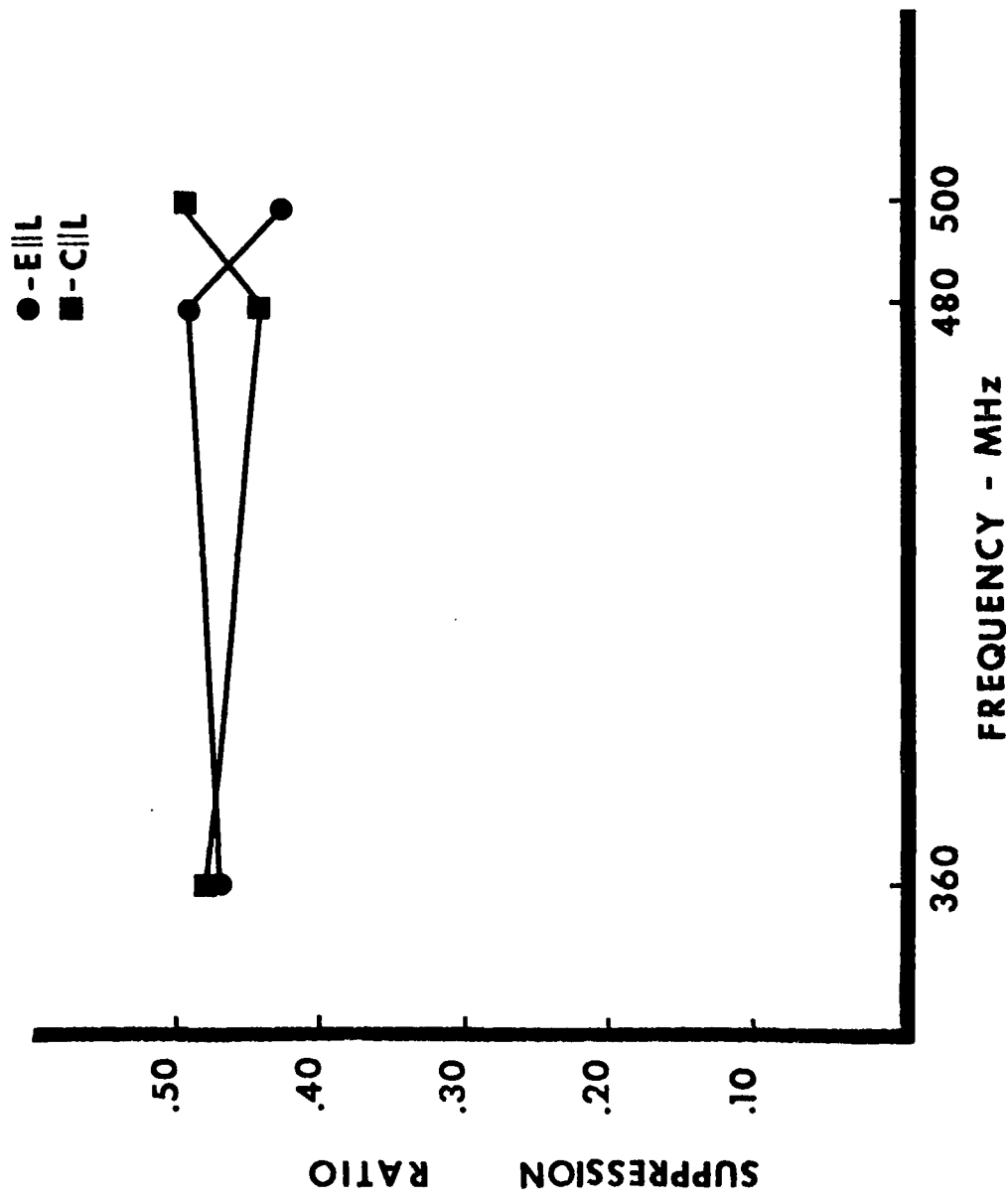


Figure 7. Mean suppression ratios of responding during microwave exposure.

daily lever-pressing sessions was also not influenced by exposure to microwave radiation. The amount of water consumed by each rat after microwave exposure until the next daily session was measured. This amount of water intake (cc) was then compared to a similar measure of water intake before microwave exposure. Figure 8 shows the mean amount and standard deviations of water consumed after microwave radiation exposure as a percentage of each animal's baseline water intake. A randomized block factorial analysis of variance [8] revealed no significant difference in water intake as a function of frequency of microwave radiation ( $p > .10$ ) and orientation of the animal in the microwave field ( $p > .10$ ).

To determine whether the effects of a particular radiation session had any effect on subsequent responding in recovery test sessions, each animal's performance during the first five minutes of the baseline session was compared to performance on the day after or two days after microwave radiation exposure. Standard suppression ratios of  $B/A + B$  were used. The animal's responding during the first five minutes of the baseline sessions is represented by the score A, whereas total responding during the first five minutes of the recovery session, either one or two days after microwave irradiation, is represented as the score B. Thus a ratio of .50 would indicate no relative change in responding during the recovery sessions compared to performance during previous baseline measures. Figure 9 shows the result of this comparison, suggesting little carryover effect from radiation sessions into recovery sessions one or two days later. A randomized block factorial analysis of variance [8] revealed that there were in fact no significant differences in the two performance measures due to either the frequency of radiation factor ( $p > .10$ ) or the orientation of the animal in the microwave field ( $p > .10$ ).

## DISCUSSION

This study was conducted to answer two questions. First, does the frequency of microwave radiation and orientation of an animal in a microwave field affect the absorption of microwave energy and consequent animal body heating? Second, can these factors, by producing differential heating, significantly alter the behavior of an animal performing in a microwave field? The data reported here support an affirmative answer to both of these questions.

The results of both experiments clearly indicate a strong effect of microwave frequency and animal body orientation in determining microwave absorption, rat body heating, and consequent suppression of behavioral responding. Animals exposed to the most absorbant frequency and body orientation combination (500 MHz,  $E \parallel L$ ) were clearly heat stressed. Vasodilation and assumption of a prone body position in these animals after radiation exposure were marked. Time to work stoppage for animals exposed under these conditions was short. For animals exposed to less absorbant frequencies and body orientations, the rate of body heating was less and consequent disruption of behavior was not evident. The high correlation between rate of body heating and time to work stoppage further supports the hypothesis that differential microwave absorption, body heating, and behavioral suppression can be governed by the factors of microwave frequency and animal body orientation in the microwave fields.

The question may be asked as to how mild hyperthermia may be responsible for suppression of a well-trained behavior in the rat. It is interesting to note that the lever-pressing animal maintained near normal average response rates during microwave irradiation. There seemed to be an abrupt cessation of lever pressing during microwave exposure, under most absorbant conditions, rather than a gradual decline in behavior below the work-stoppage criterion. This effect was unexpected, but in agreement with the earlier report by Justesen and King [9] of a similar finding in rats exposed to microwave

AD-A100 029 UTAH UNIV SALT LAKE CITY  
ELECTROMAGNETIC ENERGY ABSORPTION AND ITS DISTRIBUTION FOR MAN - ETC(U)  
NOV 78 O P GANDHI, J A D'ANDREA, M J HABMANN DAMD17-47-C-4092  
UNCLASSIFIED NL  
UTEC-MD-78-189

F/G 6/18

2 of 2  
40  
AECOD9

END  
0001  
FILED  
7-81  
DTIC

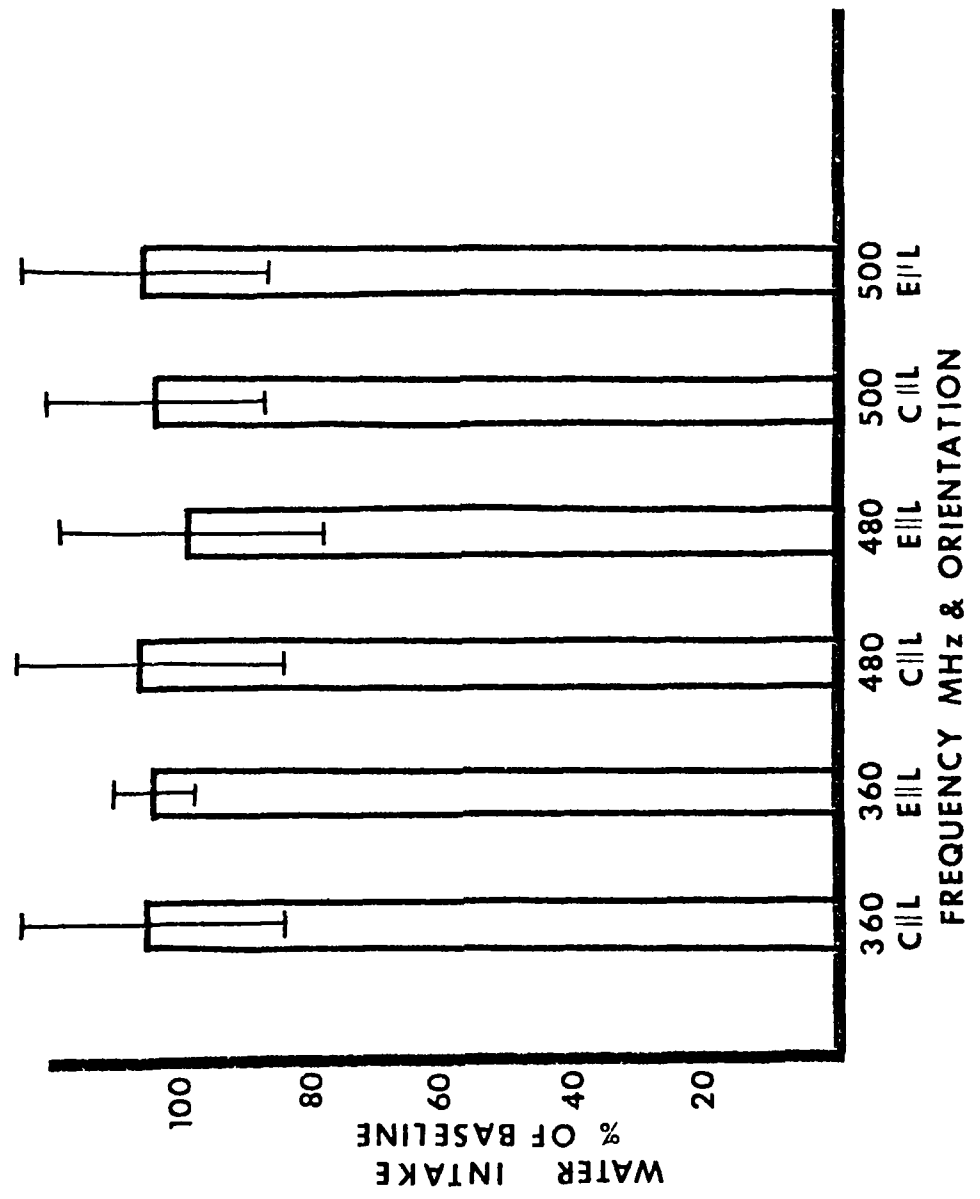


Figure 8. Water consumption after RF exposure.



Figure 9. Carryover effects suppression ratios.

radiation. Roberts, *et al.*, [10] have shown that rats, heated by raising the environmental temperature, show characteristic changes in behavioral thermoregulation. Rats heated in this fashion show an initial increased level of body grooming and activity during the first ten minutes of exposure to ambient temperatures of 37.7° C. Signs of body relaxation and extension, characteristic of the heat-stressed rat, occurred only after 45 minutes exposure to 37.7°C ambient temperature. The possibility then exists that efferent mechanisms responsible for grooming behaviors as a thermoregulatory response may also be elicited in the microwave heated rat. Mild hyperthermia induced by microwave exposure may elicit thermoregulatory behavior in the rat such as grooming which conflict with lever-pressing behavior. Thus time to work stoppage measured in this experiment may in fact, for some animals at least, be measuring time to elicitation of grooming behavior. Since microwave exposure may be a more efficient and rapid method of inducing mild hyperthermia, several classes of the classic thermoregulatory behaviors may be elicited simultaneously or in rapid succession. This latter possibility may be true for the animals exposed under the most absorbant radiation conditions. Since direct observation of each animal during irradiation could not be done, further investigation of this hypothesis is required.

It is possible that other factors may be responsible for behavioral suppression than just mild hyperthermia induction and elicitation of behavioral thermoregulation. One may speculate that evaporative water loss during microwave exposure was enhanced and that consequent thirst induction may contribute to behavioral suppression. A finding of no change in normal water intake over the 24-hour period after microwave exposure, however, seems contrary to this hypothesis. The lack of any evidence of proactive effects due to microwave exposure suggests that the most reliable effect of such exposure was body heating sufficient to suppress behavior but not intense enough to produce actual physical thermogenic damage to the animal. This may suggest that the primary effect of moderate intensity microwave exposure is to induce mild hyperthermia and consequent suppression of behavior, both of which are transient in nature.

It is important to note in Experiment I that even though each animal was allowed sufficient time for colonic thermal equilibration before exposure to microwave radiation, each animal was alert during the exposure period. It is well known that emotional reactions produce psychogenic effects in the rodent and that temperature regulation can be altered by such factors. It is difficult to rule out such reactions to the environment when using colonic temperature in the alert animal as the dependent variable. The use of habituation techniques such as familiarizing the animal to the animal holder and radiation chamber may help minimize such reactions. Nevertheless the animal cannot be readily habituated to the microwave exposure without long-term adaptation to induced heating effects. Determination of absorbed microwave power as described in this report must be distinguished as a dynamic measure, since the rat is capable of active thermoregulation during irradiation.

#### REFERENCES

1. Cleary, S. F. Uncertainties in the evaluation of the biological effects of microwave and radio frequency radiation. *Health Physics*, 25, 387-404, 1973.
2. Johnson, C. C., and A. W. Guy. Nonionizing electromagnetic wave effects in biological materials and systems. *Proc. IEEE*, 60, 692-718, 1972.
3. Milroy, W. C., and S. M. Michaelson. Biological effects of microwave radiation. *Health physics*, 20, 567-575, 1971.
4. Thompson, W. D., and A. E. Bourgeois. Nonionizing radiation. In E. Furch-

gott (Ed.) Pharmacological and biophysical agents and behavior. New York, Academic Press, 1971.

5. Gandhi, O. P. Polarization and frequency effects on whole animal absorption of RF energy. Proc. IEEE, 62, 1166-1168, 1974.
6. Gandhi, O. P. Conditions of strongest electromagnetic power deposition in man and animals, IEEE Trans. MTT, 23, 1021-1029, 1975.
7. Johnson, C. C., C. H. Durney, J. L. Lords, and G. K. Livingston. Fiber-optic liquid crystal probe for absorbed radio frequency power temperature measurement in tissue during irradiation. In Paul Tyler (Ed.) Biologic effects of nonionizing radiation. Annals of N. Y. Acad. of Sci., 247, 527-532, 1975.
8. Kirk, R. E. Experimental design. Proc. for the Behavioral Sciences. Belmont, California, Brooks Cole, 1968.
9. Justesen, D. R., and N. W. King. Behavioral effects of low level microwave irradiation in the closed space situation. In S. F. Cleary (Ed.) Biological effects and health implications of microwave radiation. U. S. Public Health Service Publication No. PB193-898, U. S. Government Printing Office, Washington, D. C. 154-179, 1970.
10. Roberts, W. W., R. D. Mooney, and J. R. Martin. Thermoregulatory behaviors of laboratory rodents. J. Comparative and Physiological Psychology, 86, 693-699, 1974.

#### ACKNOWLEDGMENT

This work was supported by the U. S. Army Medical Research and Development Command under Contract DAMD 17-74-C-4092, Om P. Gandhi, Principal Investigator, John A. D'Andrea, Coinvestigator, and Public Health Service Grant 1 R01 MH 25706-01, Raymond P. Kesner, Principal Investigator.

## I. INTRODUCTION

In electromagnetics, discretization for transforming an integral equation to a matrix equation is commonly accomplished using pulse functions as a basis [1]-[4]. More elaborate bases such as modal fields may be justified in a particular problem but are avoided in the matrix formulation for the general scattering body.

Discretization with pulse functions requires that the scattering body be partitioned into a number  $N$  of cells, where  $N$  is large enough that complex permittivity and the complex time-independent electric field may be assumed constant within each subvolume. Procedures for improving convergence with the general scattering body are of interest since the cost of computation is a rapidly increasing function of  $N$ .

This communication describes two new procedures which have been found to improve convergence in solution of the two-dimensional problem of transverse magnetic (TM) excitation of an infinite cylinder of arbitrary cross-section shape. Convergence is improved because the calculations include part of the variation of the field within each cell.

## II. REVIEW OF EARLIER SOLUTIONS USING PULSE FUNCTIONS

For TM excitation of an infinite cylinder, both incident and scattered fields have  $E$  directed parallel to the infinite dimension ( $z$  axis). The electric field is described by a scalar integral equation:

$$E_z(x, y) = E_z^i(x, y) - \frac{j k_0^2}{4} \iint [\epsilon_r(x', y') - 1] \cdot E_z(x', y') H_0^{(2)}(k_0 \rho) dx' dy', \quad (1)$$

where  $(x, y)$  and  $(x', y')$  are coordinates of the observation point and source point, respectively;  $\rho$  is the distance between the two points;  $E_z^i$  and  $E_z$  are incident and total electric field intensity, respectively, with  $e^{j\omega t}$  time dependence;  $\epsilon_r(x', y')$  is complex permittivity at the source point relative to free space;  $k_0 \equiv \omega \sqrt{\mu_0 \epsilon_0}$ ; and  $H_0^{(2)}(k_0 \rho)$  is the Hankel function of zero order.

The discrete analog of (1) consists of the  $N$ -by- $N$  system of linear equations:

$$\sum_{n=1}^N A_{mn} E_{zn} = E_{zm}^i, \quad m = 1, 2, \dots, N. \quad (2)$$

Richmond performed the discretization using pulse functions [1]. Each square cell was approximated by a circle of radius  $a$  having an equal area to simplify integration of the Bessel functions. His expressions for the matrix elements follow:

$$A_{mm} = 1 + (\epsilon_{rm} - 1) \left[ 1 + \frac{j \pi k_0 a}{2} H_1^{(2)}(k_0 a) \right] \quad (3)$$

$$A_{mn} = \frac{j \pi k_0 a}{2} (\epsilon_{rn} - 1) J_1(k_0 a) H_0^{(2)}(k_0 \rho_{mn}), \quad m \neq n. \quad (4)$$

## Procedures for Improving Convergence of Moment-Method Solutions in Electromagnetics

M. J. HAGMANN, O. P. GANDHI, SENIOR MEMBER, IEEE,  
AND C. H. DURNEY, MEMBER, IEEE

**Abstract**—Two new methods, termed "plane-wave correction" and "cylindrical-cell correction," are presented for improving the convergence of moment-method solutions in electromagnetics. Convergence is improved because the calculations include an approximation for the variation of the field within each cell.

Manuscript received November 27, 1976; revised July 13, 1977. This work was supported by U.S. Army Medical Research and Development Command under Contract DAMD 17-74-C-4092.

The authors are with the Department of Electrical Engineering, University of Utah, Salt Lake City, UT 84112.

In this method, the electric field intensity is considered to be constant over the area of a cell, an approximation that results in significant error if the cells are not very small. Larger cells can be used if the variation of the electric field is included in the calculations. A method of approximating the variation of the electric field, called "plane-wave correction," is described in the next section.

### III. PLANE-WAVE CORRECTION

Variation of  $E_z$  is initially unknown, but we may make the approximation of representing the fields within each cell by a superposition of plane waves. All member plane waves are required to have propagation vectors of magnitude  $k$  corresponding to the frequency of the incident wave and local complex permittivity of the dielectric body. If  $\alpha_i$  and  $B_i$  represent orientation of propagation and amplitude of the  $i$ th component, respectively, the superposition of plane waves may be written as

$$E_z(r', \theta') = \sum_i B_i e^{-jkr' \cos(\theta' - \alpha_i)} \quad (5)$$

If complex permittivity is constant within a cell and the approximation of circular cells is used in (1), then the diagonal matrix elements are

$$A_{mn} = 1 + \frac{jk_0^2(\epsilon_{rm} - 1)}{4E_z(0, \theta')} \int_0^a r' dr' \cdot \int_0^{2\pi} E_z(r', \theta') H_0^{(2)}(k_0 r') d\theta'. \quad (6)$$

Using (5) for  $E_z(r', \theta')$ , neglecting terms higher than second order in  $kr'$  in the expansion of the exponential, and performing the  $\theta'$  integrations,

$$A_{mm} = 1 + \frac{jk_0^2(\epsilon_{rm} - 1)}{4} \int_0^a \left[ \sum_i B_i \left( 2\pi - \frac{\pi}{2} k^2 r'^2 \right) \right] H_0^{(2)}(k_0 r') r' dr'. \quad (7)$$

Performing the integrations over the Hankel functions gives, for the diagonal elements,

$$A_{mm} = 1 + (\epsilon_{rm} - 1) \left[ (\epsilon_{rm} + 1) + \frac{j\pi k_0 a}{2} \left( 1 - \frac{\epsilon_{rm}}{4} (k_0 a)^2 \right) H_1^{(2)}(k_0 a) + \frac{j\pi}{4} \epsilon_{rm} (k_0 a)^2 H_2^{(2)}(k_0 a) \right] \quad (8)$$

In evaluating the off-diagonal matrix elements, suppose that the source point  $P'$  is in the  $n$ th cell and the observation point

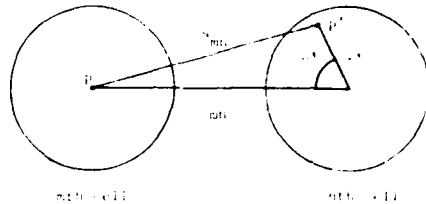


Fig. 1. Notation used in evaluation of off-diagonal matrix elements.

$P$  is at the center of the  $m$ th cell, as shown in Fig. 1. Let  $\rho_{mn}$  and  $r'$  be distances from the center of the  $n$ th cell to the observation point and source point, respectively. If the angle between  $\rho_{mn}$  and  $r'$  is  $\theta'$ , then the distance between the source point and observation point is

$$s_{mn} = \sqrt{r'^2 + \rho_{mn}^2 - 2r'\rho_{mn} \cos \theta'}. \quad (9)$$

If  $\epsilon_r$  is constant within the  $n$ th cell and the approximation of circular cells is used in (1), then the off-diagonal matrix elements are

$$A_{mn} = \frac{jk_0^2(\epsilon_{rn} - 1)}{4E_z(0, \theta')} \int_0^a r' dr' \cdot \int_0^{2\pi} E_z(r', \theta') H_0^{(2)}(k_0 s_{mn}) d\theta'. \quad (10)$$

Using Graf's addition theorem [5] in (10),

$$A_{mn} = \frac{jk_0^2(\epsilon_{rn} - 1)}{4E_z(0, \theta')} \sum_{l=-\infty}^{\infty} H_l^{(2)}(k_0 \rho_{mn}) \int_0^a j_l(k_0 r') r' dr' \int_0^{2\pi} E_z(r', \theta') \cos l\theta' d\theta'. \quad (11)$$

Using (5) for  $E_z(r', \theta')$  and neglecting terms higher than second order in  $kr'$  in the expansion of the exponential,

$$A_{mn} = \frac{jk_0^2(\epsilon_{rn} - 1)}{4} \sum_{l=-\infty}^{\infty} H_l^{(2)}(k_0 \rho_{mn}) \int_0^a j_l(k_0 r') r' dr' \cdot \int_0^{2\pi} \sum_i B_i \left[ 1 - jkr' \cos(\theta' - \alpha_i) - \frac{1}{2} k^2 r'^2 \cos^2(\theta' - \alpha_i) \right] \cos l\theta' d\theta'. \quad (12)$$

Performing the  $\theta'$  integrations in (12), and neglecting terms with  $|l| > 1$ ,

$$\begin{aligned} A_{mn} = & \frac{jk_0^2(\epsilon_{rn}-1)H_0^{(2)}(k_0\rho_{mn})}{4 \sum_i B_i} \\ & \cdot \int_0^a \left[ \sum_i B_i 2\pi \right] J_0(k_0 r') r' dr' \\ = & \frac{jk_0^2(\epsilon_{rn}-1)H_0^{(2)}(k_0\rho_{mn})}{4 \sum_i B_i} \\ & \cdot \int_0^a \left[ \sum_i B_i \frac{\pi}{2} k^2 r'^2 \right] J_0(k_0 r') r' dr' \\ + & \frac{2k_0^2(\epsilon_{rn}-1)H_1^{(2)}(k_0\rho_{mn})}{4 \sum_i B_i} \\ & \cdot \int_0^a \left[ \sum_i B_i \pi k r' \cos \alpha_i \right] J_1(k_0 r') r' dr'. \quad (13) \end{aligned}$$

The summations in all three integrands of (13) contain factors independent of the summation index that may be removed from the summations. Also changing to a dummy variable,

$$\delta_{mn} = - \frac{j\gamma\sqrt{\epsilon_{rn}}H_1^{(2)}(k_0\rho_{mn})k_0 a J_2(k_0 a)}{H_0^{(2)}(k_0\rho_{mn}) \left[ \left( 1 - \frac{\epsilon_{rn}}{4}(k_0 a)^2 \right) J_1(k_0 a) + \frac{\epsilon_{rn}}{2} k_0 a J_2(k_0 a) \right]}. \quad (19)$$

$$\begin{aligned} A_{mn} = & \frac{j\pi}{2} (\epsilon_{rn}-1) H_0^{(2)}(k_0\rho_{mn}) \int_0^{k_0 a} J_0(x) x dx \\ & - j \frac{\pi}{8} (\epsilon_{rn}-1) \epsilon_{rn} H_0^{(2)}(k_0\rho_{mn}) \int_0^{k_0 a} J_0(x) x^3 dx \\ & + \frac{\pi}{2} (\epsilon_{rn}-1) \sqrt{\epsilon_{rn}} H_1^{(2)}(k_0\rho_{mn}) \left[ \frac{\sum_i B_i \cos \alpha_i}{\sum_i B_i} \right] \\ & \cdot \int_0^{k_0 a} J_1(x) x^2 dx. \quad (14) \end{aligned}$$

Define

$$\gamma \equiv \frac{\sum_i B_i \cos \alpha_i}{\sum_i B_i}. \quad (15)$$

If quadratic and higher order terms in (6) are neglected, then

$$\gamma = \frac{j}{ka} \left[ \frac{E(a, 0) - E(0, 0)}{E(0, 0)} \right]. \quad (16)$$

Performing the integrations in (14),

$$\begin{aligned} A_{mn} = & \frac{j\pi}{2} (\epsilon_{rn}-1) H_0^{(2)}(k_0\rho_{mn}) k_0 a J_1(k_0 a) \\ & + \frac{j\pi}{4} (\epsilon_{rn}-1) \epsilon_{rn} H_0^{(2)}(k_0\rho_{mn}) (k_0 a)^2 J_2(k_0 a) \\ & - \frac{j\pi}{8} (\epsilon_{rn}-1) \epsilon_{rn} H_0^{(2)}(k_0\rho_{mn}) (k_0 a)^3 J_1(k_0 a) \\ & + \frac{\pi}{2} (\epsilon_{rn}-1) \sqrt{\epsilon_{rn}} H_1^{(2)}(k_0\rho_{mn}) (k_0 a)^2 J_2(k_0 a). \end{aligned}$$

Since only the last member in (17) is dependent on the unknown coefficients in the plane wave expansion, we will delete the term and use the first three members to calculate the diagonal matrix elements:

$$\begin{aligned} A_{mn} = & \frac{j\pi k_0 a}{2} (\epsilon_{rn}-1) H_0^{(2)}(k_0\rho_{mn}) \\ & \cdot \left[ \left( 1 - \frac{\epsilon_{rn}}{4}(k_0 a)^2 \right) J_1(k_0 a) + \frac{\epsilon_{rn}}{2} k_0 a J_2(k_0 a) \right] \quad (17) \end{aligned}$$

The use of (18) is justified only if the last member of (17) is small. The fractional error in  $A_{mn}$  due to neglecting the last member of (17) is

$$\text{Since the magnitude of the ratio of the Hankel functions is greatest for a small argument, we set } \rho_{mn} = \sqrt{\pi}a \text{ for adjacent cells. Expanding the Bessel functions for small arguments and using (16) to estimate } \gamma, \text{ we obtain}$$

$$|\delta_{mn}| \leq \frac{1}{4\sqrt{\pi} \ln \left( \frac{2}{\Gamma\sqrt{\pi}k_0 a} \right)} \left| \frac{E(a, 0) - E(0, 0)}{E(0, 0)} \right|, \quad (20)$$

where  $\Gamma \approx 1.78107$ .

In the plane wave correction method, (8) and (18) are used for the matrix elements, and the solution corresponds to the value of  $E_z$  at each cell center. Numerical considerations suggest that deletion of the last member in (17) is the principal source of error. Equation (20) requires that if  $4\sqrt{\pi} \ln(2/(\Gamma\sqrt{\pi}k_0 a))$  exceeds the condition number of the matrix, then the error in  $E_z$  calculated for the cell centers will be less than the variation of  $E_z$  within each cell relative to values at the cell centers. Hence the plane wave correction will account for much of the variation of  $E_z$  within each cell. We must have  $a < 0.0876\lambda_0$  or the criterion will not be satisfied even for a

condition number of unity. Similar convergence criteria are not available in the method using pulse functions that is described in Section II. A second method of approximating the variation of the electric field, called "cylindrical-cell correction," is described in the next section.

#### IV. CYLINDRICAL-CELL CORRECTION

In the methods described in Sections II and III, the scattering body is divided into cells that are approximated by circular cylinders in calculation of the matrix elements. The method of cylindrical-cell correction, which is presented for the first time in this communication, emphasizes the properties of such a model of the original body.

Let the cross section of the scatterer be divided into square cells, each having side  $s$ . For the model, replace each cell with a circular cylinder having radius  $a$  and assume properties of free space between the cylinders. For the chosen geometry [6], the effective relative complex permittivity  $\epsilon_{\text{eff}}$  of the model and the complex permittivity  $\epsilon_r'$  of each cylinder are related by

$$\epsilon_{\text{eff}} = 1 + \frac{\pi a^2}{s^2} (\epsilon_r' - 1). \quad (21)$$

If we require that the effective relative complex permittivity of the model equal that of the original scatterer, then

$$\epsilon_r' = 1 + \frac{s^2}{\pi a^2} (\epsilon_r - 1). \quad (22)$$

If the electrical size of the cylinders is sufficiently small, the inhomogeneities of the model will have no significant effect, so that scattering from the model satisfying (22) will duplicate that of the physical scatterer. The model is useful since we may approximate the variation of the electric field within each cylinder. A circular cylinder with TM excitation will have internal fields given by

$$E_z = \sum_{n=0}^{\infty} b_n J_n(kr) \cos(n\theta + c_n), \quad (23)$$

where the  $b_n$  and  $c_n$  are determined by the excitation. If the cylinder is sufficiently small, the zero-order term will dominate, so we may use the approximation

$$E_z = b_0 J_0(kr). \quad (24)$$

From (6) and (24), the diagonal matrix elements are given by

$$A_{mm} = 1 + \frac{\pi k_0^2 (\epsilon_{rm}' - 1)}{4} \int_0^a J_0(k'r') H_0^{(2)}(k_0 r') dr' \cdot \int_0^{2\pi} d\theta', \quad (25)$$

where  $k' \equiv \sqrt{\epsilon_{rm}' - 1}$ .

Performing the  $\theta'$  integration and using a relationship from [7] for the  $r'$  integration, we obtain the following expression

used to calculate the diagonal matrix elements:

$$A_{mm} = \frac{j\pi}{2} [k'a J_1(k'a) H_0^{(2)}(k_0 a) - k_0 a J_0(k'a) H_1^{(2)}(k_0 a)]. \quad (26)$$

From (10) and (24), the off-diagonal matrix elements are given by

$$A_{mn} = \frac{j k_0^2 (\epsilon_{rn}' - 1)}{4} \int_0^a r' dr' \cdot \int_0^{2\pi} J_0(k'r') H_0^{(2)}(k_0 s_{mn}) d\theta'. \quad (27)$$

Using Graf's addition theorem [5] and the notation of Fig. 1,

$$A_{mn} = \frac{j k_0^2 (\epsilon_{rn}' - 1)}{4} \sum_{l=-\infty}^{\infty} H_l^{(2)}(k_0 \rho_{mn}) \cdot \int_0^a J_l(k_0 r') J_0(k'r') r' dr' \int_0^{2\pi} \cos(l\theta') d\theta'. \quad (28)$$

Performing the  $\theta'$  integration, which collapses the summation, and using a relationship from [7] for the  $r'$  integration, we obtain the following expression used to calculate the off-diagonal matrix elements:

$$A_{mn} = \frac{j\pi}{2} H_0^{(2)}(k_0 \rho_{mn}) [k'a J_1(k'a) J_0(k_0 a) - k_0 a J_0(k'a) J_1(k_0 a)], \quad m \neq n. \quad (29)$$

In the cylindrical-cell correction method, (26) and (29) are used for the matrix elements, and the solution corresponds to the value of  $E_z$  at each cell center. A solution is defined for any ratio of  $a/s$ , but only two cases have been studied: 1) tangent cylindrical cells

$$a = \frac{s}{2}, \quad \epsilon_r' = 1 + \frac{4}{\pi} (\epsilon_r - 1)$$

and 2) overlapping cylindrical cells

$$a = \frac{s}{\sqrt{\pi}}, \quad \epsilon_r' = \epsilon_r.$$

For very large or very small values of  $a/s$ , the structure of the model differs significantly from that of the scatterer, so that the solution, which actually corresponds to scattering from the composite of circular cylinders, will differ from that for the desired scatterer. Advantages of the method will be seen in the example in Section VI.

#### V. CALCULATION OF POWER ABSORPTION

With both plane-wave correction and cylindrical-cell correction, the solution corresponds to the value of  $E_z$  at each cell center. The plane-wave correction leaves the variation of

$E_z$  within each cell undefined, but with cylindrical-cell correction, (24) describes the approximate variation of  $E_z$  within each circular cylinder of the model.

If the value of power absorption is desired, then  $1/2 \sigma E_z E_z^*$  may be computed within each cell using the values of  $E_z$  found using pulse functions or plane-wave corrections. In this section the approximate variation of  $E_z$  within each cell is used for an improved expression for power absorption if cylindrical-cell correction is used.

Total power absorption in one circular cylinder is given by

$$P = \int_0^a \int_0^{2\pi} \frac{1}{2} \sigma' E_z E_z^* r dr d\theta. \quad (30)$$

From (22) the conductivity of the cylinder is related to that of the scatterer by

$$\sigma' = \frac{s^2}{\pi a^2} \sigma. \quad (31)$$

Substituting (24) and (31) in (30) gives

$$P = \frac{s^2 \sigma}{a^2} h_0 h_0^* \int_0^a J_0(k'r) J_0^*(k'r) r dr. \quad (32)$$

Using a relationship from [7] for the  $r'$  integration and simplifying, the average absorbed power density within the cell is given by

$$P_d = \frac{\sigma}{2} E_z E_z^* \left[ \frac{\text{Im}[k'a J_0^*(k'a) J_1(k'a)]}{\text{Re}(k'a) \text{Im}(k'a)} \right]. \quad (33)$$

where  $E_z$  is the calculated value of  $E_z$  found for the cell center using cylindrical-cell correction.

#### VI. NUMERICAL EXAMPLE: THE INFINITE CYLINDER MODEL OF MAN

The infinite cylinder has been suggested for use as a model for body extremities or the chest cavity in the evaluation of biological hazards from electromagnetic radiation [8]. Approximation of an extremity or the whole body by an infinite cylinder may be made using the ratio of volume to length for the cross-sectional area.

The model considered in this example is an infinitely long cylinder with square cross section of 20 by 20 cm, having TM excitation by a plane wave incident perpendicular to one of the four congruent faces. The body is homogeneous with values of permittivity and conductivity that are typical for muscle, skin, and other tissues having high water content [9].

The methods described in this communication have been used to calculate average specific absorbed power for the model. Suitability of the model can only be justified at high frequencies where end effects may be neglected, but calculations have been made over a wide range of frequencies to allow comparison of convergence with the different methods.

Fig. 2 illustrates the frequency dependence of average specific absorption rate (SAR) for the model. The values obtained using the accepted method of pulse functions with 100 cells are the standard for comparison. Values obtained using pulse functions with 81 cells were found to differ from

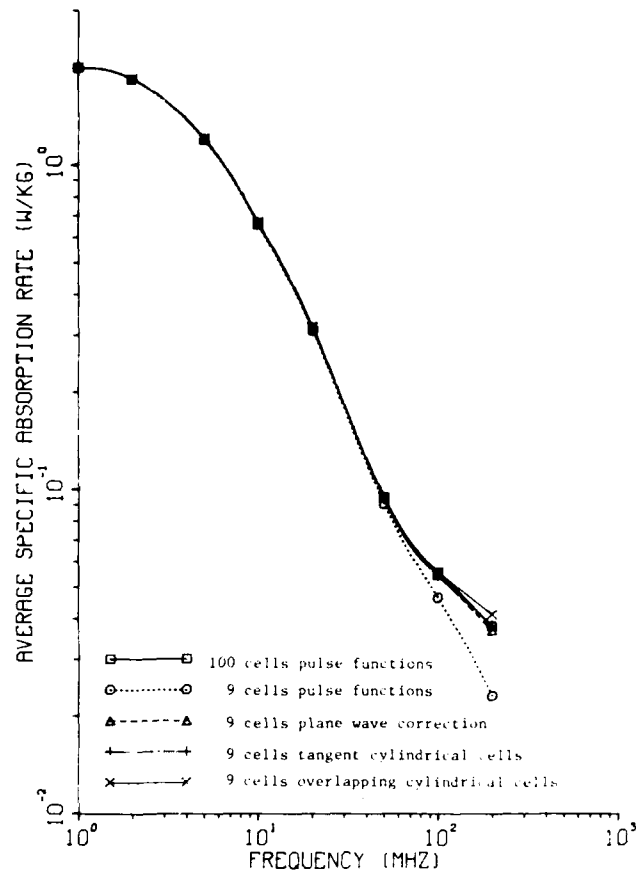


Fig. 2. Variation of average specific absorption rate with frequency for infinite cylinder model of man. Incident power density is 1 mW/cm<sup>2</sup>.

those with 100 cells by less than 1 percent for frequencies up to 200 MHz. Values found using 9 cells with pulse functions, plane wave correction, and cylindrical-cell correction with tangent and overlapping cells are also given in the figure. For 9 cells, all four calculations are in good agreement with the standard at low frequencies, where the cells have small electrical size. Calculations with the new methods appear to have comparable accuracy and appear to offer a significant improvement in convergence when compared to pulse functions.

The criterion  $a < 0.0876\lambda_0$  suggests that the plane wave correction with 9 cells will cease to be useful for frequencies exceeding 700 MHz, but the exact limit depends on the condition number as mentioned in Section III. Increasing error is observed for frequencies exceeding 200 MHz which is consistent with the convergence criteria.

#### VII. CONCLUSIONS

Two methods have been found which improve convergence in solution of the two-dimensional problem of TM excitation of an infinite cylinder of arbitrary cross-section shape. The extension to the three-dimensional problem has not yet been completed.

Convergence is improved because the calculations include approximation for the variation of the field within each cell. The new methods give expressions for the matrix elements

that are different from those found using pulse functions, but values of the matrix elements are in good agreement for electrically small cells.

The matrix elements found with the new methods do not require a substantial increase in computational effort. For a homogeneous scatterer, if equal size cells are used, the new methods require one-time computation of several additional Bessel functions, but time for calculation of the matrix elements is dominated by recalculation of the zero-order Hankel function which is needed with or without the corrections made in the new methods. If the scatterer is not homogeneous or if different cell sizes are used, then time for calculation of each matrix element is approximately doubled in the new methods. Time spent in calculation of the matrix elements is proportional to  $N^2$ , whereas time spent in solving the matrix equation is proportional to  $N^3$ , so for large numbers of cells there is still no significant increase in computation time with the new methods.

#### REFERENCES

- [1] J. H. Richmond, "Scattering by a dielectric cylinder of arbitrary cross section shape," *IEEE Trans. Antennas Propagat.*, vol. AP-13, pp. 334-341, May 1965.
- [2] J. H. Richmond, "TE-Wave scattering by a dielectric cylinder of arbitrary cross section shape," *IEEE Trans. Antennas Propagat.*, vol. AP-14, pp. 460-464, July 1966.
- [3] G. W. Hohmann, "Three-dimensional induced polarization and electromagnetic modeling," *Geophysics*, vol. 40, pp. 309-324, April 1975.
- [4] D. E. Livesay and K. M. Chen, "Electromagnetic fields induced inside arbitrarily shaped biological bodies," *IEEE Trans. Microwave Theory Tech.*, vol. MTT-22, pp. 1273-1280, Dec. 1974.
- [5] M. Abramowitz and I. A. Stegun, Eds., *Handbook of Mathematical Functions*, National Bureau of Standards, 1964.
- [6] L. K. H. Van Beek, "Dielectric behaviour of heterogeneous systems," *Progress in Dielectrics*, vol. 7, pp. 69-114, 1967.
- [7] P. M. Morse and H. Feshbach, *Methods of Theoretical Physics*. New York: McGraw-Hill, 1953.
- [8] T. K. Wu and L. L. Tsai, "Numerical analysis of electromagnetic fields in biological tissues," in *Proc. IEEE*, vol. 62, pp. 1167-1168, Aug. 1974.
- [9] C. C. Johnson, C. H. Durney, and H. Massoudi, "Long-wavelength electromagnetic power absorption in prolate spheroidal models of man and animals," *IEEE Trans. Microwave Theory Tech.*, vol. MTT-23, pp. 739-747, Sept. 1975.

## APPENDIX J

904

IEEE TRANSACTIONS ON MICROWAVE THEORY AND TECHNIQUES, VOL. MTT-26, NO. 11, NOVEMBER 1978

# Improvement of Convergence in Moment-Method Solutions by the Use of Interpolants

MARK J. HAGMANN, STUDENT MEMBER, IEEE, OM P. GANDHI, SENIOR MEMBER, IEEE, AND CARL H. DURNEY, MEMBER, IEEE

**Abstract**—Two interpolants are described that may be used to correct the results of a moment-method solution using pulse functions as a basis and delta functions for testing. The interpolants allow for some of the variation of the fields within each cell and thereby increase accuracy and improve convergence. The interpolants are usable for a general scatterer and typically require about 1 percent of the cost of the initial numerical solution.

## I. INTRODUCTION

MOMENT-METHOD solutions for electromagnetic scattering with a general dielectric object often use pulse functions as a basis and delta functions for testing [1]–[5]. The object of this paper is to show that an interpolant may be used to allow for some of the variation of the fields within each cell and thereby increase accuracy and improve convergence. The computational expense of using the interpolant is typically about 1 percent of the cost of the initial numerical solution.

A numerical solution using a pulse function basis results in a single value representing  $E$  within each cell. The delta functions used for testing enforce the integral equation at the center of each cell so that the calculated  $E$  values are most representative of the cell centers. Experimental tests have shown that the error in  $E$  calculated for the cell centers is relatively small even when adjacent cells have values which may differ by an order of magnitude [6]. Since the values of  $E$  may be assigned to points in space, interpolation is possible.

The present study has been restricted to piece-wise interpolation in which the value of the corrected specific absorption rate (SAR) is calculated for one cell at a time. In this paper, two interpolants that have been developed by the authors are described. The triquadratic interpolant is usable when cell centroids are on a Cartesian product mesh. The NEWSUD interpolant is useful for problems in which the cubical cells may have different sizes and general locations.

Manuscript received September 20, 1977; revised January 12, 1978. This work was supported by the U.S. Army Medical Research and Development Command, Washington, DC, under Contract DAMD 17-74-C-4092.

The authors are with the Department of Electrical Engineering, Merrill Engineering Building, University of Utah, Salt Lake City, UT 84112.

## II. TEST OF A ONE-DIMENSIONAL INTERPOLANT

Moment-method solutions with any subsectional basis, such as pulse functions, require that the scatterer be approximated by a composite of cells [1]–[5]. Since analytical solutions for such composites are unknown in three-dimensional problems, a test of convergence has been made for a one-dimensional problem.

Consider the one-dimensional problem of a plane wave polarized in the  $x$  direction incident upon a dielectric slab which extends from  $z=0$  to  $z=a$ . The electric field is described by a scalar integral equation:

$$E_x(z) = E'_x(z) - \frac{jk_0}{2} \int_0^a (\epsilon_r(z') - 1) E_x(z') e^{-jk_0 \rho} dz' \quad (1)$$

where  $z$  and  $z'$  are coordinates of the observation point and source point, respectively,  $\rho$  is the distance between the two points,  $E'_x$  and  $E_x$  are the incident and total electric-field intensity, respectively, with  $e^{j\omega t}$  time dependence,  $\epsilon_r(z')$  is the complex permittivity at the source point relative to free space, and  $k_0 \equiv \omega \sqrt{\mu_0 \epsilon_0}$ .

The discrete analogue of (1) consists of the  $N$ -by- $N$  system of linear equations:

$$\sum_{n=1}^N A_{mn} E_{xn} = E'_{xm}, \quad m=1, 2, \dots, N \quad (2)$$

where the dielectric is partitioned into  $N$  cells which are thin slabs, and  $n$  and  $m$  are indices for the cells.

The matrix elements are readily evaluated using (1) with the procedure in [2]:

$$A_{mn} = 1 + (\epsilon_{rn} - 1)(1 - e^{-jk_0 \Delta/2}) \quad (3)$$

$$A_{mn} = j(\epsilon_{rn} - 1)e^{-jk_0 \rho_{mn}} \sin\left(\frac{k_0 \Delta}{2}\right), \quad m \neq n \quad (4)$$

where  $\Delta$  is the thickness of each cell and  $\rho_{mn}$  is the distance between the centers of the  $m$ th and  $n$ th cells.

The analytical solution for a homogeneous dielectric slab is given by

$$E_x(z) = \frac{E'_x(0) [2\sqrt{\epsilon_r} \cos \sqrt{\epsilon_r} k_0(a-z) + 2j \sin \sqrt{\epsilon_r} k_0(a-z)]}{2\sqrt{\epsilon_r} \cos \sqrt{\epsilon_r} k_0 a + j(1+\epsilon_r) \sin \sqrt{\epsilon_r} k_0 a} \quad (5)$$

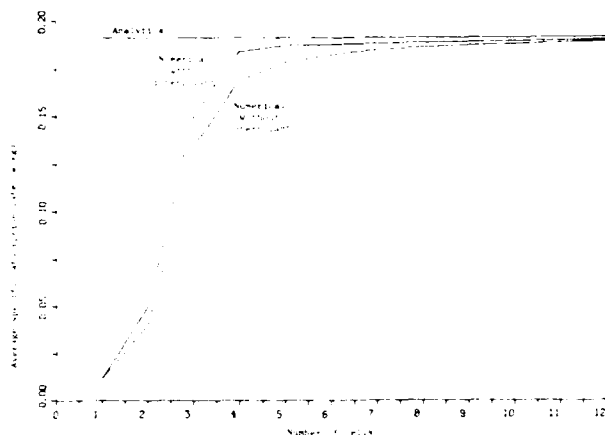


Fig. 1. Calculated average specific absorption rate for a 2-cm thick layer of muscle at 2450 MHz. Incident power density is  $1 \text{ MW/cm}^2$ .  $\epsilon_r = 50$ ,  $\sigma = 2.2 \text{ mho/m}$ .

Fig. 1 gives the average SAR for a 2-cm thick layer of muscle at 2450 MHz for three different computational procedures. The analytical value was found by integration of  $1/2 \sigma \vec{E} \cdot \vec{E}^*$  using (5). Numerical solutions were obtained using (2)-(4). Numerical values without the interpolant were found by averaging  $1/2 \sigma \vec{E} \cdot \vec{E}^*$  for each cell. Numerical values were also obtained by using a piece-wise quadratic interpolant [7] to obtain an expression for  $\vec{E}$  within each cell and then integrating the expressions for a volume average of  $1/2 \sigma \vec{E} \cdot \vec{E}^*$ .

It is readily seen in Fig. 1 that the interpolant causes a significant improvement in convergence to the known analytical solution. We may relate the improvement in convergence to the well-known preference of Simpson's rule to the trapezoidal rule for numerical quadrature. Simpson's rule requires fitting a piecewise quadratic through the data points and generally gives a better approximation of the integrand function for greater accuracy than the trapezoidal rule.

### III. TRIQUADRATIC INTERPOLANT

We have developed a triquadratic interpolant which may be used when the cell centroids are on a Cartesian product mesh. As the name suggests, quadratic interpolation is used parallel to each of the three Cartesian axes.

A total of 27 cells is used in the stencil for each calculation. Fig. 2 shows the location of the 26 cells surrounding the cell in which the correction is made. The Cartesian product is shown for  $X = -1, 0, 1$ ,  $Y = -1, 0, 1$ ,  $Z = -1, 0, 1$ , but scaling is readily used to adjust to a specified cell size.

Quadratic interpolation may be used with univariate data for the function  $F(X)$  at the three points  $X = -1, 0, 1$  by the rule

$$F(X) = F(-1) \frac{X}{2} (X-1) + F(0)(1-X) \\ \cdot (1+X) + F(1) \frac{X}{2} (X+1). \quad (6)$$

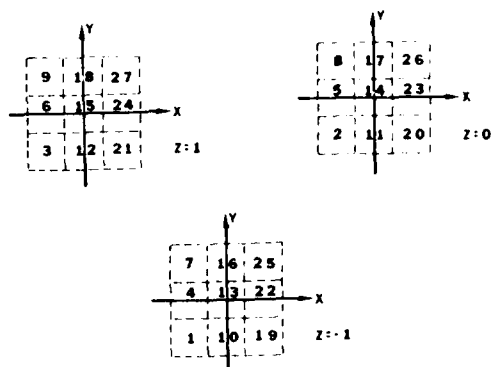


Fig. 2. Location of cells in stencil for the triquadratic interpolant

Triquadratic interpolation may be performed on the stencil shown in Fig. 2 by using products formed from three univariate interpolants. For example, the contribution of the function value at  $X = -1$ ,  $Y = -1$ ,  $Z = 0$  (cell number 2) is

$$F(-1, -1, 0) \frac{X}{2} (X-1) \frac{Y}{2} (Y-1)(1-Z)(1+Z).$$

Triquadratic interpolation as described in the last paragraph is only usable for corrections in a cell surrounded by 26 other cells, as shown in Fig. 2. It is possible to use a single interpolation rule based on the full 27-cell stencil if  $\vec{E}$  values are estimated for unoccupied positions by means of a series of fill-in rules. We have used the following series of rules in which the  $\vec{E}$  values are filled in the order of increasing distance from the central cell by averaging  $\vec{E}$  values known in adjacent cells.

1) Fill in the six closest cells (numbers 5, 11, 13, 15, 17, 23). If any are unoccupied, use the value of  $\vec{E}$  in the central cell.

2) Fill in the twelve next closest cells (numbers 2, 4, 6, 8, 10, 12, 16, 18, 20, 22, 24, 26). If any are unoccupied, use one-half the sum of  $\vec{E}$  for the pair from the six closest cells of part 1 which share a face with the unoccupied cell.

3) Fill in the eight corner cells (numbers 1, 3, 7, 9, 19, 21, 25, 27). If any are unoccupied, use one third the sum of  $\vec{E}$  for the three cells sharing a face with the unoccupied cell

Application of triquadratic interpolation to the general scatterer requires the following calculations be made for each cell. First, a sieve is used to find which of the 26 surrounding cells are occupied. Next, the fill-in rules are used as required to complete the stencil. Finally, the triquadratic interpolant is used to evaluate the integral of  $1/2 \sigma \vec{E} \cdot \vec{E}^*$  over the central cell. If the cells have different complex permittivities, both the fill-in and interpolation rules must be modified by suitably multiplying by the ratio of permittivities so that the interpolant has both  $D$  normal and  $E$  tangential to each boundary continuous. We have made such modifications and have used interpolation in solutions for inhomogeneous dielectric scatterers.

Since analytical solutions are not available for arrays of cubes, a standard for evaluating results obtained by



Fig. 3. Calculated average specific absorption rate for a 12-cm cube of muscle at 1 MHz without interpolation. Incident power density is 1 MW/cm<sup>2</sup>,  $\epsilon_r = 2000$ ,  $\sigma = 0.556$  mho/m.

TABLE I  
ERROR IN CALCULATED AVERAGE SPECIFIC ABSORPTION RATE  
FOR A 12-cm CUBE OF MUSCLE AT 1 MHz.  $\epsilon_r = 2000$ ,  $\sigma = 0.556$   
mho/m

Number of Cells	Error Without Interpolant	Error With Interpolant
1	-44.6	-44.6
8	-37.67	-34.17
27	-26.37	-20.92
64	-20.27	-15.97
216	-13.5	-9.01
512	-10.17	-5.897

numerical methods is not easily obtained, but one convergence test has been made for the triquadratic interpolant. Fig. 3 gives the average specific absorption rate calculated without interpolation for a 12-cm cube of muscle with plane wave at 1 MHz normally incident on one face. Linear convergence is demonstrated in the figure. Extrapolation using the values for 216 and 512 cells gives an SAR of  $0.3275 \times 10^{-6}$  W/kg for an incident power density of 1 MW/cm<sup>2</sup>. Table I gives the estimated errors in SAR without interpolation and with the triquadratic interpolant found by comparison with the extrapolated value of SAR. Results in Table I suggest that the triquadratic interpolant causes a significant improvement in convergence.

#### IV. NEWSUD INTERPOLANT

We have developed the NEWSUD interpolant which may be used when the cells have different sizes and/or arbitrary placement. The NEWSUD interpolant is more general than the triquadratic interpolant and does not require fill-in rules but is limited to linear rather than quadratic correction. The name NEWSUD is an acronym of the words "north," "east," "west," "south," "up," and

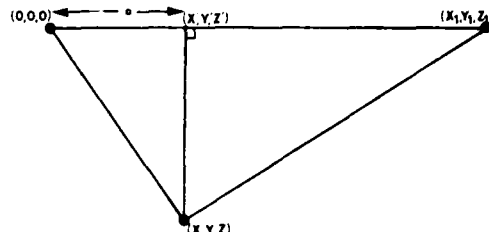


Fig. 4. Configuration for linear interpolation in the NEWSUD method.

"down" since the stencil contains only one cell near each of the six faces of a central cube for calculations within that cube.

When the NEWSUD interpolant is used for calculations within a cell, first, one imaginary plane is passed through each edge of the cube and the cell centroid. The planes divide the cube into six congruent pyramids as well as dividing the exterior into six corresponding solid angles. Next, each solid angle is searched to find a cell centroid as close as possible to the interpolated cube. Interpolation is performed separately in each of the six pyramids using only the centroids of the interpolated cube and corresponding external cell. If a solid angle does not contain an external cell centroid within a reasonable distance, say one side of the central cell or less, the uninterpolated value of  $E$  is used within the corresponding pyramid.

The configuration for linear interpolation within a pyramid in the NEWSUD method is shown in Fig. 4. The point at which interpolation is desired ( $X$ ,  $Y$ ,  $Z$ ), the centroid of the external cell ( $X_1$ ,  $Y_1$ ,  $Z_1$ ), and the centroid of the interpolated cell which is used as the origin determine a plane which is used for the figure.

The equation of the plane perpendicular to the line connecting  $(X_1, Y_1, Z_1)$  to the origin and passing through the point  $(X, Y, Z)$  is

$$XX_1 + YY_1 + ZZ_1 = a\sqrt{X_1^2 + Y_1^2 + Z_1^2} \quad (7)$$

where  $a$  is the distance from the origin to the plane. The linear interpolation used in the NEWSUD method when an external cell is found corresponding to a pyramid of the interpolated cell is accomplished by the approximation of identifying  $\bar{E}(X, Y, Z)$  with  $\bar{E}(X', Y', Z')$  so that

$$\begin{aligned} \bar{E}(X, Y, Z) &= \frac{a\bar{E}(X_1, Y_1, Z_1)}{\sqrt{X_1^2 + Y_1^2 + Z_1^2}} \\ &\quad + \left[ 1 - \frac{a}{\sqrt{X_1^2 + Y_1^2 + Z_1^2}} \right] \bar{E}(0, 0, 0). \end{aligned} \quad (8)$$

Linear interpolation defined by (7) and (8) is used to evaluate the integral of  $1/2 \sigma \bar{E} \cdot \bar{E}^*$  in a pyramid for which a corresponding external cell is found. If the cells have different complex permittivities, (8) must be modified by suitably multiplying by the ratio of permittivities

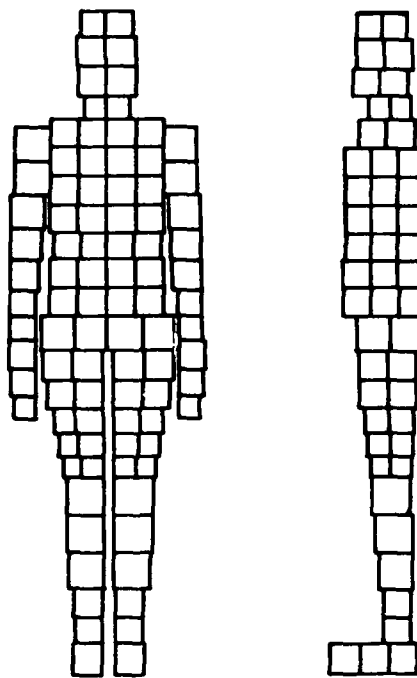


Fig. 5. An improved model of man for numerical calculations.

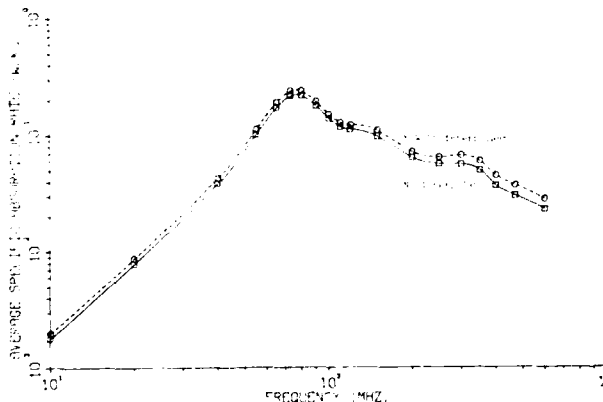


Fig. 6. Whole-body SAR for a homogeneous model of man.  $E \parallel \hat{L}$ ,  $k$ : front-to-back, incident intensity = 1 MW/cm<sup>2</sup>.

so that both  $D$  normal and  $E$  tangential to a boundary are continuous.

Fig. 5 illustrates a model of man which has been used for numerical calculations [8]. Moment-method solutions have been made for the model using pulse functions as a basis and delta functions for testing. The NEWSUD interpolant has been used in calculations since the model has cells which are cubes of different sizes. Fig. 6 shows the frequency dependence of the average SAR calculated for the model of man with a vertically polarized plane wave having frontal incidence. Values found both with and without interpolation are given.

If the local  $E$  values are exact samples and if there is appreciable variation between adjacent cells, then statistical procedures may be used to calculate confidence limits

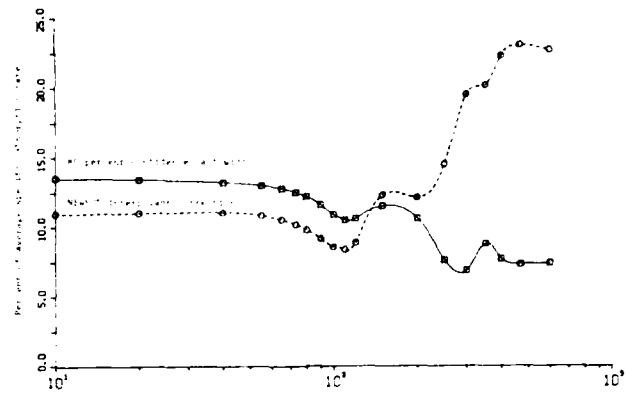


Fig. 7. Correction to whole-body SAR for homogeneous model of man.

for values of the average SAR found without aid of interpolants [9]. The 80-percent confidence half widths for average SAR values have been calculated and plotted in Fig. 7. The percent correction which the NEWSUD interpolant makes is also shown in Fig. 7.

The frequency-dependent variation of the true  $E$  must cause increasing error in calculations of local  $E$  at frequencies greater than 200 MHz for the cell sizes used with the model of man [10]. The 80-percent confidence half widths shown in Fig. 7 are not valid at frequencies above 200 MHz since their calculation requires the assumption that the local  $E$  values are exact samples. Fig. 7 shows that the NEWSUD interpolant makes relatively little correction to the SAR at low frequencies where relatively little error is expected, but the correction increases sharply at frequencies for which the error is expected to increase.

## V. CONCLUSIONS

The interpolative correction to calculated values of the average SAR has been tested in a one-dimensional problem in which the analytical solution is available for comparison with numerical solutions. A test was also made in a three-dimensional problem in which the true solution was estimated by extrapolation. In both tests the interpolant makes small corrections when few cells are used since sampling is insufficient to allow proper estimation of the variation of the fields. The fractional correction is also observed to decrease as many cells are used since the interpolated and uninterpolated solutions must converge to the same answer. In both tests the interpolant was found to provide a significant reduction in error for a negligible increase in computational expense.

It is hoped that the two interpolants presented in this paper are only the first steps in the development of a procedure which will find general usage as a follow-up to moment-method solutions. Use of the interpolant for calculation of the external scattered fields and development of a general interpolant consistent with the wave equation appear to be the next necessary steps.

## REFERENCES

- [1] J. H. Richmond, "Scattering by a dielectric cylinder of arbitrary cross section shape," *IEEE Trans. Antennas Propagat.*, vol. AP-13, pp. 334-341, May 1965.
- [2] —, "TE-wave scattering by a dielectric cylinder of arbitrary cross-section shape," *IEEE Trans. Antennas Propagat.*, vol. AP-14, pp. 460-464, July 1966.
- [3] G. W. Hohmann, "Three-dimensional induced polarization and electromagnetic modeling," *Geophysics*, vol. 40, pp. 309-324, Apr. 1975.
- [4] D. E. Livesay and K. M. Chen, "Electromagnetic fields induced inside arbitrarily shaped biological bodies," *IEEE Trans. Microwave Theory Tech.*, vol. MTT-22, pp. 1273-1280, Dec. 1974.
- [5] R. F. Harrington, *Field Computation by Moment Methods*. New York: Macmillan, 1968.
- [6] B. S. Guru and K. M. Chen, "Experimental and theoretical studies on electromagnetic fields induced inside finite biological bodies," *IEEE Trans. Microwave Theory Tech.*, vol. MTT-24, pp. 433-440, July 1976.
- [7] P. J. Davis, *Interpolation and Approximation*. New York: Dover, 1975.
- [8] M. J. Hagmann, O. P. Gandhi, and C. H. Durney, "Numerical calculation of electromagnetic energy deposition for a realistic model of man," presented at the 1977 USNC/URSI Meeting, Airlie, VA.
- [9] W. Mendenhall and R. L. Schaeffer, *Mathematical Statistics with Applications*, North Scituate, MA Duxbury, 1973.
- [10] M. J. Hagmann, O. P. Gandhi, and C. H. Durney, "Upper bound on cell size for moment-method solutions," *IEEE Trans. Microwave Theory Tech.*, vol. MTT-25, pp. 831-832, Oct. 1977.

DISTRIBUTION LIST

Director (ATTN: SCRD-UWZ-C)  
Walter Reed Army Institute of Research  
Walter Reed Army Medical Center  
Washington, DC 20012

USAMRDC (SGRD-RMS)  
Fort Detrick  
Frederick, MD 21701

Defense Technical Information Center (DTIC)  
ATTN: DTIC-DDA  
Cameron Station  
Alexandria, VA 22314

Dean  
School of Medicine  
Uniformed Services University  
of the Health Sciences  
4301 Jones Bridge Road  
Bethesda, MD 20014

Commandant  
Academy of Health Sciences, US Army  
ATTN: AHS-COM  
Fort Sam Houston, TX 78234